PFC/RR-86-15 DOE/ET-51013-186

EXPERIMENTAL RESULTS FROM THE CONSTANCE B MAGNETIC MIRROR

October 1983 - June 1986

Smatlak, D.L., Chen, X., Garner, R.C., Goodman, D.L.,
Hokin, S.A., Irby, J.H., Lane, B.G., Liu, D.K.,
Post, R.S., Smith, D.K., J. Trulsen*

August 21, 1986

Plasma Fusion Center
Massachusetts Institute of Technology
Cambridge, MA 02139

*Present address: University of Tromso, Tromso, Norway

Preface

The intention of the authors in compiling this report has been to collect, in a compact form, most of the data which has been taken on the Constance B mirror machine from its beginnings in October, 1983 to date. The report is intended primarily for the benefit of the members of the Constance group, present and future. Therefore the reader will note that the style is somewhat informal. Because this is the first document of its kind for our experiment, we have included some basic information on the diagnostic set and the machine itself which will not be included in future reports of this type. Those topics which are thesis research are only briefly covered here since they will be detailed in subsequent Ph.D. theses and publications.

Table Of Contents

A. Introduction

In this report the Constance B mirror facility at the Massachusetts Institute of Technology is described and the experimental research which has been carried out from October 1983 through June 1986 is summarized. Constance B is a plasma confinement device of the quadrupole, or minimum-B, magnetic mirror geometry. Electron cyclotron resonance heating (ECRH) is used to create and heat high beta (beta = plasma pressure/magnetic field pressure), hot electron plasmas for thermonuclear fusion research. The typical operating parameters achieved in the machine are shown below.

Table 1. Constance B Operating Parameters

Midplane Magnetic Field	B_o = 3.2 kG
Mirror Ratio	R_m = 1.9
Mirror Length	L_m = 80 cm
Estimated Plasma Volume	V_p = 8 liters
Hot Electron Temperature	T_h = 450 keV
Hot Electron Density	$n_h \sim 2 \times 10^{11} cm^{-3}$
Potential	ϕ = 100 V
Cold Electron Temperature	T_c = 60 eV
Cold Electron Density	$n_c = 2 \times 10^{11}\ cm^{-3}$
Ion Temperature	$T_i \sim 20$ eV
Beta	β = 20%
Neutral Pressure	8×10^{-7} torr
Pulse Length	3 seconds
ECRH Frequency	10.5 GHz
ECRH Power	2 kW

The main areas of research which have been investigated are: Hot electron equilibrium, hot electron microinstability, ECRH-induced electron velocity space diffusion, ICRH (ion cyclotron resonance heating), ion drift pumping, and radial potential control. The selection of these topics has been driven by the role of Constance as a support machine for the U.S. tandem mirror fusion program. Highlights of 1985 include:

* Completion of the electron microinstability studies. This work experimentally characterizes the whistler instability and its effect on confinement in a reactor-like hot electron plasma. This work has shown that the driving mechanism for this instability is the free energy associated with the 1-5 keV electrons and that the hot electrons (E>100 keV) are microstable.

* Studies of ECRH induced electron endloss in which rf induced endloss rates have been measured which are up to 100 times the collisional loss rate.

* Measurements of the equilibrium diamagnetic fields outside the hot electron plasma. These are the first detailed measurements of the 3-dimensional equilibrium on a high beta plasma.

* Initiation of the ICRH and drift pumping experiments.

* Detailed measurements of the axial profile of the hot electron temperature and the x-ray flux. This contributes to our understanding of the hot electron distribution function.

* The first visible light images of a minimum-B hot electron plasma. These pictures suggest that the hot electrons are concentrated along a thick baseball seam which is the drift surface for the deeply trapped hot electrons. This implies that the equilibrium cannot be described using a P(B) formalism.

The Constance program is funded by the Applied Plasma Physics division of the United States Department of Energy, Office of Fusion Energy. The

group consists at this writing of one full-time scientist, four part-time (5-15%) scientists from the Tara tandem mirror group, five graduate students, and one full-time technician.

B. Machine Operations

A photograph of Constance B is shown in figure 1. Basic machine construction was completed in October 1983. The cylindrical fan tanks on each end provide large surfaces for pumping and allow the field lines to expand and hit the end walls at low magnetic field. The expansion reduces the end wall plasma density and limits the secondary electron currents from the wall. This decouples the plasma from the walls as evidenced by the high plasma potential compared to the similar previous experiment INTEREM[1]. Pumping is achieved with a 250 l/sec turbo-molecular pump and titanium gettering in the fan tanks. The typical base pressure is 2×10^{-8}torr with the main impurity at these pressures being argon. The vacuum chambers are made of aluminum.

The magnet is a water cooled copper conductor baseball coil. Figure 2 shows the field lines and the surfaces of constant magnetic field (mod-B surfaces) which are generated by this magnet. Note that the field lines have strong curvature. The magnet is run pulsed and pulse lengths of 5 seconds with a 3% average duty cycle are typical.

The first Constance B baseball magnet was obtained from the Lawrence Livermore National Laboratory. It was the spare for an early experiment,

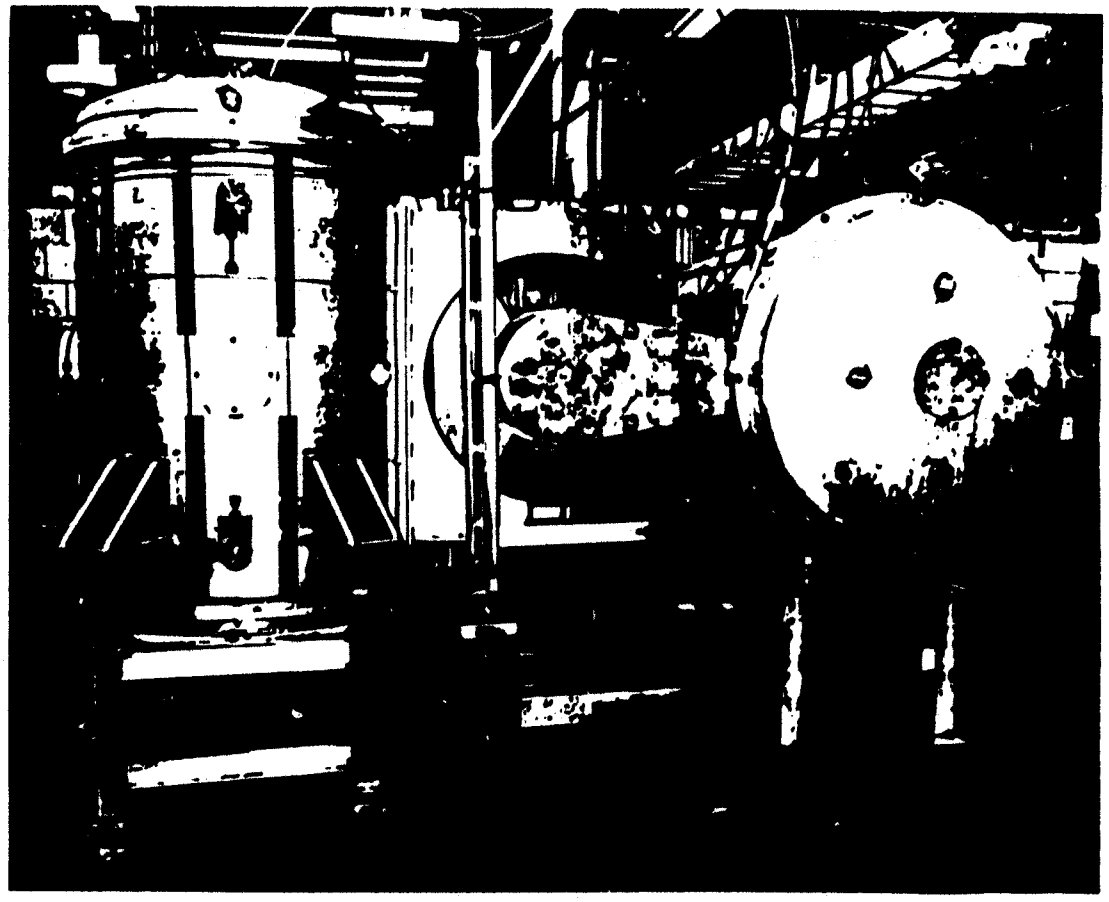

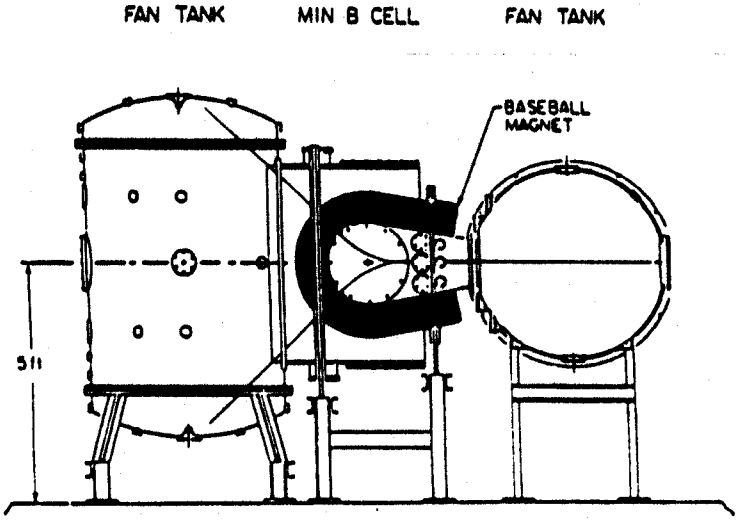

Fig. 1) Photograph and diagram of the Constance B mirror machine.

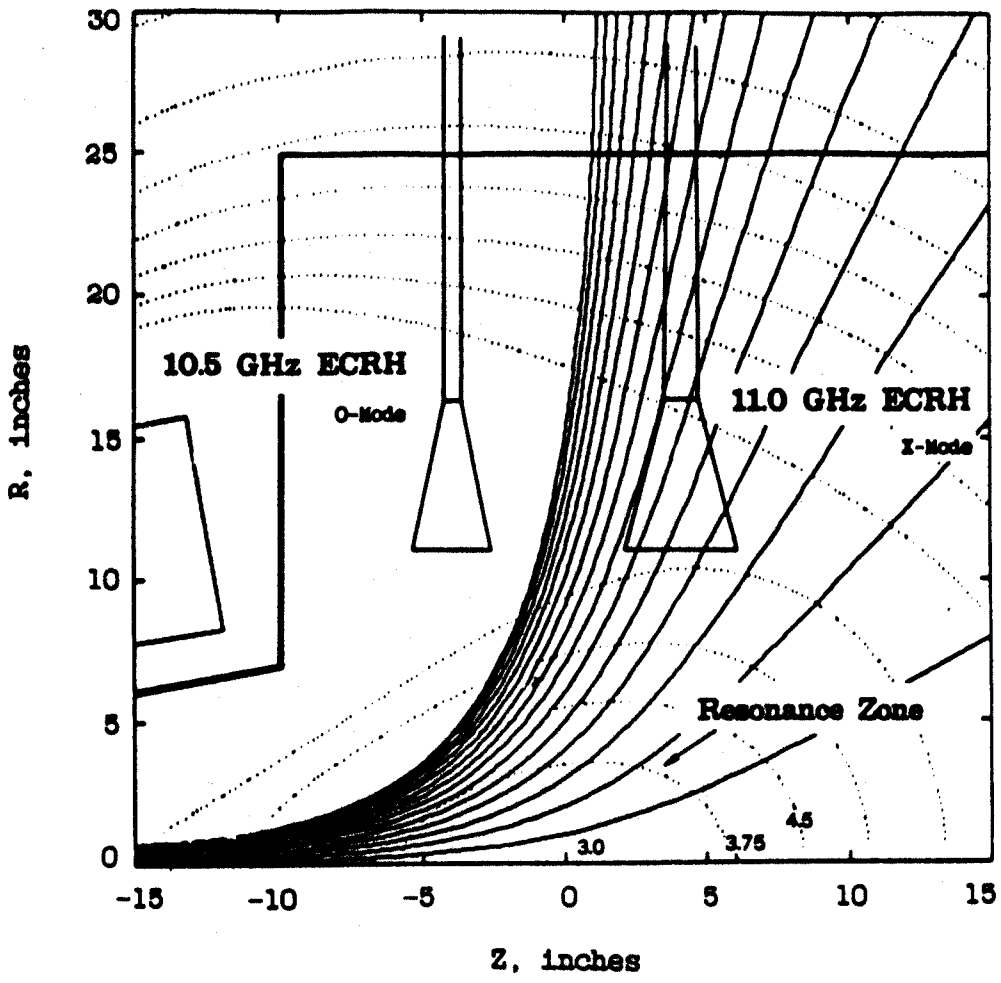

Fig. 2) The magnetic field geometry in Constance B. The microwave antennas are also shown.

but had been in an outdoor display area since the completion of that program. This coil shorted twice in 1984, and the second short, in December 1984, could not be repaired. A new coil arrived in late April, 1985 and full operation of the experiment was resumed in June 1985.

In 1985 there were 4500 shots taken on the machine from May 30 until December 31, of which 1336 were taken in the month of October. In the first half of 1986, over 5000 shots have already been taken. By comparison, 376 shots were taken in 1983, and 2900 in 1984. Operation with the new baseball magnet has been trouble-free. The machine is typically run up to 10 hours per day, 5 days a week except for scheduled up-to-airs and other maintenance.

Timing and safety interlock functions on the machine are controlled by a Gould Modicon 484 programmable controller. The data system is CAMAC based and runs on the Tara Vax 11/750 computer. This year online storage space for Constance was increased to 88 Mbytes, enough for 250 shots, or approximately three days worth of shots. The rf and power equipment used by the experiment is listed below.

Table 2. Constance B Equipment

600 W 11.0 GHz CW klystron amplifier
5 kW 10.5 GHz CW klystron amplifier
2 kW CW 3-5 MHz ICRH transmitter
50 kW pulsed 100-150 kHz drift pumping transmitter
1 MW X-band pulsed magnetron ECRH system
Gould Modicon 484 Programmable Logic Controller
Magnet power supplies
Computerized data collection - CAMAC digitizers

The diagnostics which have been developed for use on the machine are listed in Table 3 below. Major diagnostics which are in the process of being added to the machine include a time-of-flight analyser and an x-ray crystal spectrometer. A magnetic endloss analyzer is in the design stage.

Table 3. Constance B Diagnostics

4	Diamagnetic loops *
2	NaI(Tl) hard x-ray PHA systems
1	24 GHz interferometer
1	1/2 m Ebert visible spectrometer *
1	CCD TV camera *
2	Plastic scintillator probes
3	Fast pressure gauges
11	Gridded end loss analyzers *
11	Faraday cups *
11	Net current detectors *
3	Emissive probes
5	B-dot probes *
2	Langmuir probes
1	Admittance probe *
2	Skimmer probes
2	H-alpha detectors *
1	Cs cell charge exchange analyzer *
3	Microwave cavity power monitors
1	rf spectrum analyser
1	Microwave spectrum analyzer
1	Acousto-optic spectrometer (AOS)
1	Thermistor probe
1	BB dropper system *
1	Ge soft x-ray system (borrowed) *
4	Surface barrier diodes *
1	X-ray pinhole camera *

* Quantity increased or new diagnostic in 1985

C. Basic Plasma Measurements

The typical operating parameters of the Constance B mirror were shown in Table 1. Figure 3 shows the time evolution of the diagnostic signals during a typical shot. The machine parameters are 3.6 kG, $1x10^{-6}$ torr, and 3 kW of ECRH at 10.5 GHz. A typical time evolution of the x-ray temperature is given in fig. 4, where this data is the result of averaging over 10 shots. Note that the endloss, the density, and the potential rise to their peak values within 50-100 ms, while the diamagnetism and the x-ray temperature continue to increase at a slower rate. The initial x-ray temperature rise is linear in time. The spikes in the endloss and the rf emission signals are the result of the hot electron microinstability (section F). The diagnostic methods used to obtain the data in fig. 3 will be discussed in this section. The location of some of the diagnostics in the machine is shown in figure 5.

The hot electron temperature is determined by pulse height analysis of the bremsstrahlung x-ray spectrum between ~50 keV and 1.5 MeV measured with a 2"x2" or 3"x3" sodium iodide crystal detector. The detector sees the chord-averaged flux through a volume which intercepts approximately 1 cm^2 at the center of the plasma. The average energy moment of the measured pulse height spectrum can be computed and compared to the average energy moment of a Maxwellian distribution of temperature T_h. In most cases Maxwellian spectra are a very good fit to the experimental data. The calculation takes into account the attenuation due to the air and the aluminum vacuum window.

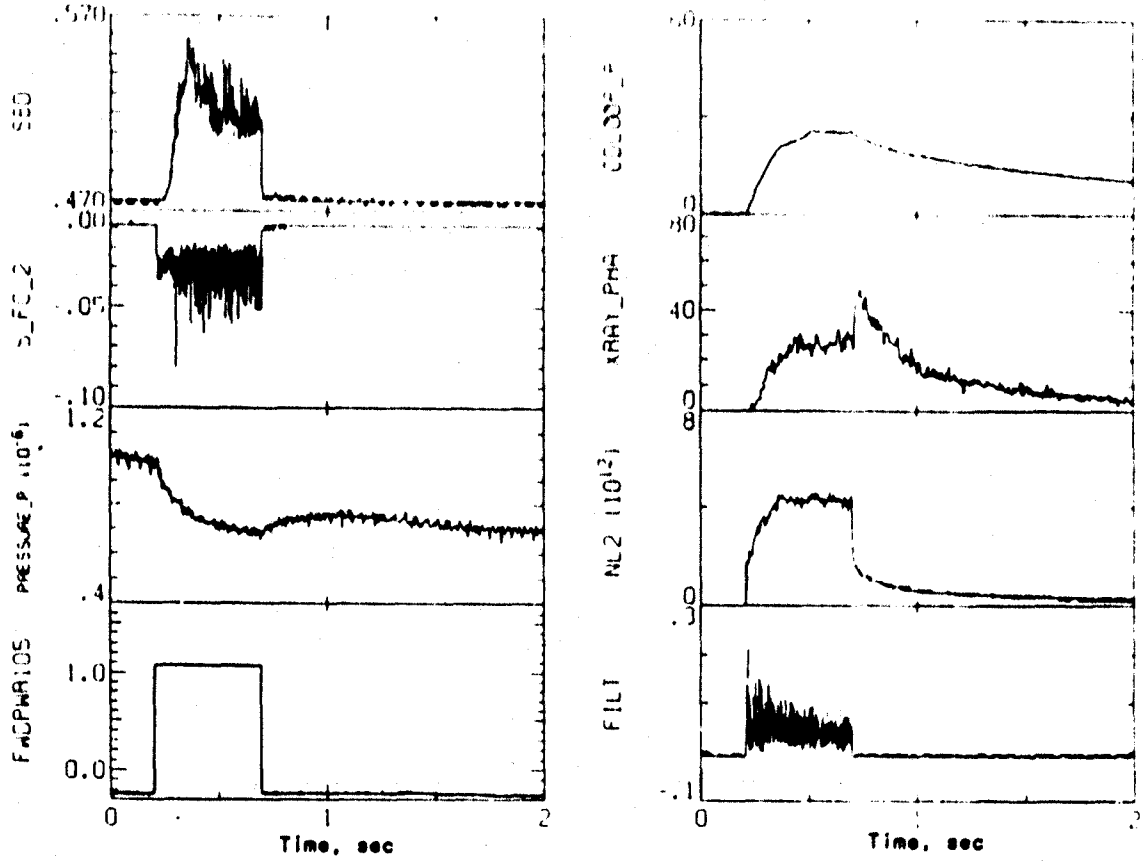

Fig. 3) Diagnostic signals from a shot with 3 kW of ECRH and midplane magnetic field of 3.6 kG. The signals on the left, from top to bottom, are the surface barrier detector, an endwall Faraday cup, the edge neutral pressure, and the ECRH power. On the right, the diamagnetic loop signal, the x-ray flux, the line density, and the microwave emission at frequencies other than the ECRH frequency are shown.

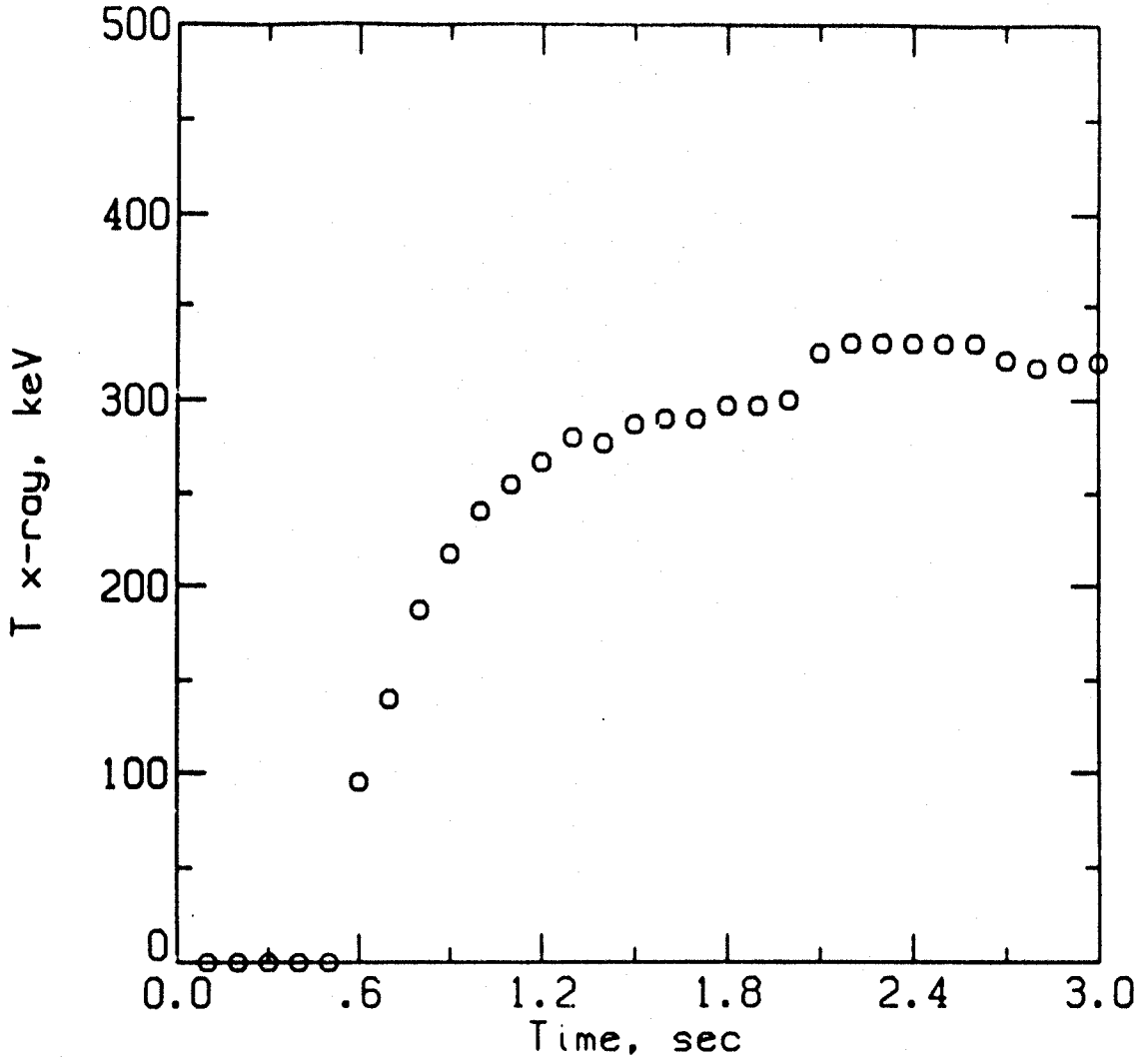

Fig. 4) Time evolution of the x-ray temperature as measured by the NaI detector. The ECRH is turned off at 2.0 sec. B=3.2 kG, P=1 kW, P_o = 8 x 10^{-7} torr.

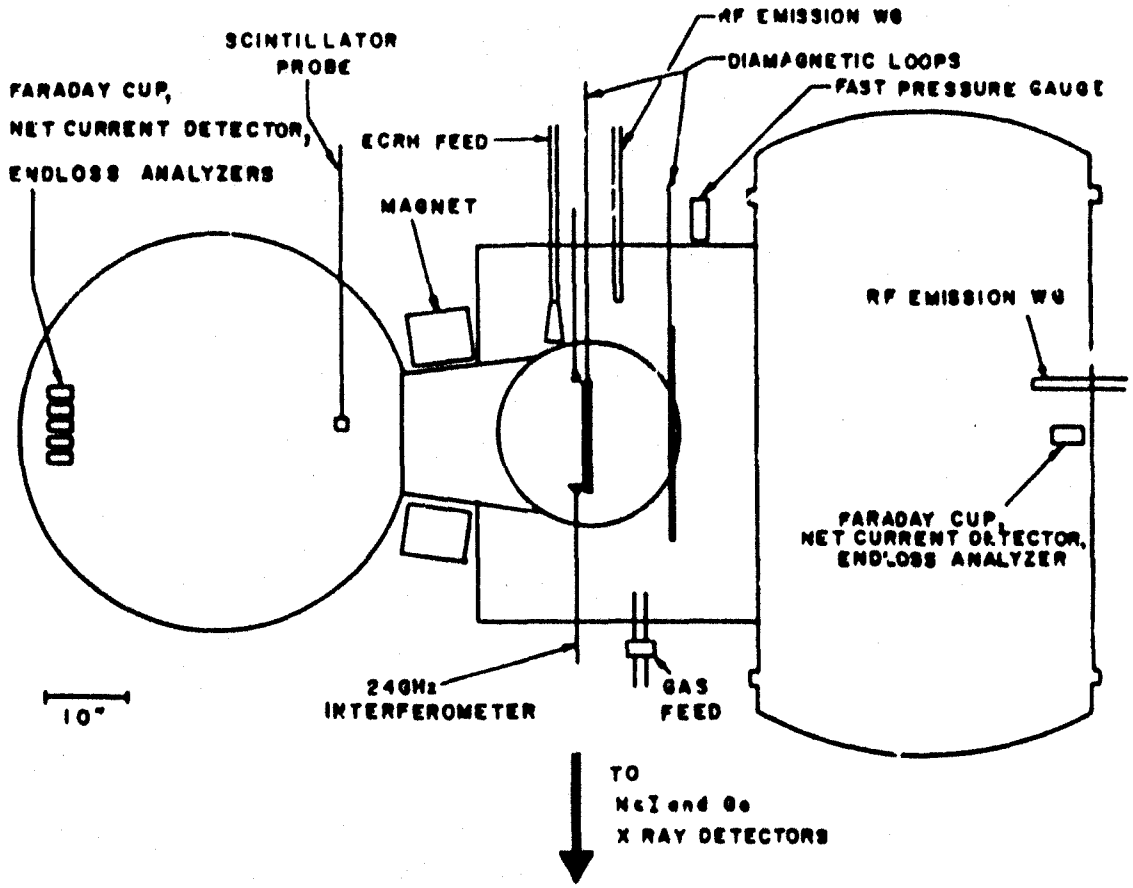

Fig. 5) Location of diagnostics on the Constance B mirror.

and is fully relativistic. A typical spectrum is shown in figure 6. The hot electron temperature varies from 200 to 500 keV depending on the ECRH power, magnetic field, or neutral pressure. The detailed scaling data will be presented in section E. It is important to remember that the measured temperature is the line-averaged hot electron temperature weighted by the electron and target density profiles.

In early 1986 we borrowed the Tara/ASE intrinsic planar Ge soft x-ray detector to measure the bremsstrahlung x-ray spectrum between 2 keV and 150 keV. This detector indicates that the spectrum is Maxwellian down to 2 keV and the temperatures match the values measured by the NaI hard x-ray system (fig. 7).

The cold electron temperature has been measured with the endloss analyzer. The data is shown in figure 8. In 1986 a **v x B** energy analyzer will be designed and built to look at electron endloss in the range from 5 keV to 150 keV, the range that is not covered by the endloss analyzers or plastic scintillator probes.

The plasma potential can be measured by two methods. The knee on a swept endloss analyzer curve will give a measure of the peak potential in the machine. Emissive probes can also be used for local potential measurements in regions where there are no hot electrons. The two come into agreement when the emissive probe is placed on axis near the mirror peak (fig. 9). The emissive probe has better time response (100 kHz) than the swept endloss analyzer, so that the emissive probe is useful for studying

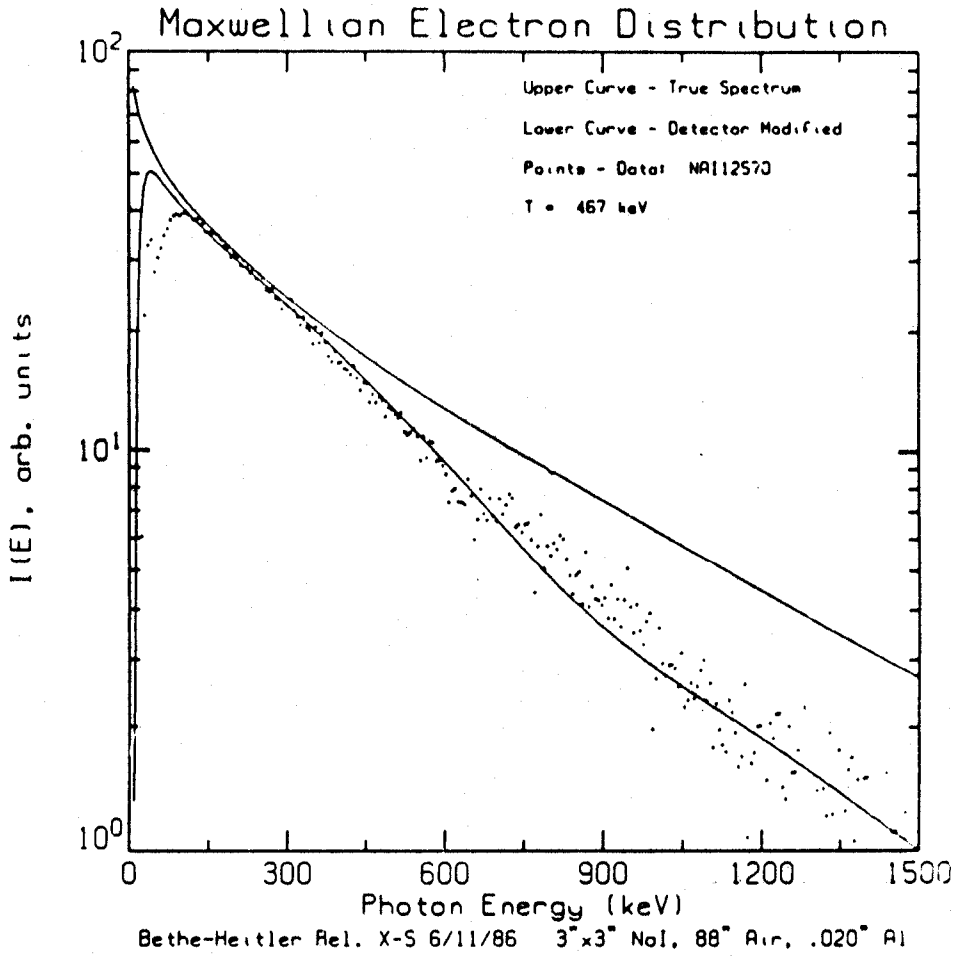

Fig. 6) Hard x-ray bremsstrahlung spectrum measured with a 3" × 3" NaI detector for a 2 kW, 3.2 kG, 5×10^{-7} torr shot. The data is summed for the first 250 ms after rf turn-off.

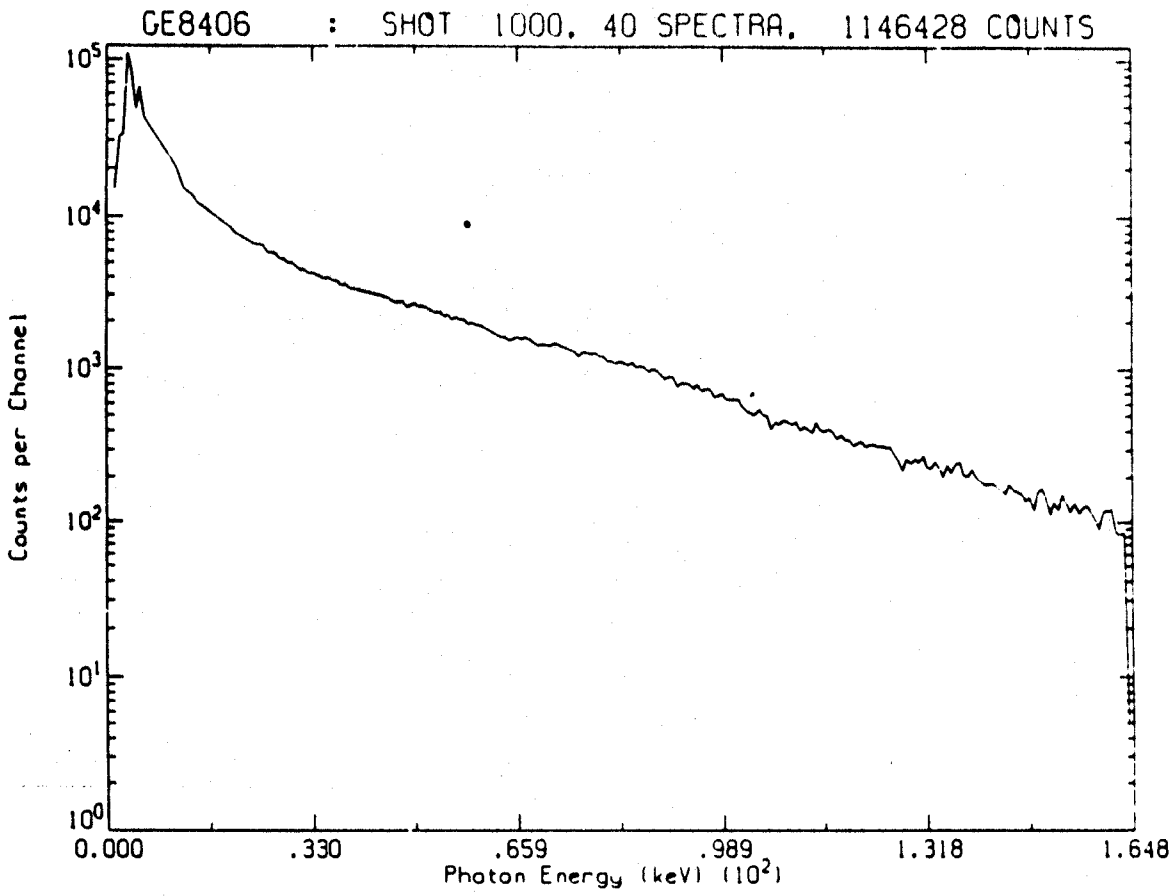

Fig. 7) Soft x-ray bremsstrahlung spectrum measured with an intrinsic planar germanium detector. The spectrum is summed over 33 shots with conditions of 3.2 kG, 1 kW, and 2×10^{-6} torr.

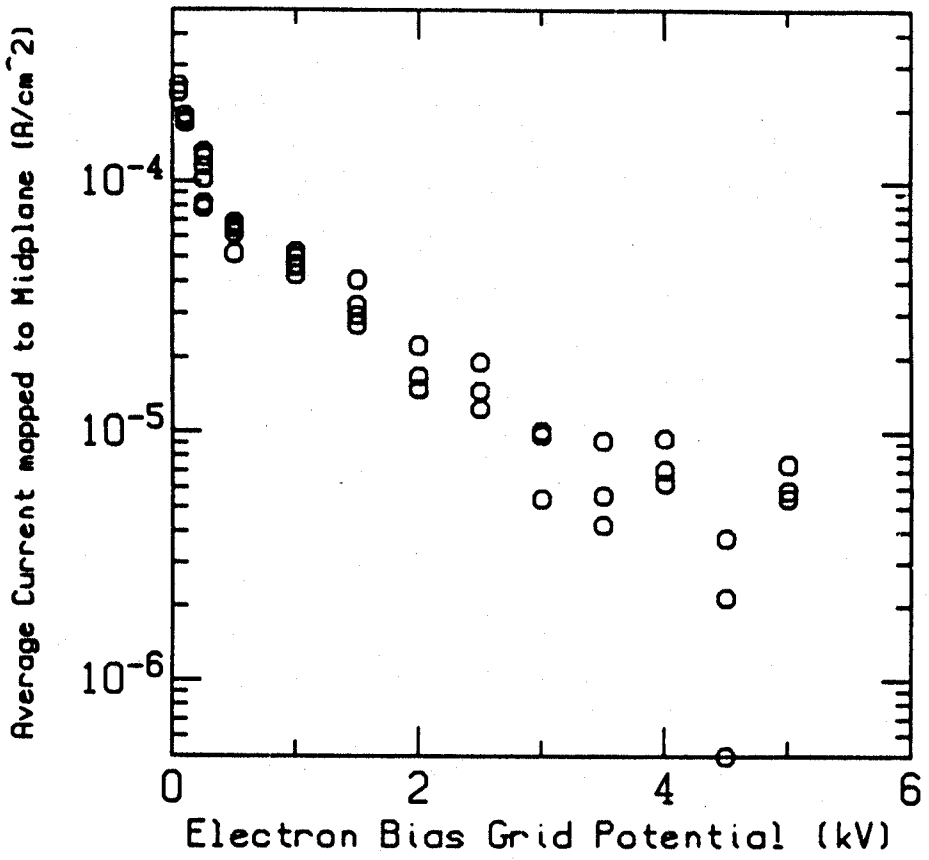

Fig. 8) Electron endloss current as a function of endloss analyzer repeller voltage. Each point is for a different shot. B=3 kG and P=1 kW.

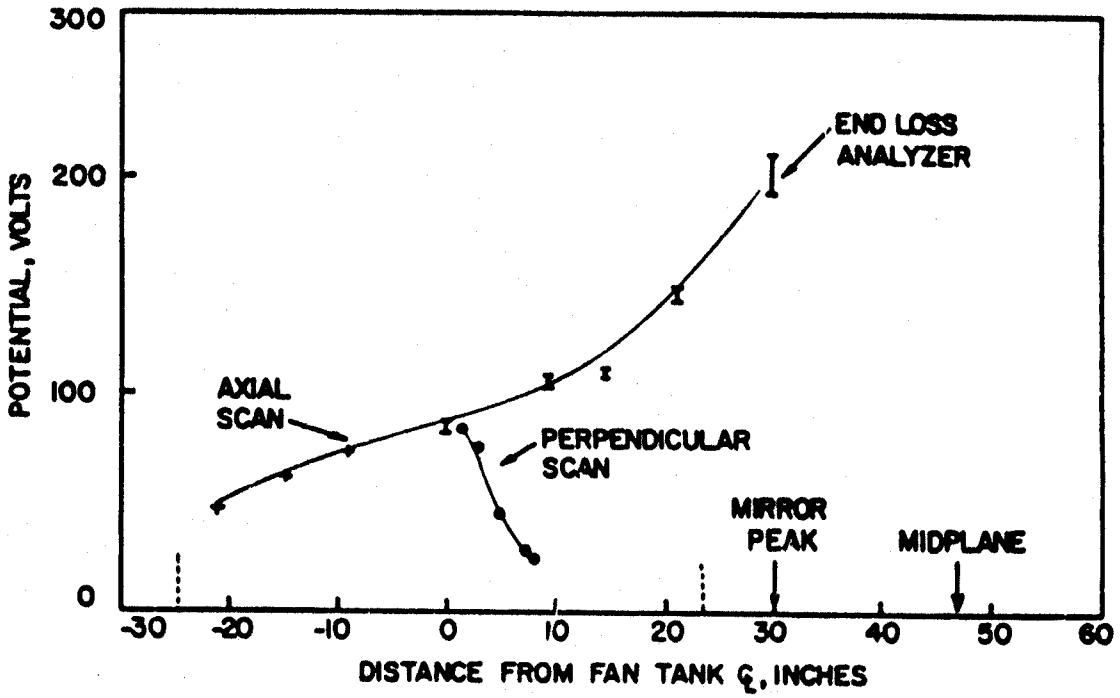

Fig. 9) Axial and radial potential profiles measured by an emissive probe in the north fan tank. The potential measured by the swept end loss analyzer is shown for comparison. The radial (labeled perpendicular) scan is taken at the center of the fan tank.

the potential fluctuations due to the electron microinstabilities (section F).

A positively swept endloss analyzer will also give the parallel ion endloss temperature. Data will be presented in section N. Recall that the endloss temperature is not necessarily the same as the temperature inside the plasma. Measurements of the hydrogen and helium line widths yield an ion temperature of ~15 eV, which is lower than the ~60 eV ion endloss temperature. Initial tests of a cesium cell charge exchange analyzer have been made and this diagnostic will provide another measure of the ion temperature when it is operational.

Skimmer probes are used to infer the hot electron plasma size. The principle behind the skimmer probe is that it acts as a limiter to prevent hot electron production at radii greater than the position of the probe tip. The position at which the probe begins to affect the plasma diamagnetism is usually interpreted as the edge of the hot plasma (fig. 10). The skimmer probe data and the television camera pictures indicate that the midplane plasma radius is determined by the vacuum ECRH resonance zone. Additional skimmer probe data will be discussed in section D.

Electron density measurements are made with a 24 GHz interferometer on the midplane which looks through the plasma perpendicular to the axis and at an angle of 45 degrees to the horizontal. The line density measured by the interferometer is usually converted to density by assuming that the density profile is flat with a 20 cm width. This model gives a lower bound on the

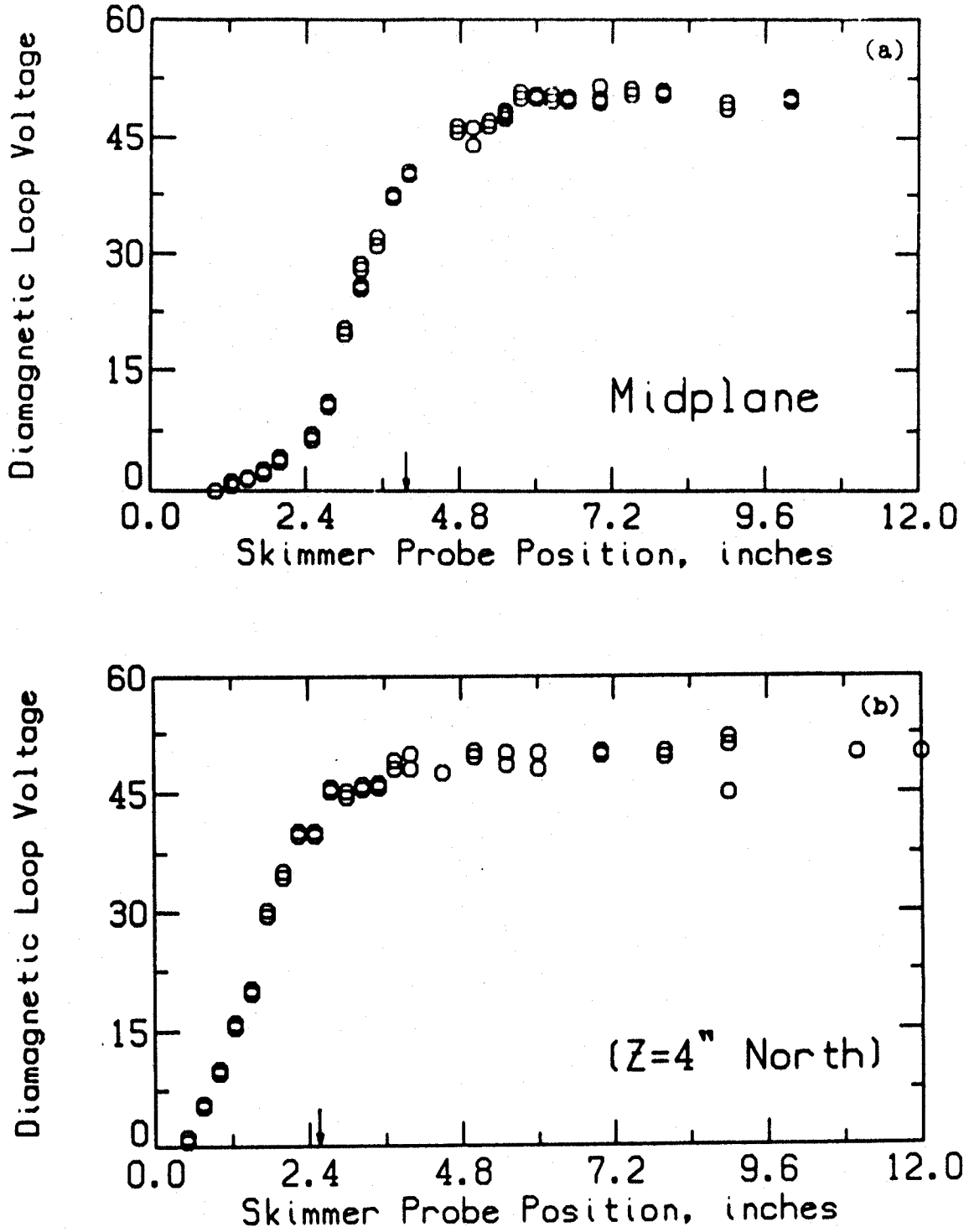

Fig. 10) Variation of the diamagnetic loop signal with the position of a 1/4" diameter skimmer probe inserted radially at (a) the midplane and (b) 4" north of the midplane. The vacuum ECRH resonance zone is marked by the arrows.

density. Any radial dependence of the density will lead to higher peak densities.

However, the interferometer, in effect, does not measure all of the hot electron density because the phase shift in a relativistic plasma is reduced relative to that of a cold plasma of equal density. We use the formula derived by Mauel [2] for the index of refraction of a relativistic plasma:

$$N^2 = 1 - \frac{\omega_p^2}{\omega^2} \left\langle \frac{1}{\gamma} \right\rangle$$

where $\left\langle \frac{1}{\gamma} \right\rangle$ is the average of the inverse mass of the hot electrons. This formula implies that for the typical Constance parameters about half of the hot electron density will be measured by the interferometer. The time behavior of the interferometer signal (fig. 11) verifies that some hot electrons are measured since there is some signal present after the ECRH is turned off, and long after the cold electrons have scattered out. The drop in line density after the rf is turned off gives a lower bound on the fraction of hot electrons in the plasma of about 1/2 when the rf is on.

The hot electron density measurement from the interferometer can be compared to the hot density calculated from the stored energy measured by the diamagnetic loop and the x-ray temperature. The comparison between these two methods is shown in fig. 12. Recall that we are dividing a peak value (model-dependent) by a line averaged value. The fact that the two methods agree to even within a factor of 2 is encouraging.

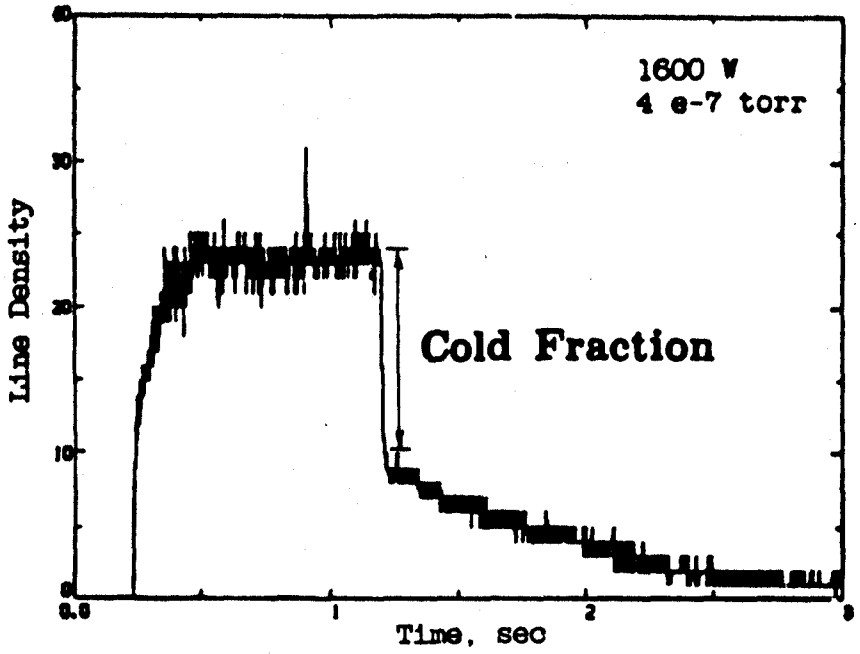

Fig. 11) Time evolution of the interferometer signal. The fast drop at ECRH turn-off is due to the loss of cold electrons.

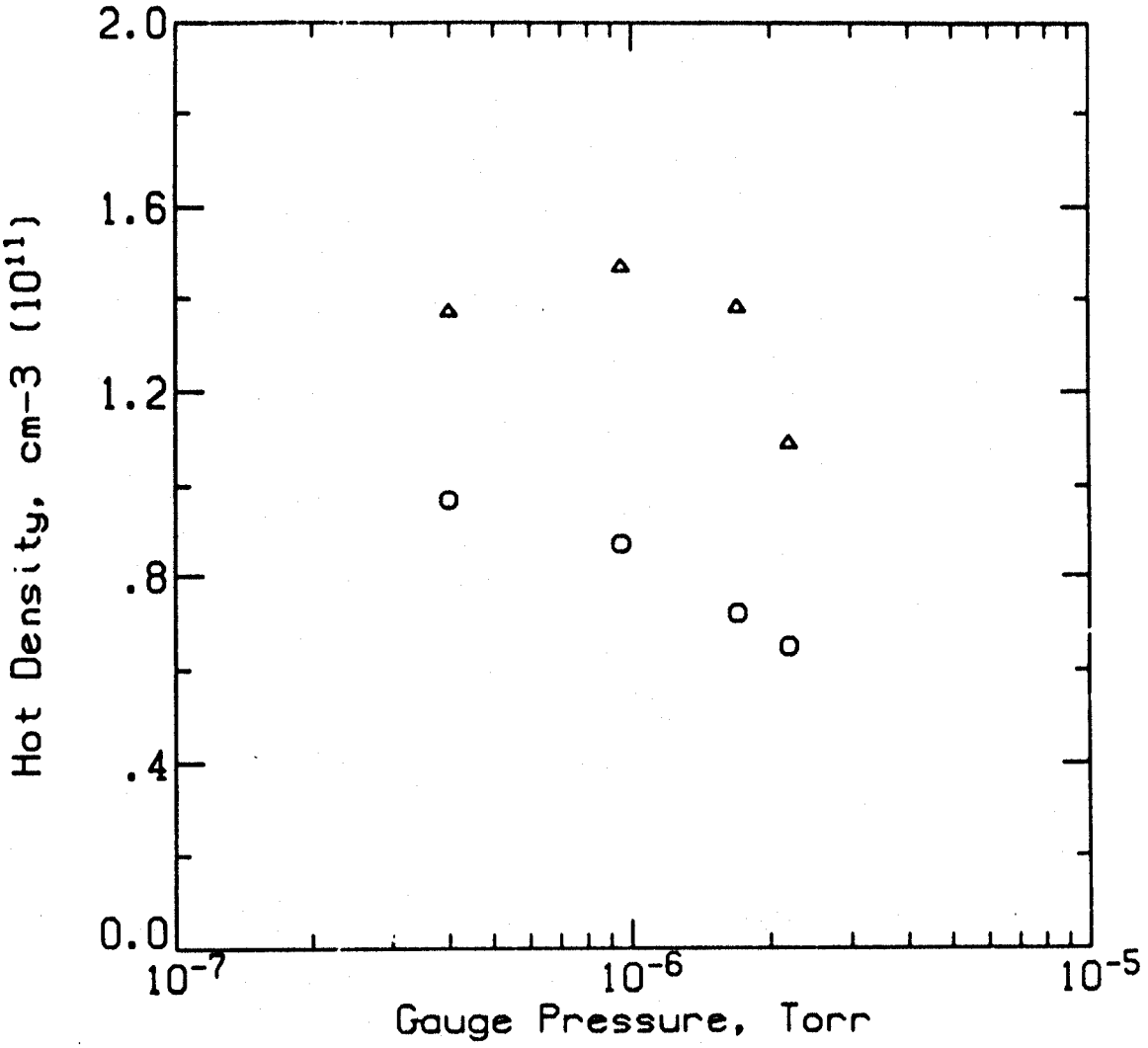

Fig. 12) Comparison of the hot electron density inferred from the interferometer (triangles) to the density calculated using the diamagnetic loop signal and the measured x-ray temperature (circles) as a function of neutral pressure. P=1 kW, B=3 kG.

Profile effects are also important in the diamagnetic loop measurements. In order to convert the measured loop voltage to a useful quantity such as beta ($\beta = \frac{8\pi nT}{B^2}$), the plasma size and the pressure profile must be known. This is not easily determined in a hot electron plasma. Measurements to do just this are in progress on Constance and will be discussed in section H. At this point it will be sufficient to point out that for a given diamagnetic loop voltage, beta can vary by more than a factor of 1.5 between a hollow and a flat pressure profile of the same size. For example, the diamagnetic loop signal which was shown in figure 3 can correspond to betas between 6% and 20% depending on the exact hot electron pressure profile which is used. The number usually used to calculate beta from the experimental data is that for a flat profile of radius determined by the skimmer probe so that it is a conservative estimate and in fact beta may well be higher. For details of the effect of profiles on beta see the memos by X. Chen [3]. In Constance, diamagnetic loops of different sizes at multiple locations are employed. A diamagnetic loop shaped like the baseball magnet has also been used. From axial arrays of loops and a pressure model one can calculate the hot electron temperature anisotropy, $T_\perp/T_{||}$. The diamagnetic loop data suggests a value of anisotropy near five.

As a part of the effort to infer the hot electron profile, experiments have been conducted in which an 1/8" diameter aluminum BB is dropped through the plasma at different locations. The BB should sweep out all the hot electrons as it falls through the plasma since the hot electron drift time (.1 μs) and bounce time (6.6 ns) are much shorter than the BB transit time ($\sim$ 10 ms). The BB's are found to be molten when they hit the opposite wall.

One can calculate that at least 40 joules of stored energy is necessary to melt this amount of aluminum, if we assume that the BB was uniformly molten. This gives a lower bound on the plasma stored energy and consequently a lower bound on beta of 15% if an 8 liter plasma volume is used. Since the BB only reduces the diamagnetic loop signal by half on dropping through, the actual values can be higher. Although visual inspection of the BB indicates it was probably uniformly molten, the transient heat conduction problem should be calculated in order to verify this assumption. We also note that the BB's are not heated to drive off surface gases before they are dropped into the plasma. As a result some fraction of the drop in diamagnetism is probably caused by the BB's gas cloud.

The edge neutral pressure is monitored using a fast pressure gauge in the central chamber. Gauges are also installed in the fan tanks. Pump-out by the plasma is seen (see fig. 3). These gauges have not yet been calibrated in the magnetic field, so they are only accurate to within a factor of two. The agreement between the fast pressure gauges and the Bayard-Alpert gauge will vary as a function of time after an up-to-air. Immediately following an up-to-air the fast pressure gauge reads 4 times higher than the Bayard-Alpert and within 2 days they agree to within a factor of 2.

Given the plasma parameters which have been described above, it is instructive to construct a table of the typical frequencies of plasma motion in Constance. This table is shown below, for the plasma parameters which were given in Table 1.

Table 4. Plasma Frequencies

Midplane electron cyclotron frequency	f_{ce} = 8.95 GHz
ECRF heating frequency	$f_{\mu w}$ = 10.5 GHz
Midplane electron plasma frequency	f_{pe} ~ 4.0 GHz
Midplane ion cyclotron frequency	f_{ci} = 4.88 MHz
Upper hybrid frequency	f_{uh} ~ 9.8 GHz
Hot electron drift frequency	f_{de} ~ 7 MHz

The plasma emission at many of these frequencies can be measured by the acousto-optic spectrometer, or AOS. The AOS is a high speed, high frequency spectrum analyzer. It measures rf power in 500 MHz bands from 5 MHz to 4 GHz with 2 MHz resolution at power levels as low as 1 nanowatt in 2 ms, or 100 nW in 20 microseconds. The AOS measures 60 such spectra consecutively, or at preset intervals, storing the data in computer memory for later study.

Some early data from the AOS is shown in figure 13 [4]. The signal from a magnetic probe at the edge of the plasma which has been processed by the AOS shows activity over a wide range of frequencies. The plasma frequency near the probe is between 2 and 3 GHz.

D. Profiles

Insight into the hot electron pressure profiles in Constance was provided by the visible light images of the plasma taken with a CCD television camera. Typical pictures are shown in figure 14. These figures show that, from the sides, the area of brightest intensity is c-shaped and the end view is that of four balls. The pictures are from one frame (30 ms)

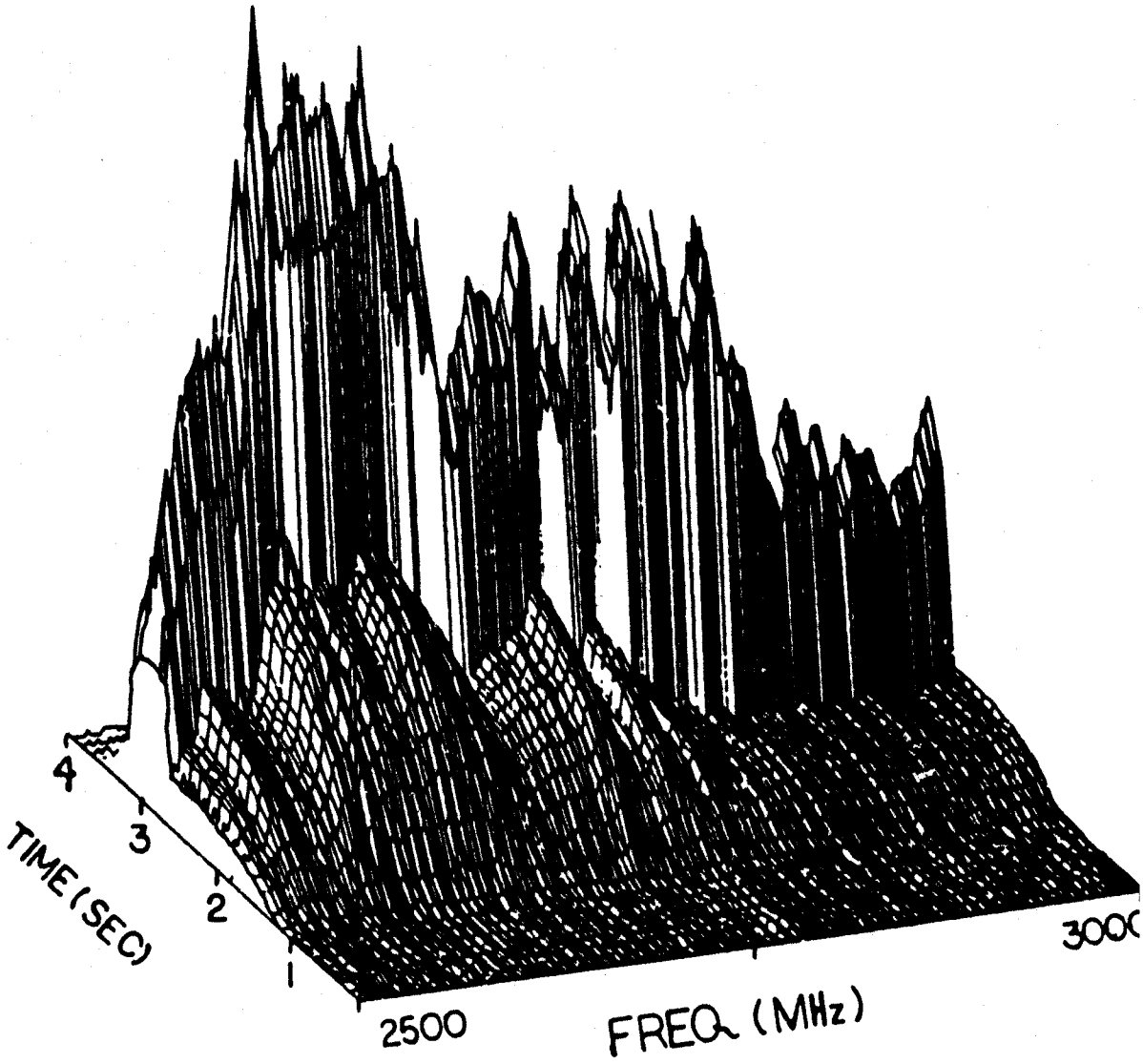

Fig. 13) Early results from the AOS show broadband rf generated by the hot electron plasma. The signal was coupled to the AOS receiver via a four turn b-dot probe 10 cm from the axis and 10 cm from the midplane. 600 W of ECRH at 11 GHz is applied 1 second into the shot. At 3 seconds the ECRH is turned off, resulting in a burst of emission.

CONSTANCE B PLASMA

Visible Light - ECRH off

(a)

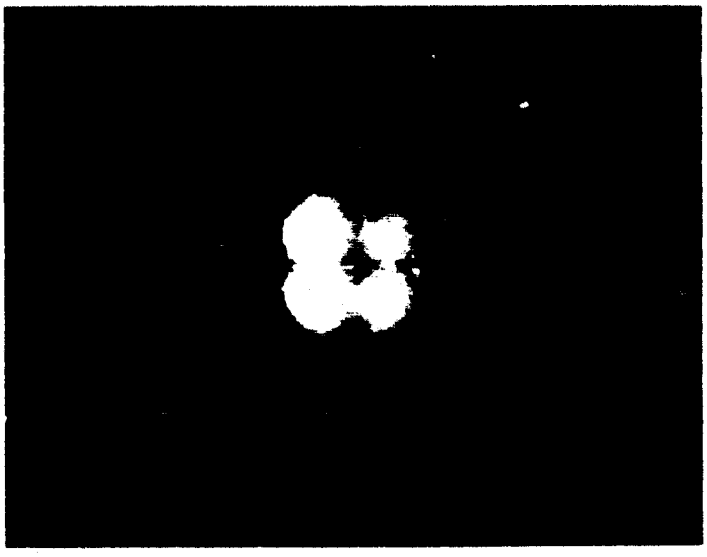

(b)

Fig. 14) Visible light images of the Constance B plasma taken over a 30 ms interval after the ECRH has been turned off. In the side view (a) the vertical fan is to the right and the vacuum ECRH resonance zone is near the edge of the image; (b) is the end view. The bright spots are x-rays which strike the CCD chip in the video camera.

taken after the ECRH is turned off. Note the absence of plasma on the center in the end view. The white spots are caused by x-rays which strike the CCD chip in the camera. From these pictures we believe that in three dimensions the bright area is shaped like a baseball seam (like the magnet). These patterns persist for fractions of a second after rf turn-off when there are only hot electrons, suggesting that the hot electrons are confined along the baseball curve. This trajectory is the drift surface for the deeply trapped electrons.

To lowest order electrons will drift on surfaces of constant J, where $J(\epsilon,\mu,\alpha,\beta)$ is the longitudinal invariant $J=\int v_{||} ds$, ϵ is the total energy, μ is the magnetic moment, and α and β are flux coordinates. To the extent that the confining geometry is long and thin, particles all drift on the same flux surface. Numerical computations [5] on a similar experiment, Baseball-II, show that at a radius of 10 cm the surfaces of a shallowly trapped particle and a deeply trapped particle are separated by approximately 1 cm. Thus within an error of 10% all the particles drift on the same surface, a property sometimes referred to as omnigenity. In Constance the error is in fact less than this since the plasma is not observed to extend to the mirror peak at R=2 but is typically confined to R<1.2. If all the particles drift on approximately the same flux surface we can investigate the nature of this surface by examining a particular class of particles, those electrons that are deeply trapped. The drift velocity of a deeply trapped particle is

$$v_{drift} = \frac{B \times \mu \nabla B}{m_e \omega_{ce} B}$$

Thus a particle drifts on a mod-B surface, which in Constance is a closed ellipsoidal surface. Since it remains a deeply trapped particle as it drifts, the particle must drift on a path on the mod-B surface along with the field lines are just tangent to this surface. In Constance this path has the shape of a baseball seam. Near the axis the baseball seam degenerates to a circle but because of the large curvatures in the Constance geometry at radii of 10 cm the baseball seam nature of the drift surface is quite pronounced.

The fact that the visible light pictures resemble a baseball seam from the side and that an end view shows little light from the axis suggests that the hot electrons in the afterglow peak at a flux surface off the axis. This is plausible since the heating due to the ECRH is stronger where the field gradients are weak. Thus particles on field lines which are nearly tangent to the resonant mod-B surface would be more strongly heated than particles on the axis since the axis field line and the resonant mod-B surface are perpendicular at the point that they intersect.

Calculations using model pressure profiles which have been line-integrated to simulate what is seen by the camera show that the profile must be peaked off the axis for the end view pictures to look like 4 balls. Figure 15 shows the comparison between the line-integral of profiles which are (a) flat, and (b) peaked off the axis. The ball-like structure only appears in the peaked off-axis, or hollow, profile. This has been verified over a wide class of profiles. Note that even for the flat profile the line-integrated end view is strongly peaked on the axis - so a profile which is peaked on the axis would have an even more strongly peaked end view.

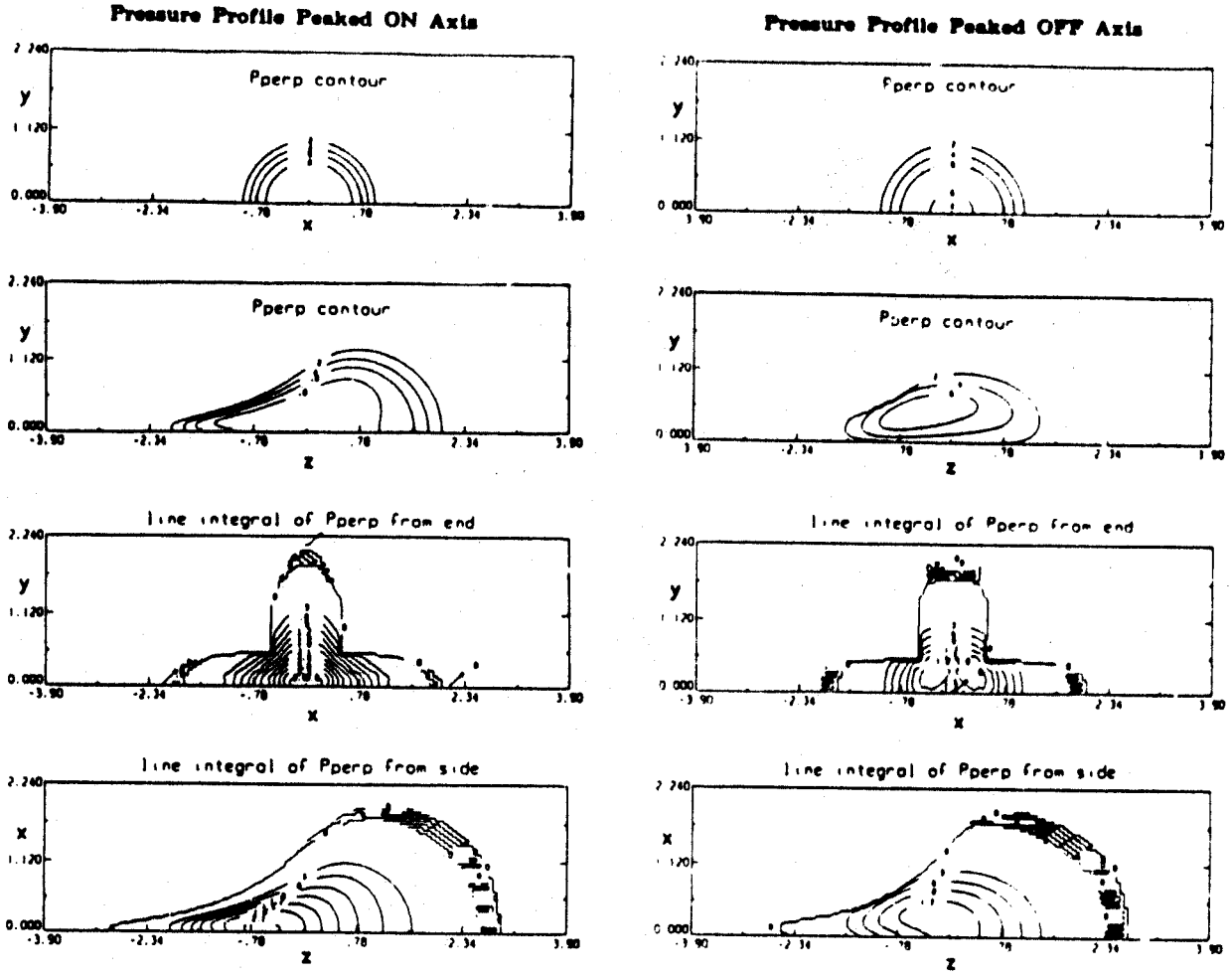

Fig. 15) Model calculations of the pressure profiles. The top two panels show cuts of the pressure profiles at the midplane and in the y-z plane for a case which is peaked off axis and a case which is peaked on axis. The lower 2 panels show the result of line integrating the profiles from the end and from the side in order to model what is seen by the TV camera.

The profile in fig. 15 which is peaked off the axis does not have quadrupole symmetry at the midplane. It is azimuthally symmetric at the midplane which is not consistent with the baseball seam model. Figure 16 shows the calculated profiles for a model which has midplane quadrupole symmetry. This model will be referred to as the drift, or baseball, model in future discussions.

Other diagnostics have corroborated the visible light images. X-ray pinhole photographs from the side also show a c-shaped plasma. The pictures are made using x-ray film which is exposed for approximately 8 shots. The fact that the c-shape is clear indicates that the shape is the same during most of the shot, since the film is integrating throughout the entire shot- i.e. during build-up and magnet ramp-down when the hot electrons hit the walls. The low energy cut-off of the x-rays which make the image is determined by the paper which covers the x-ray film, and this is not known. The vacuum window is aluminized Kimfoil, which transmits above 400 eV.

The 1/2 m Ebert visible light spectrometer was used to measure the radial H-alpha profile. The results are shown in figure 17 for a vertical scan at the midplane at the end of the ECRH pulse. The profile is hollow and the peak in the Abel-inverted profile occurs at approximately 2" in radius on the midplane which is similar to the region of maximum intensity on the CCD camera images of the plasma. Of course, the Abel inversion was done assuming cylindrical symmetry, which is incorrect for the Constance plasma, so agreement between the two may be merely fortuitous. The H-alpha emission is a function of the electron density and temperature profile, and the neutral profile. The electron contribution is due to the hot electrons

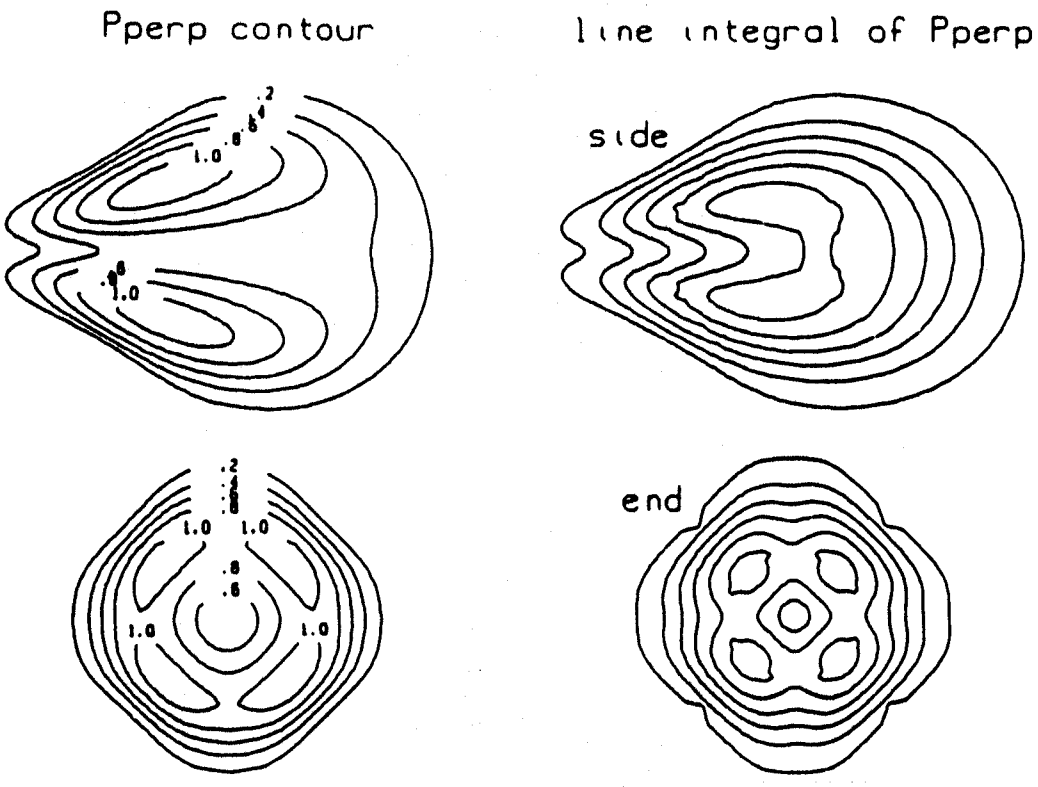

Fig. 16) Drift model pressure profile. The plots labelled P_{perp} contours are cuts at the midplane and in the y-z plane.

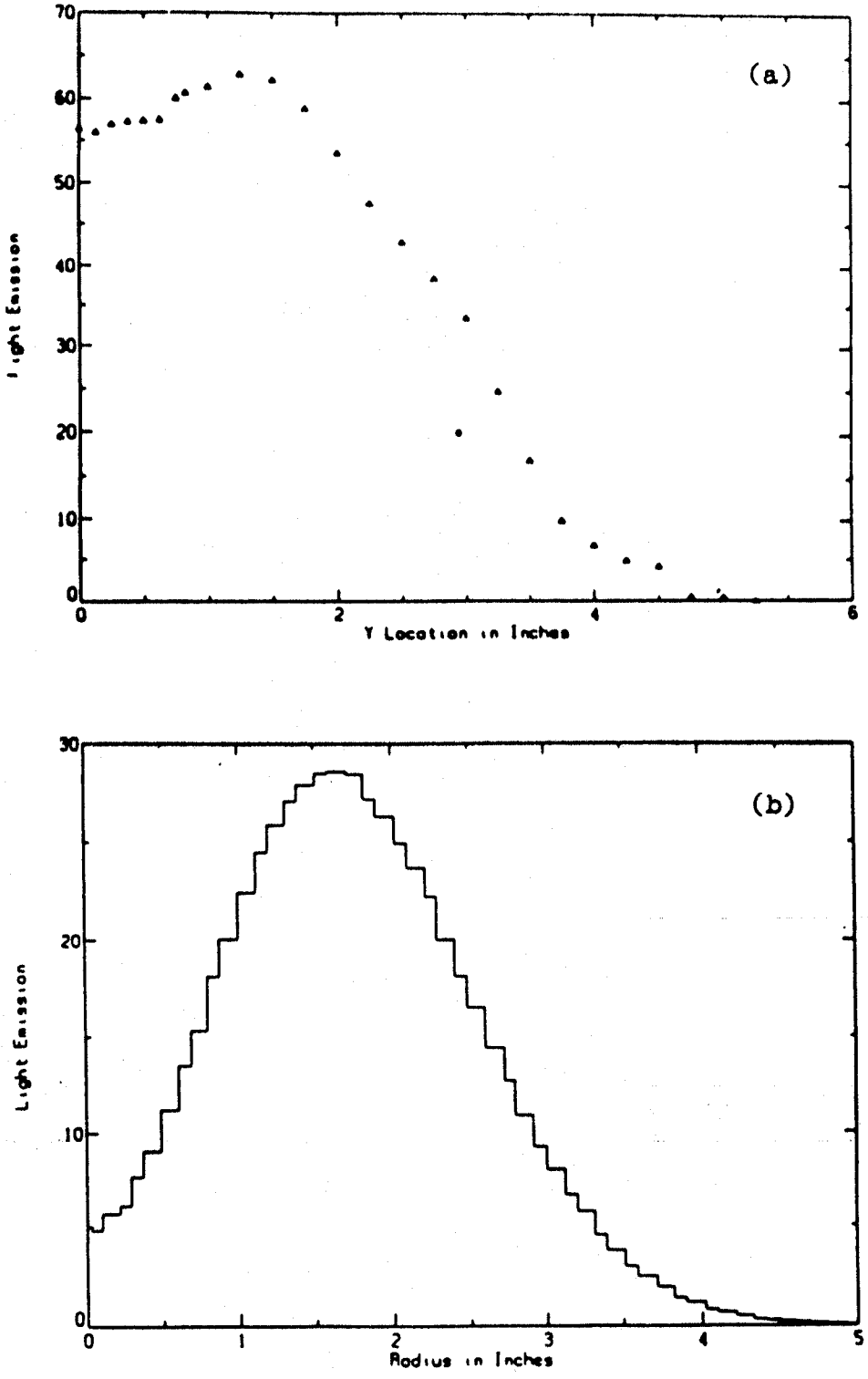

Fig. 17) Radial scan of the H-alpha intensity at the midplane during ECRH. The (a) raw data has been smoothed and Abel-inverted to get the result shown in (b). This vertical scan was taken for shot conditions of 3.2 kG, 1 kW, and 1×10^{-6} torr.

and the cold electrons, but since the cross-section is lower for the hot electrons we assume that most of the radiation is due to the cold electrons when the ECRH is on. This is verified by the behavior when the rf is turned off and the image intensity fades by factors of 3 to 5. The calculations of neutral penetration indicate that the plasma is transparent to neutrals for our parameters, so that neutrals are distributed uniformly throughout the plasma volume. This then implies that the cold electron density profile is hollow. Note that this suggests that the cold density will be higher than we have calculated because of the profile effects. Using the H-alpha profile shape as a model implies that a peak electron density near 10^{12} cm^{-3} can be present in Constance, under conditions where we measure the maximum line density. Axial measurements of the H-alpha profile have also been made and are shown in figure 18. Note that they show the axial asymmetry which is characteristic of the TV camera pictures.

Measurements of the axial variation of the hot electron temperature and the x-ray flux are shown in figure 19. The measurements covered the center third of the plasma, from R=1.2 on the thin side of the fan to R=1.2 on the thick side. Plasma conditions were 3.2 kG, 1 kW of ECRH and a neutral pressure of 5×10^{-7} torr. For these conditions the axial x-ray flux profile when the ECRH is on is the same as the H-alpha profile. This is to be expected if the main target is neutral hydrogen.

The axial x-ray profiles are in good agreement with predictions using a bi-Maxwellian distribution with an anisotropy, $T_{\perp}/T_{||}$, equal to five. Poor agreement is obtained when an isotropic Maxwellian or a loss cone

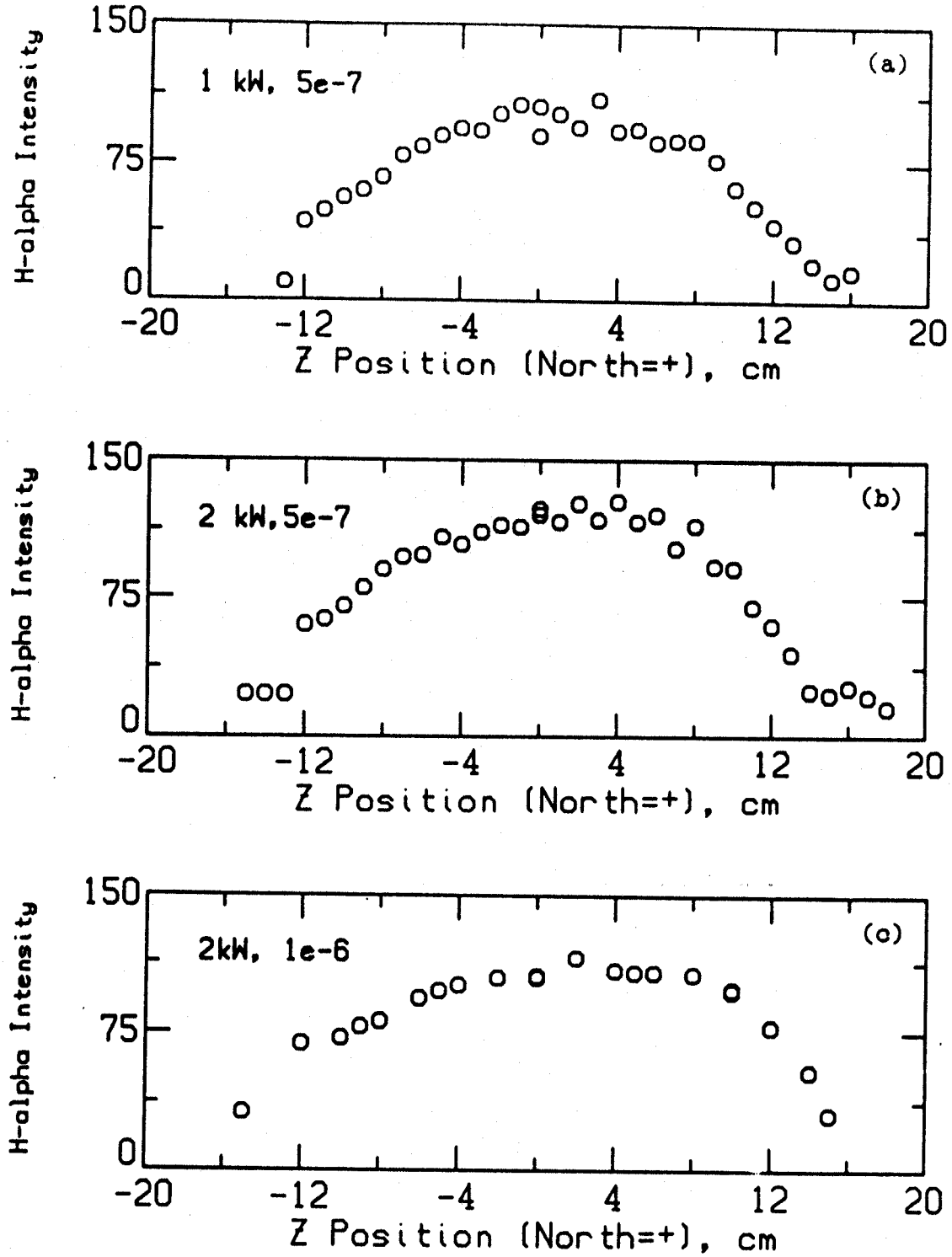

Fig. 18) Axial scan of the H-alpha intensity at y=0 for three different plasma conditions during ECRH. The axial asymmetry is consistent with the TV camera pictures. B = 3.2 kG.

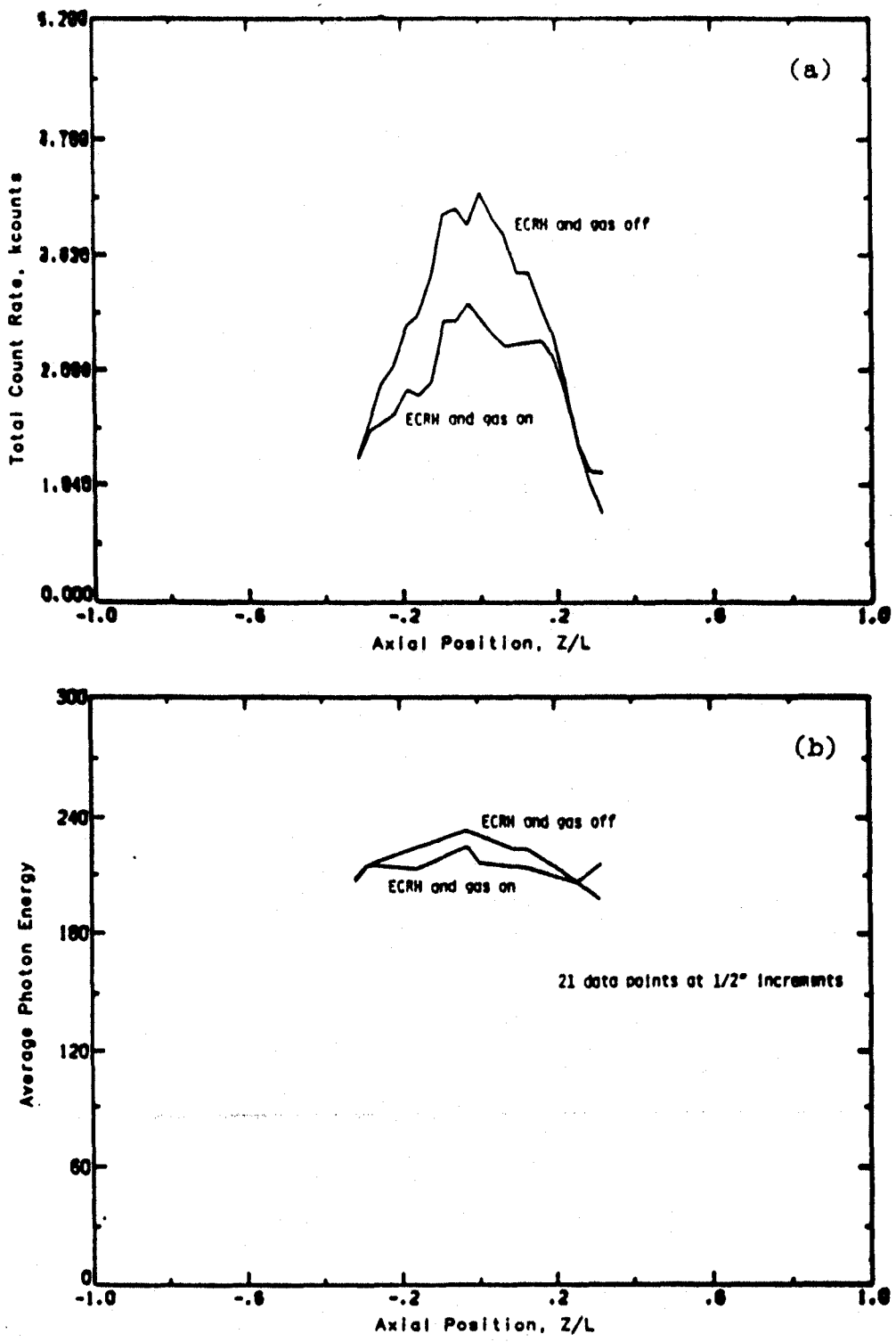

Fig. 19) Axial scan of the (a) x-ray flux and the (b) average photon energy for 3.2 kG, 1 kW, 5×10^{-7} torr plasma conditions.

distribution function is used. For a pure Maxwellian, the profile would be strongly peaked to the south, since it goes as the chord length, and a loss cone profile would be flatter than the data.

Figures 20 and 21 show the radial measurements of the x-ray flux and the hot electron temperature at 5 positions on the midplane at 2 different neutral pressures. This is the raw, uninverted data. Note that the temperature is approximately flat across the plasma and that the line-integrated flux can appear hollow or peaked depending on the neutral pressure.

Skimmer probes have been inserted to the axis at the axial position which corresponds to the opening in the baseball "c". This can be done without affecting the measured diamagnetism or density, verifying that there are no hot electrons at this position. However the probe must be very thoroughly cleaned - usually by putting it into the plasma for several shots - or the diamagnetism will be affected.

We note that the initial theoretical analysis of this hollow configuration suggests that it should be unstable to hot electron interchange modes fluting inward. The observed long term stability is therefore of great interest. In addition, we note that the equilibrium cannot be described as was first anticipated by a simple P(B) pressure function. To the extent that the particles all drift on the same flux surface the pressure can be modelled by a pressure profile which is function of B and flux surface with the condition that the flux surface is also a drift surface. In general the pressure must be derived from a microscopic distribution function $F(\epsilon, \mu, J)$.

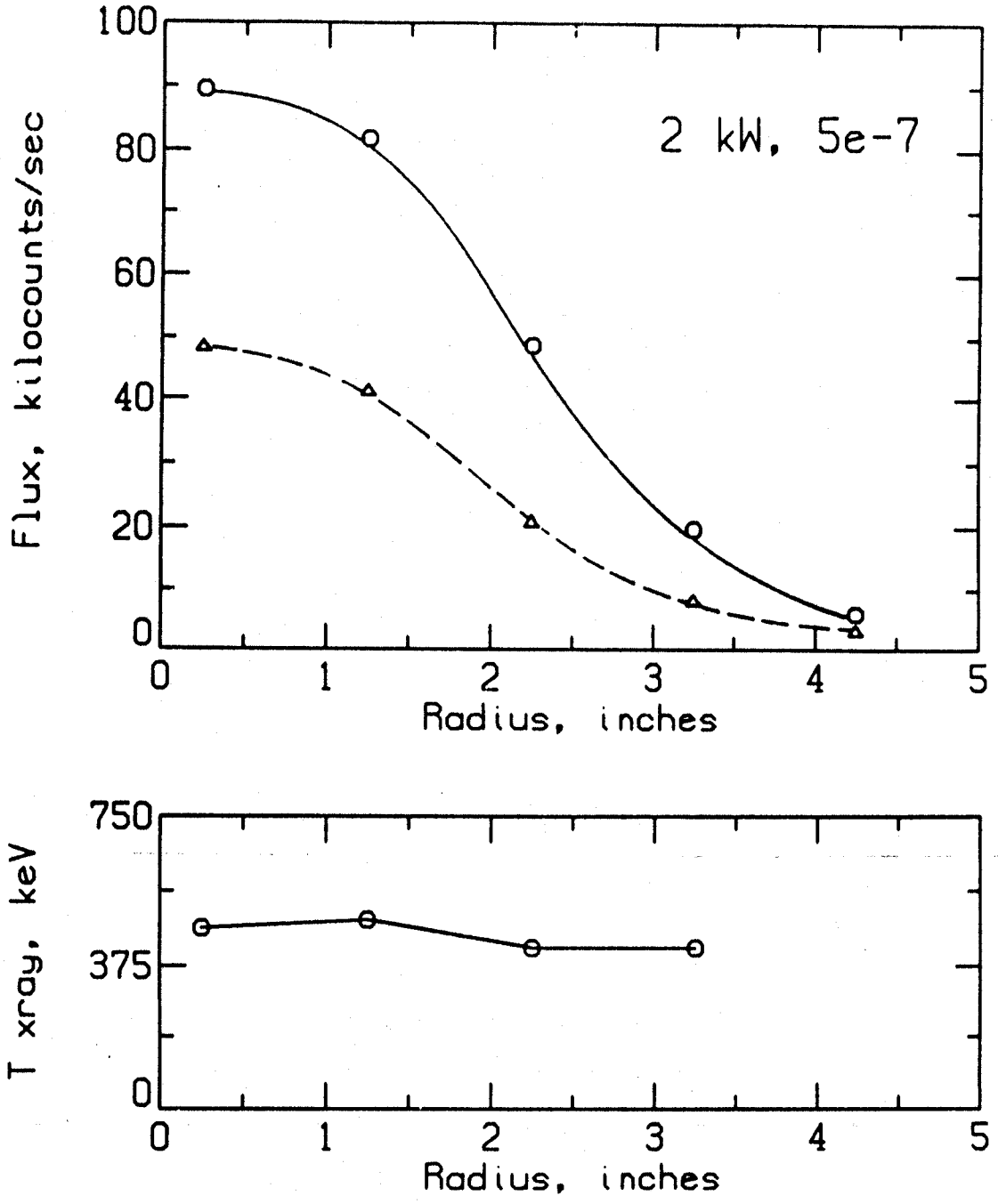

Fig. 20) Radial midplane scan of the x-ray flux and temperature for 3.2 kG, 2 kW, and 5×10^{-7}torr. The data is summed for the first 50 ms following rf turn-off. The 3" × 3" NaI detector was used. The triangle data is the counts between 100 and 1500 keV, and the circles are for all counts in the spectrum. The data has not been inverted.

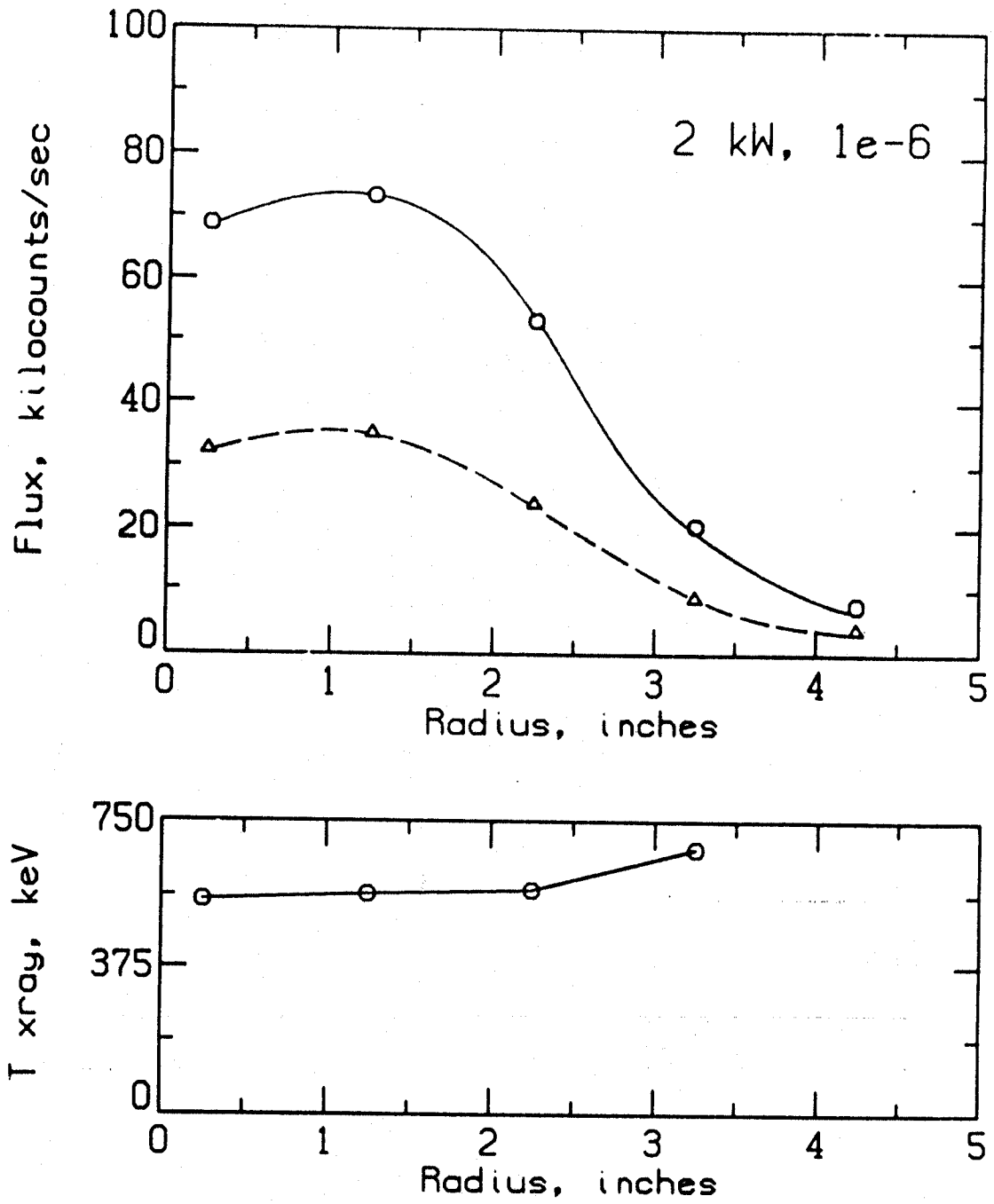

Fig. 21) Radial midplane scan of the x-ray flux and temperature for 3.2 kG, 2 kW, and 1 x 10^{-6} torr. The data is summed for the first 50 ms following rf turn-off. The 3" x 3" NaI detector was used. The triangle data is the counts between 100 and 1500 keV, and the circles are for all counts in the spectrum. The data has not been inverted.

e further note that the non-omnigenity of particles combined with the ECRH hich changes particle pitch angles has implications for hot electron ransport which have not to our knowledge been explored.

Scaling Studies

The plasma parameters in Constance B shown in Table 1 can change ignificantly with changes in the neutral pressure, the microwave power evel, and the magnetic field. The scaling results to date are presented in his section.

Some of the observations from the neutral pressure scaling studies are: (1) MHD stable hot electron plasmas are obtained over a wide range of neutral pressures - from 10^{-7} torr to 5×10^{-5} torr of hydrogen, (2) optimum hot electron parameters occur near 10^{-6} torr, and (3) the cold electron density increases with pressure. The data is shown in figures 22 through 24. This type of detailed data will be used to understand the particle and power balance in the machine. There are also indications that changes in the equilibrium occur as a function of neutral pressure.

The ECRH power scaling data shows that under most operating conditions the plasma stored energy saturates when the microwave power is increased above about 1.2 kW (fig. 25a). This is apparently due to a drop in the achieved hot electron temperature (fig. 26a). The hot density also saturates (fig. 26b), as does the microinstability-induced rf emission One

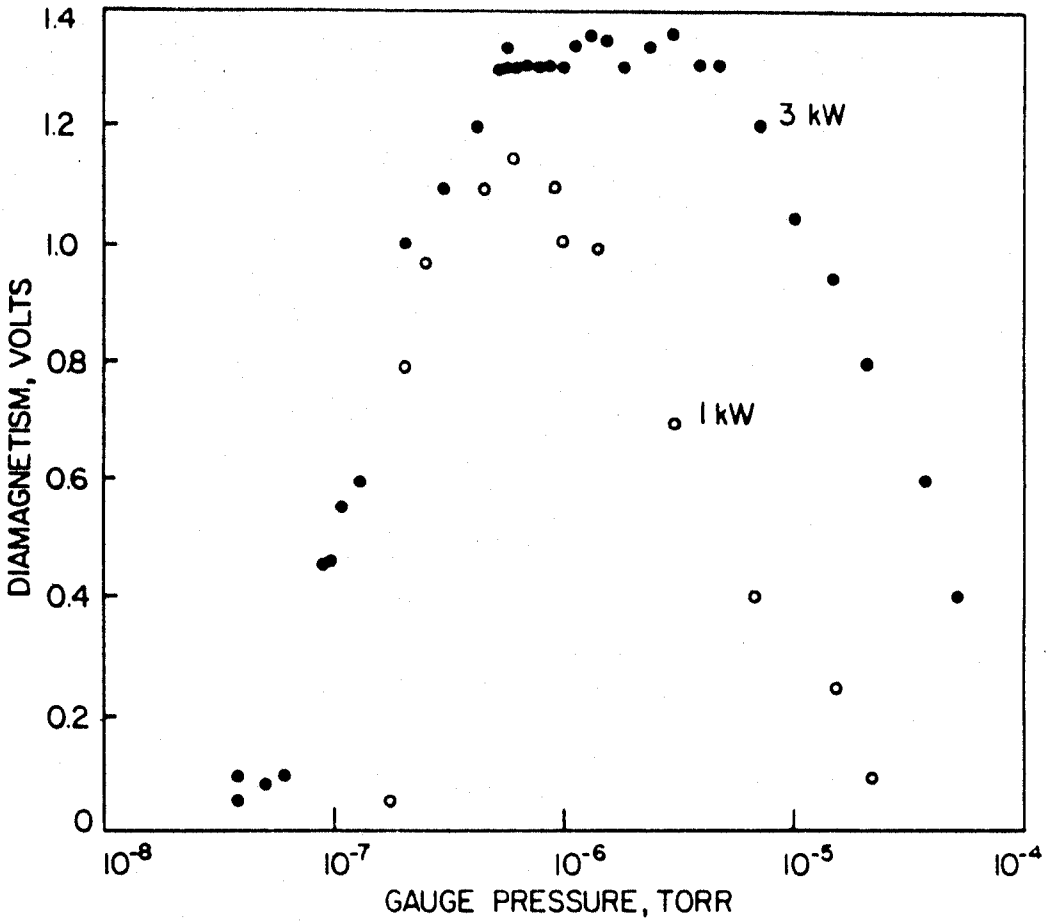

Fig. 22) Diamagnetism as a function of pressure. In this plot, the pressure read on the Bayard-Alpert gauge has been used. B=3 KG.

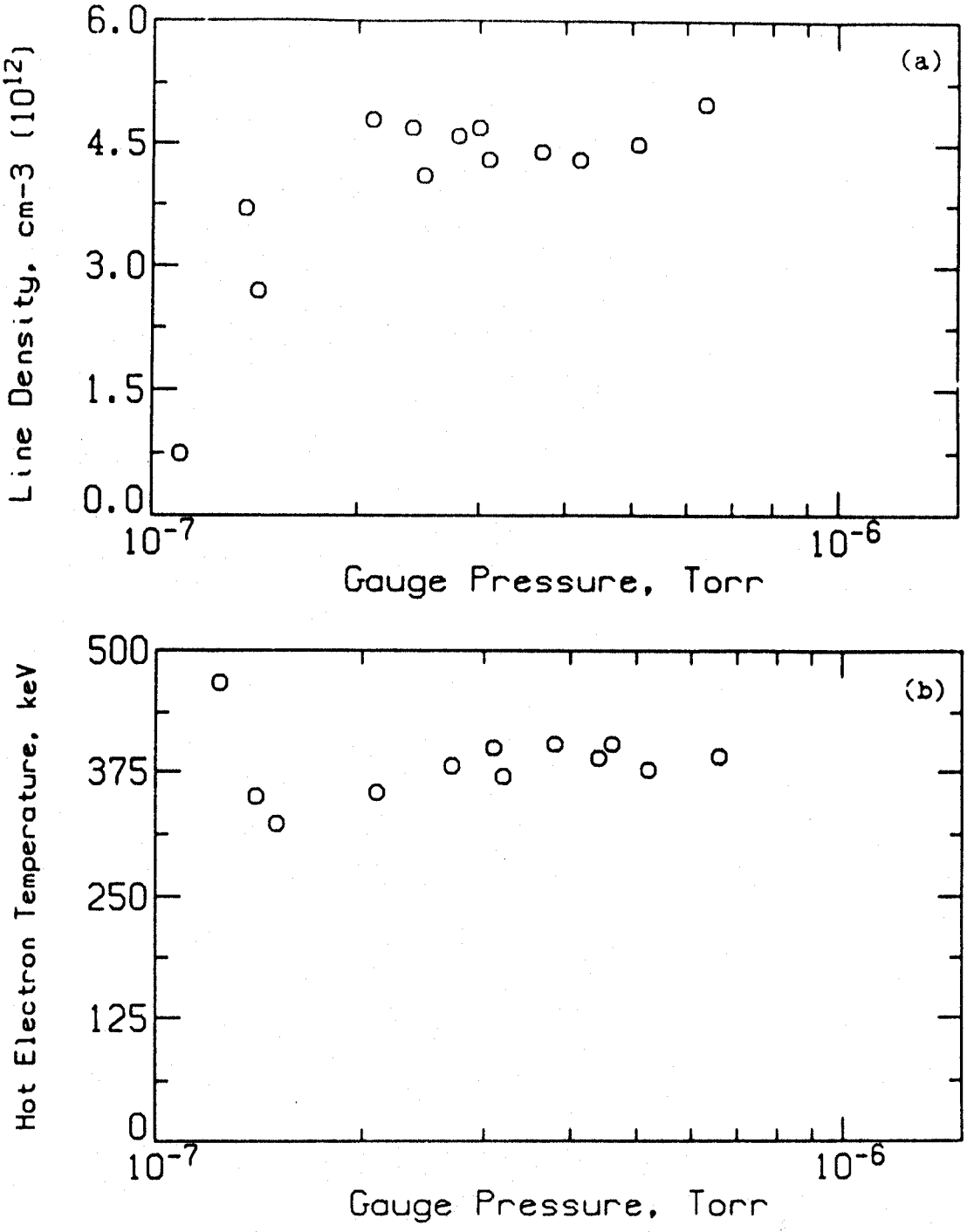

Fig. 23) Variation of the electron density and the x-ray temperature with neutral pressure for plasma conditions of 3 kG and 3 kW.

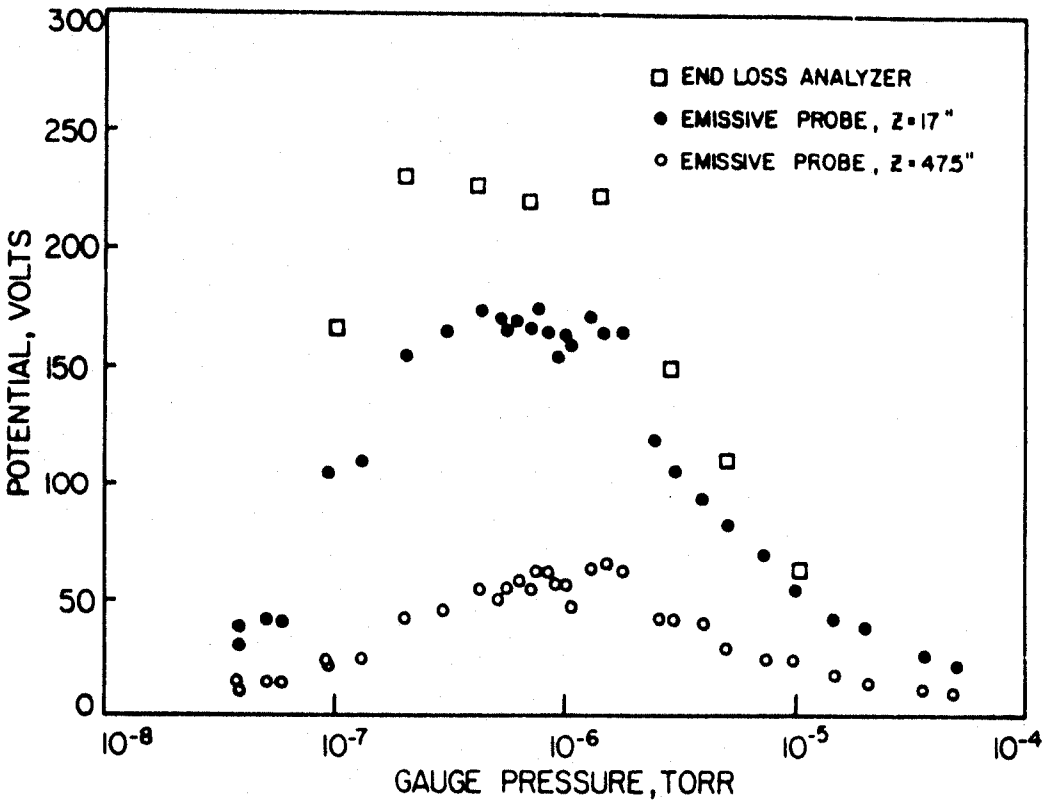

Fig. 24) Potential as a function of neutral pressure. In this plot, the pressure on the Bayard-Alpert gauge has been used.

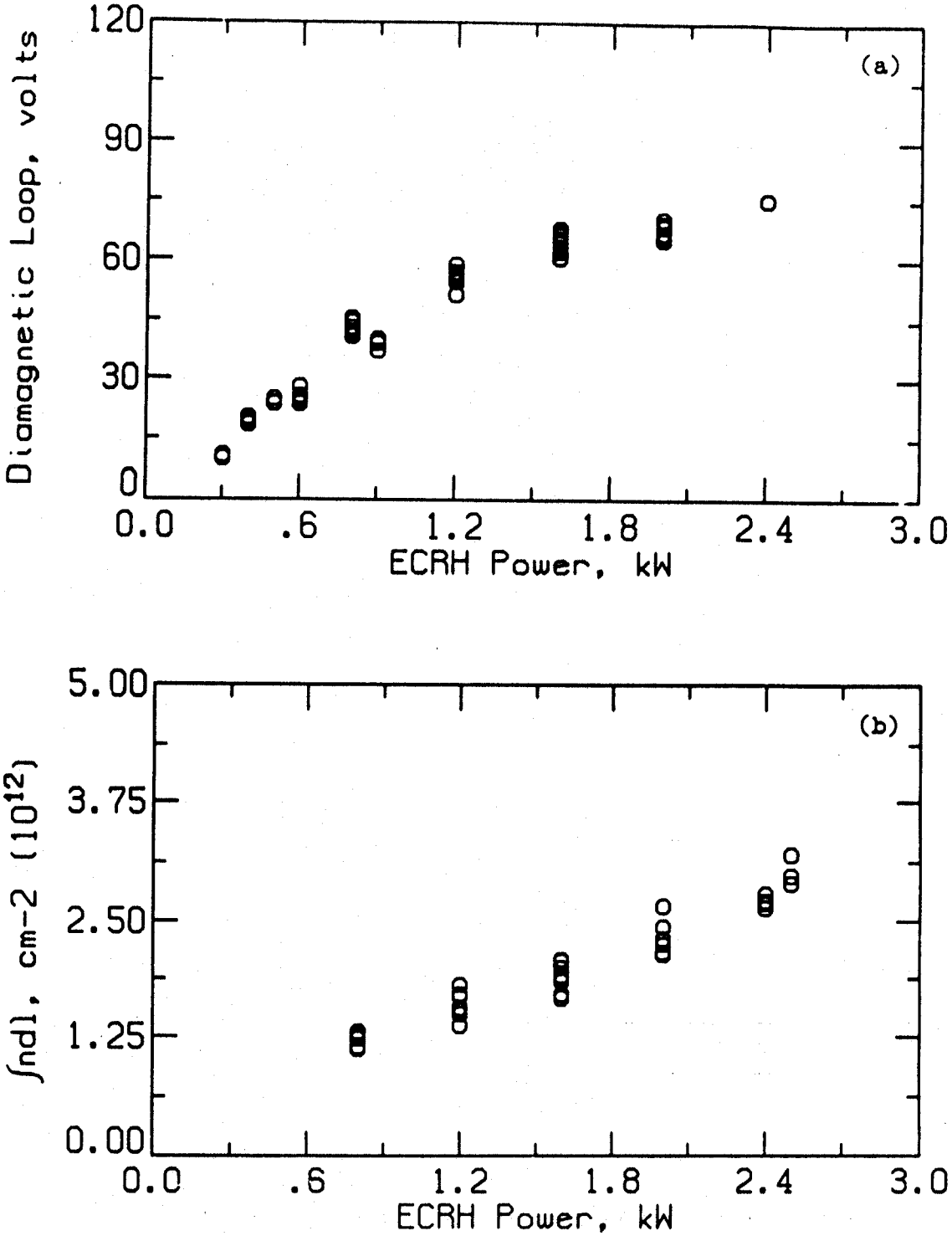

Fig. 25) (a)Variation of the diamagnetic loop voltage and (b) line density measured with the interferometer with ECRH power for 3 kG and 4 × 10^{-7}torr plasmas.

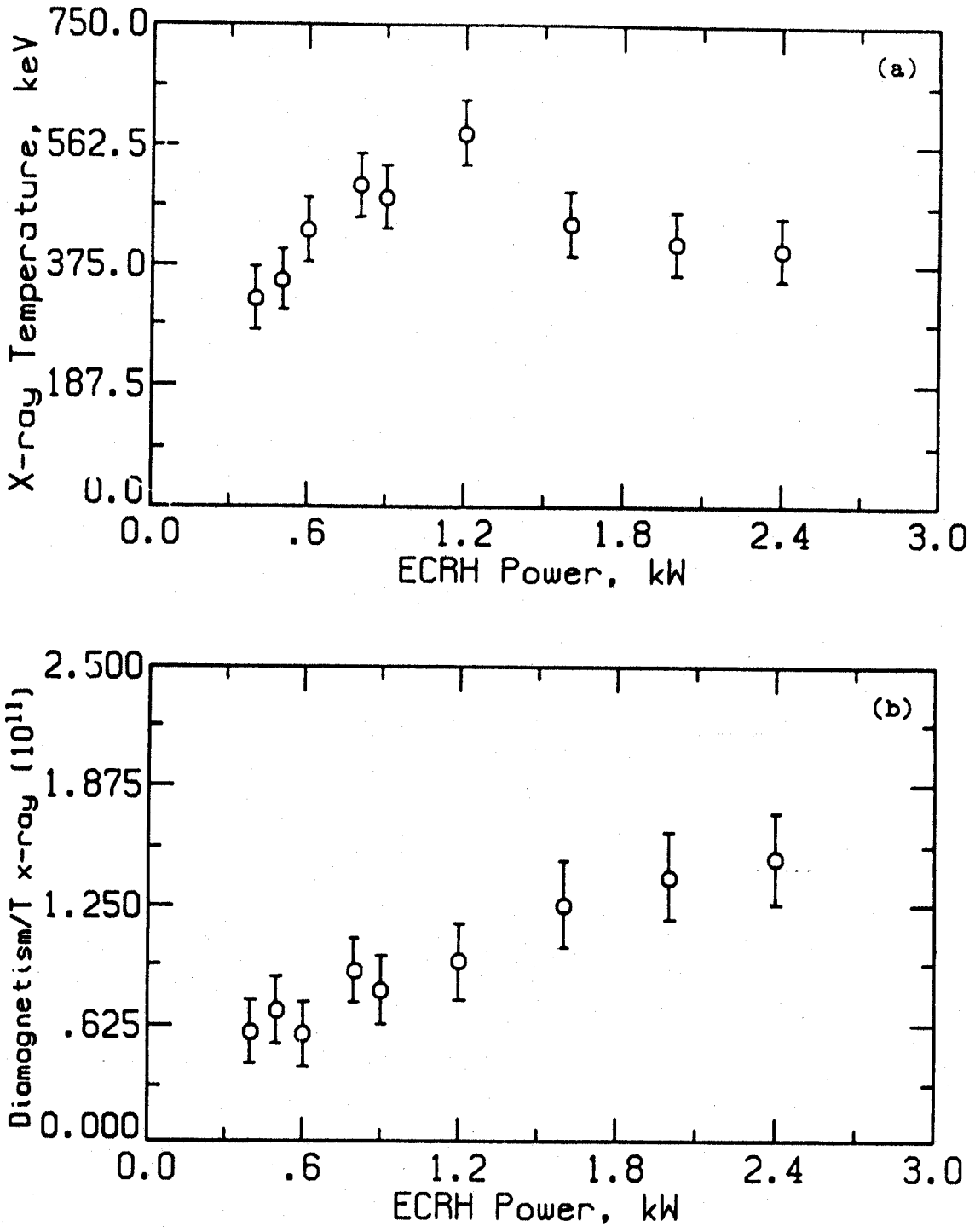

Fig. 26) Variation of (a) hot electron temperature and (b) "nhot" with ECRH power for B=3 kG, p= 4×10^{-7}torr. The hot electron temperature is measured at rf turn-off with the 2" × 2" NaI detector.

parameter which continues to rise above this ECRH power is the level of cavity microwave emission (fig. 27b). Therefore we postulate that this indicates a decrease in the strength of the ECRH absorption by the plasma. This hypothesis is supported by the cavity power signal and the reflected power as a function of time during a single shot (fig. 28). It can be seen that the cavity power signal increases when the diamagnetism begins to saturate. However, in general the cavity power is not a reproducible enough measure of the ECRH absorption.

According to our calculations, the change in density is not sufficient to cause such a large change in the ECRH absorption. However given the apparent strong profile effects it may be that somewhere in the plasma cutoff density for the ECRH is being approached and so the absorption goes down. Also since the x-ray temperature is measured on the midplane it may be that the temperature in the baseball seam is still increasing. This will be investigated using a vertical array of NaI detectors. Once we have a better understanding of the density and temperature profiles in the plasma we may be able to explain the saturation effects which are observed.

The decay time of the diagmagnetic loop signal as a function of neutral pressure is shown in figure 29. Because the hot electron temperature does not change rapidly after the ECRH is turned off, the decay of the diagmagnetism is essentially due to the change in the hot electron density. Hot electrons are collisionally lost via pitch angle scattering on ions and neutrals. The decay rate will have two slopes. It will initally be fast because of the presence of the cold electrons and their ions. After they scatter out (within ~ 100 ms), the hot electron scattering is reduced and

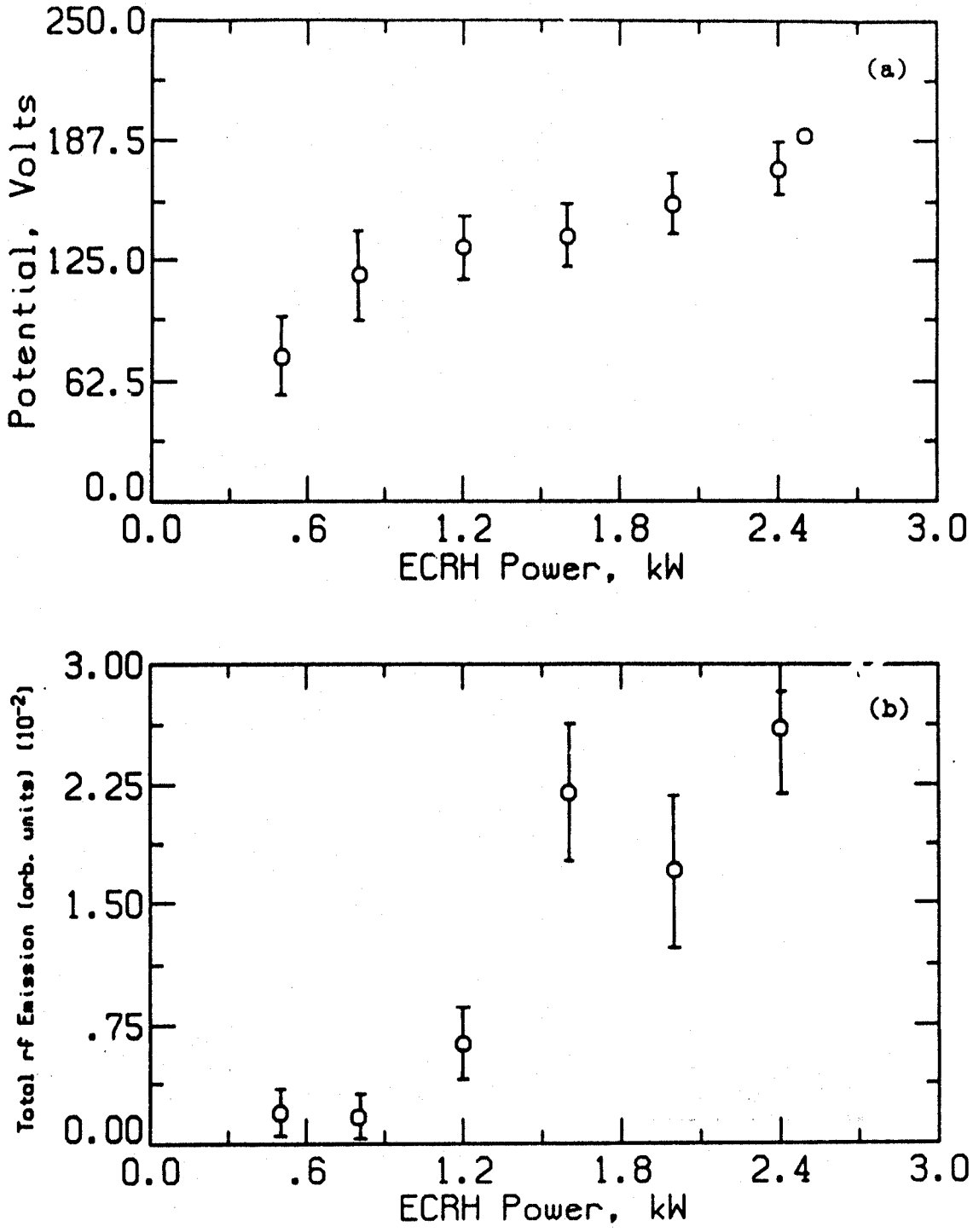

Fig. 27) The variation of (a) the potential measured by the endloss analyzer and (b) the cavity power with ECRH power is shown. Note that the cavitv power increases significantly above 1.2 kW.

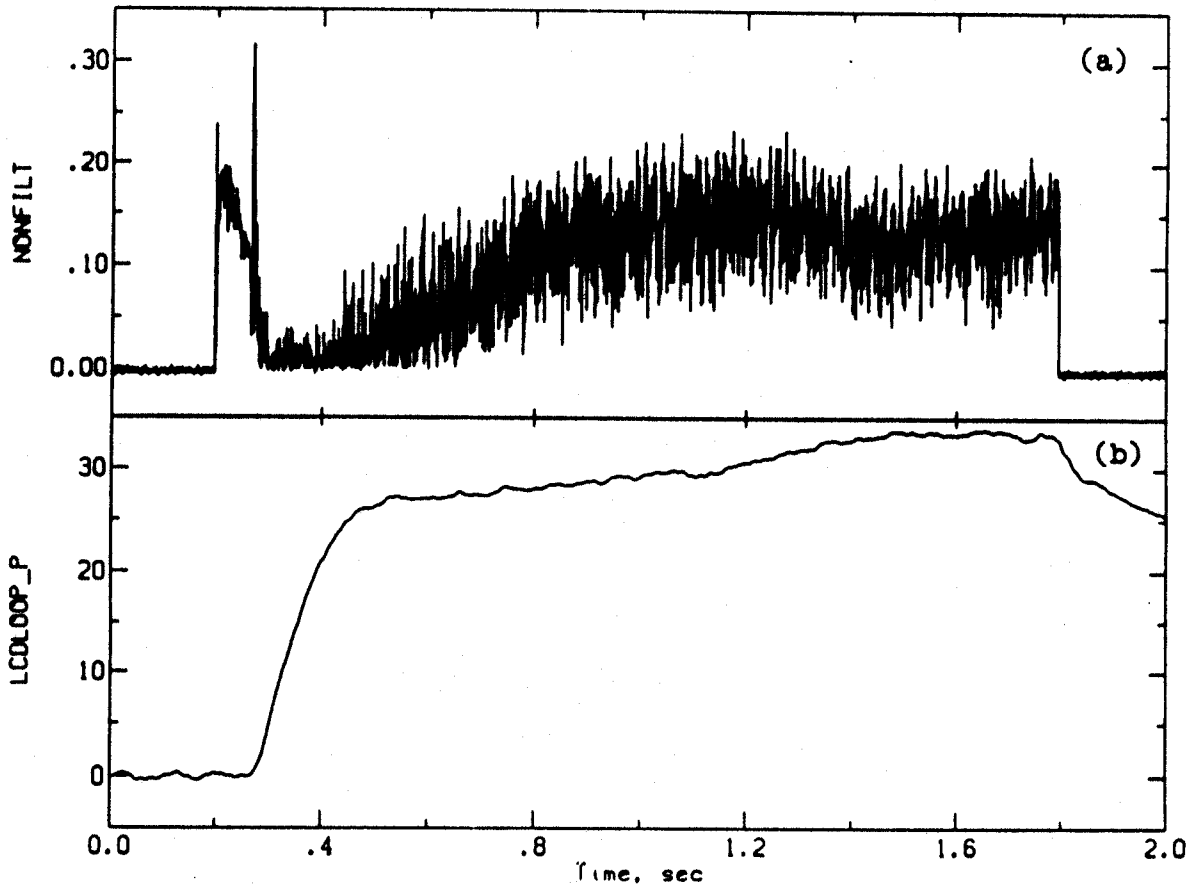

Fig. 28) (a) The cavity power and (b) the diamagnetic loop signal as a function of time during a shot. Note that the cavity power is low as the plasma is building up. When the diamagnetism begins to saturate, the cavity power begins to rise. A second rise in diamagnetism beginning about 1.2 seconds coincides with a drop in cavity power.

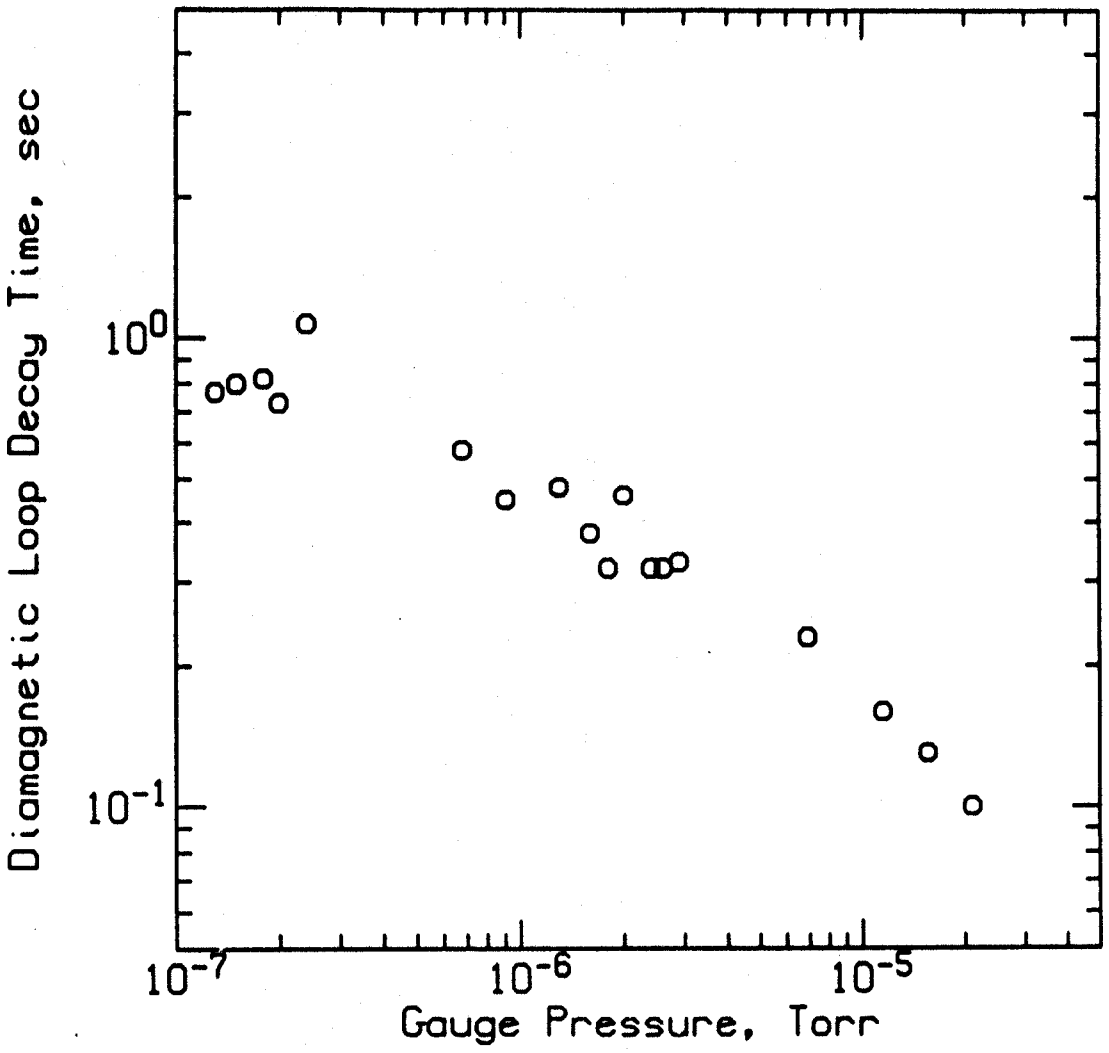

Fig. 29) Diamagnetic loop decay time as a function of neutral pressure. B=3 kG.

the decay time is longer. Notice that at neutral pressures $\geq 3 \times 10^{-6}$ torr (H_2) the neutral density becomes comparable to the ion density. Using Te_h = 450 keV and $n_i = n_{eh} + n_{ec} = 4 \times 10^{11}$ cm^{-3} the calculated collisional scattering time is 2.2 sec. However, this calculation assumed $Z_{eff} = 1$ and section L will show that $Z_{eff} = 1.26$(at 5×10^{-7}torr), which brings the decay time down to 1.4 seconds, which is in reasonable agreement with the data.

An interesting, but confounding, feature of the plasma was discovered in the course of a detailed pressure scan. It was found that given sufficient ECRH power (typically > 2kW), over a very narrow range in neutral pressure, the diamagnetic loop signal will continue to rise throughout the ECRH pulse, instead of saturating as discussed previously. Typical examples are shown in figure 30. We now believe that the increase in the signal is not due to additional beta but instead the result of high frequency fluctuations (>100 kHz). These fluctuations can be integrated along with the equilibrium diagmagnetic flux when a certain type of our integrators is used. It also appears that a change in the plasma size occurs at this particular gas pressure. From the TV camera we see that plasma is hitting the diamagnetic loop and causing it to glow in one spot. At pressures above or below the critical pressure, no glow is observed. The baseball equilibrium is seen at both lower and higher pressures.

Figure 31 shows the variation of the diamagnetic loop signal and the line density with magnetic field. Note that the plasma size is changing

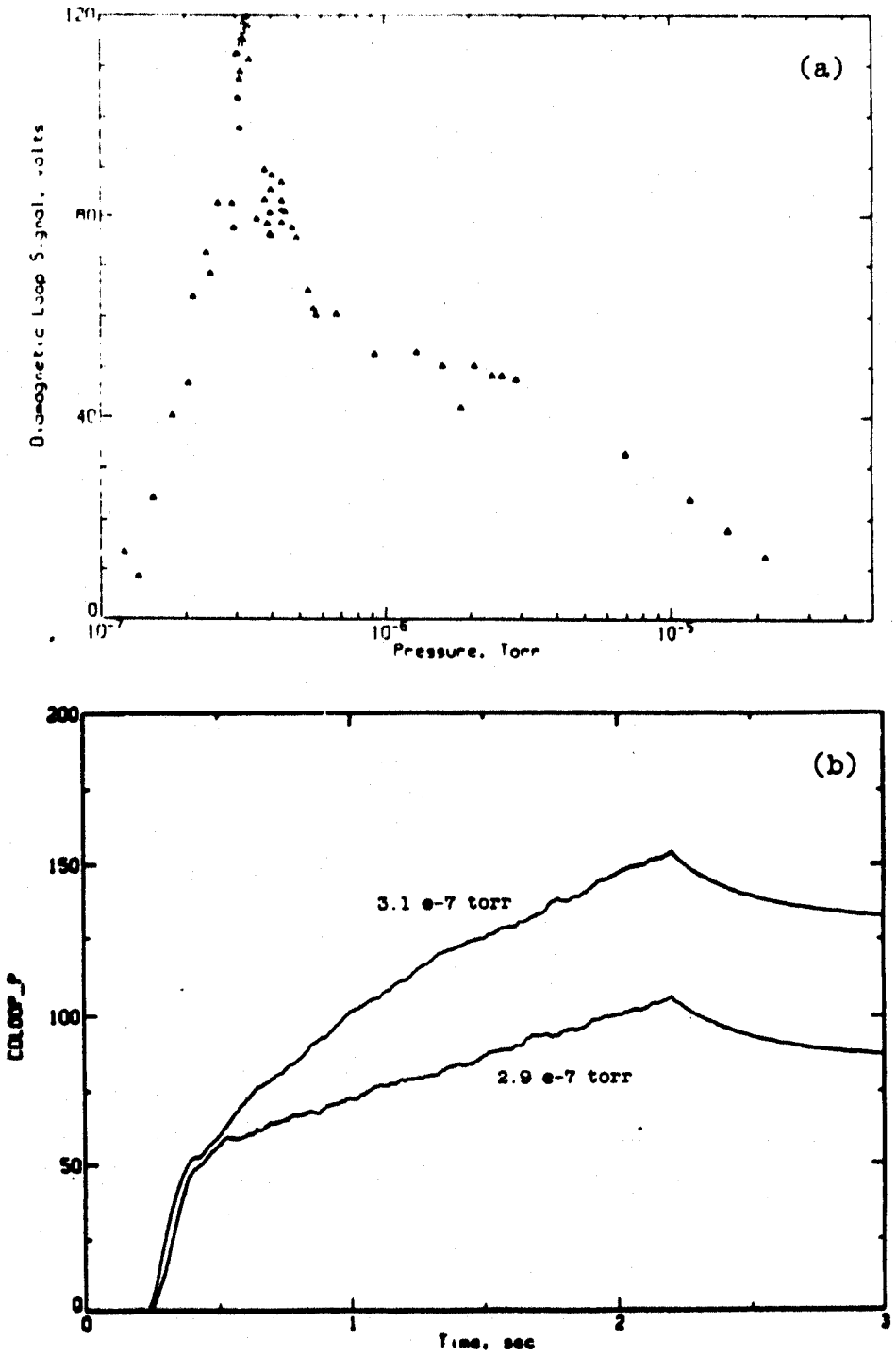

Fig. 30) (a) Diamagnetic loop voltage at t=1 sec. for a detailed pressure scan when the integrators with input filters are used. (b) A 5% change in the neutral pressure leads to a 50% change in the diamagnetic loop signal.

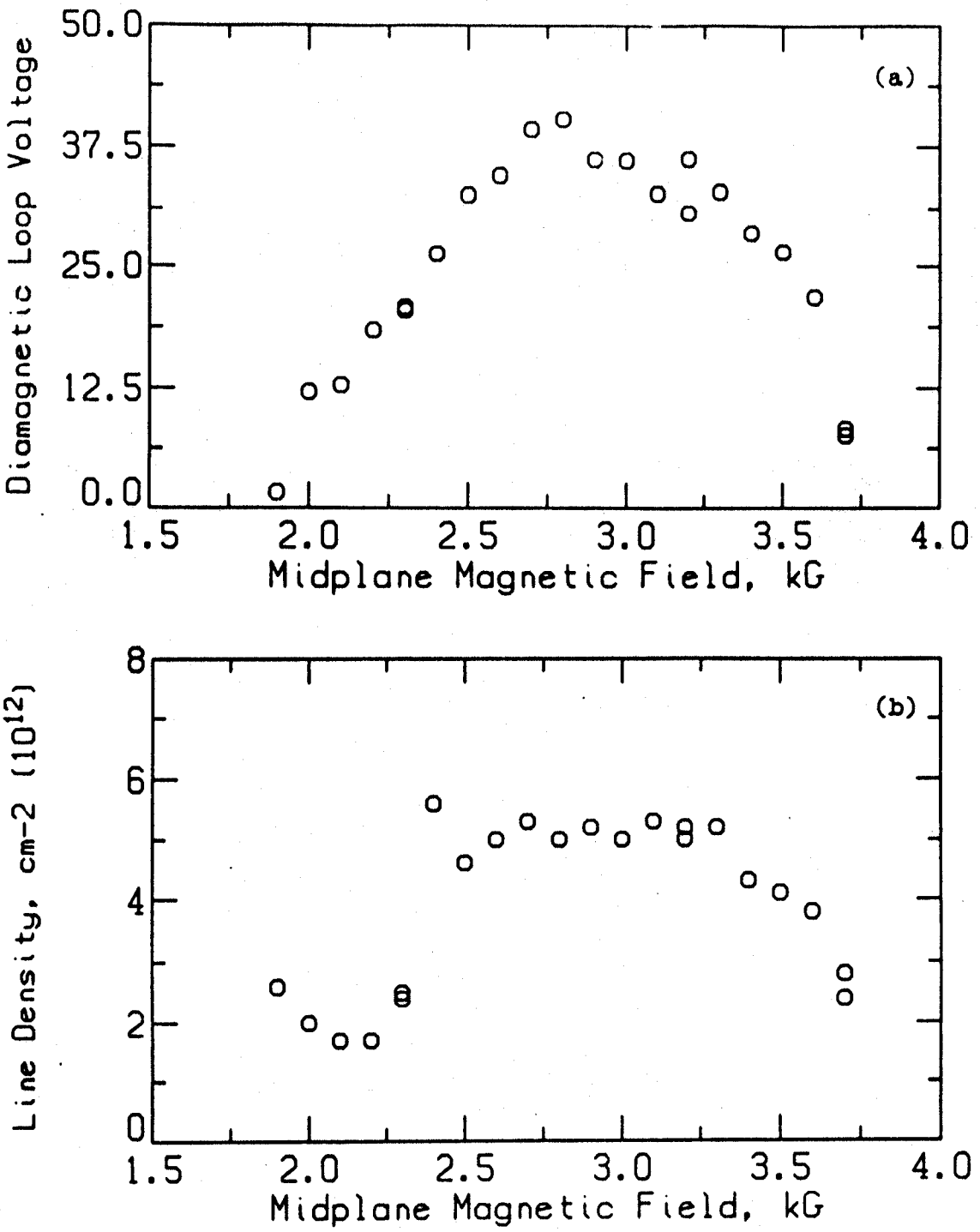

31) (a) Diamagnetic loop signal and (b) interferometer line density as a function of magnetic field. P=4 kW and $P_o = 1 \times 10^{-6}$ torr.

magnetic field and these values are not directly proportional to beta or density. Plasmas cannot be created when the fundamental or the second harmonic ECRH resonance is at the midplane.

F. Electron Microinstability

Studies of electron microinstabilities in Constance are described in detail in reference 6. Two types of microinstability emission are observed in Constance B. Dispersion relation calculations identify both as being due to the whistler instability. Whistler B emission occurs in regular bursts which correlate with bursts of ion and electron endloss, and with diamagnetism and potential fluctuations (fig.32). The rf emission occurs in a band of frequencies below the midplane cyclotron frequency. The whistler C emission occurs continuously in time and is associated with continuous enhanced electron endloss. The frequency range of the whistler C emission extends from approximately the upper frequency bound of the whistler B emission up to the ECRH frequency (10.5 GHz).

The whistler C emission is associated with the off-axis field lines and the whistler B emission is associated with all field lines. The whistler C emission occurs at higher frequencies because the density is higher on the outer field lines. The burst rate of the whistler C emission is much greater than the whistler B emission burst rate because the heating rate increases for increasing radial distance from the axis, due to the decrease in the magnetic field gradients.

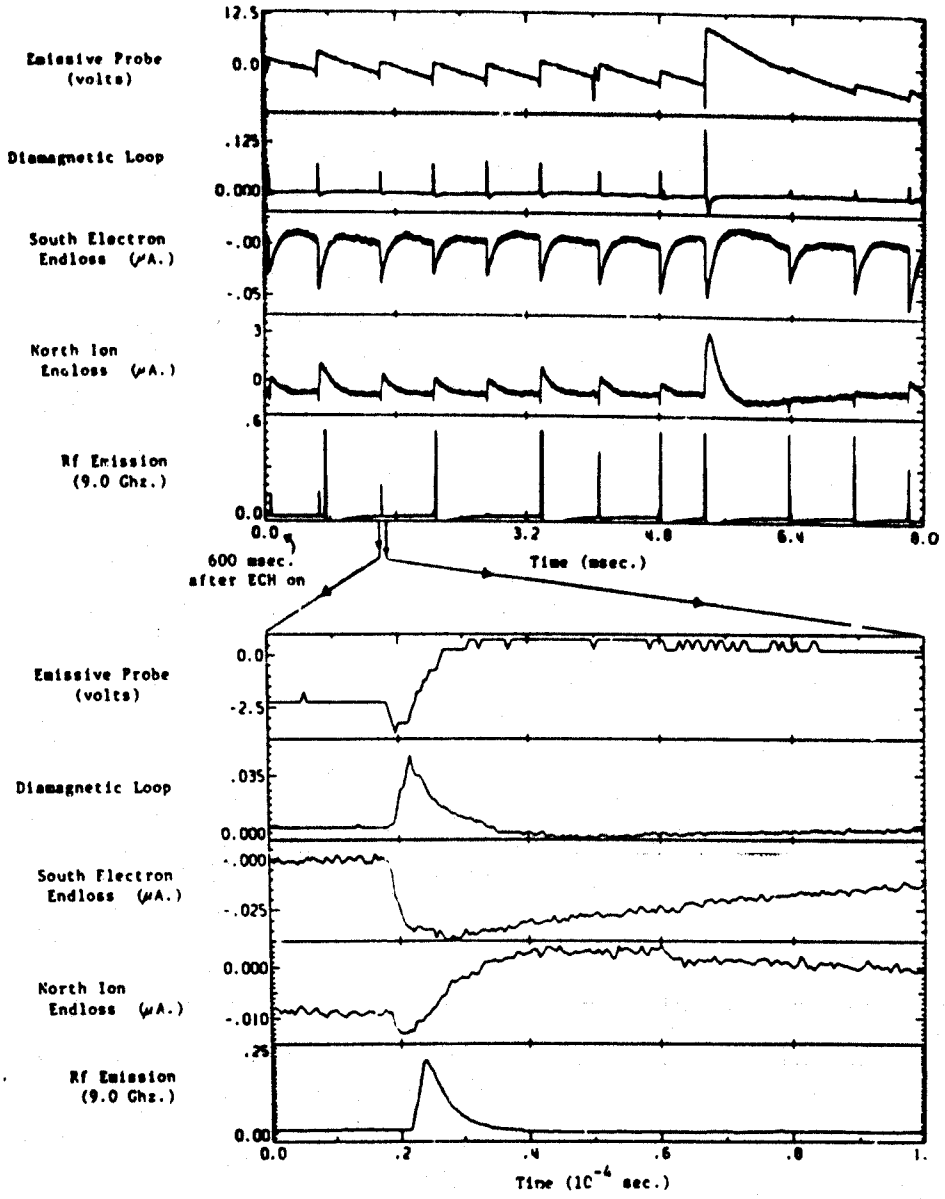

Fig. 32) Bursting nature which characterizes the whistler microinstability in the Constance B plasma. The top set of plots show the bursts over an 8 ms time window, and the plots below show one particular burst on a faster time scale.

Experimental observations and theoretical calculations indicate that the microinstabilities in the Constance B plasma are driven primarily by the low energy, magnetically trapped electrons with energies in the 1-5 keV range. Electrons of energies greater than 100 keV form a quiescent background which have little effect on the instability. The following experimental evidence supports these conclusions:

1) The unstable emission remains constant throughout the entire shot, starting a few hundred microseconds after gas breakdown and continuing until a few milliseconds after the ECRH is turned off even though the hot electron temperature and the diamagnetism are increasing with time.

2) The variation of the unstable emission power with gas pressure is different from the scaling of the diamagnetism with pressure (fig. 33).

3) Greater than 99% of the electrons which are lost axially as a result of the microinstability have energies less than 5 keV and have an effective temperature of approximately 2 keV. This is independent of the time in a shot.

4) During shots where the neutral gas is allowed to decay while the ECRH is left on, a plasma which is primarily composed of hot electrons is formed. During such shots the unstable rf emission and microinstability induced endloss cease at some point during the decay of the neutral gas pressure, when new, ECRH created plasma is no longer being formed at such a high rate (fig. 34).

Theoretical calculations have identified both instabilities as Whistler instabilities [6]. To model the plasma, an analytical approximation of a Fokker-Planck type distribution was used in a relativistic Vlasov dispersion relation calculation. This distribution resembles the solutions of the Fokker-Planck codes which calculate the electron distribution function in the presence of ECRH heating. The frequency regime in which the

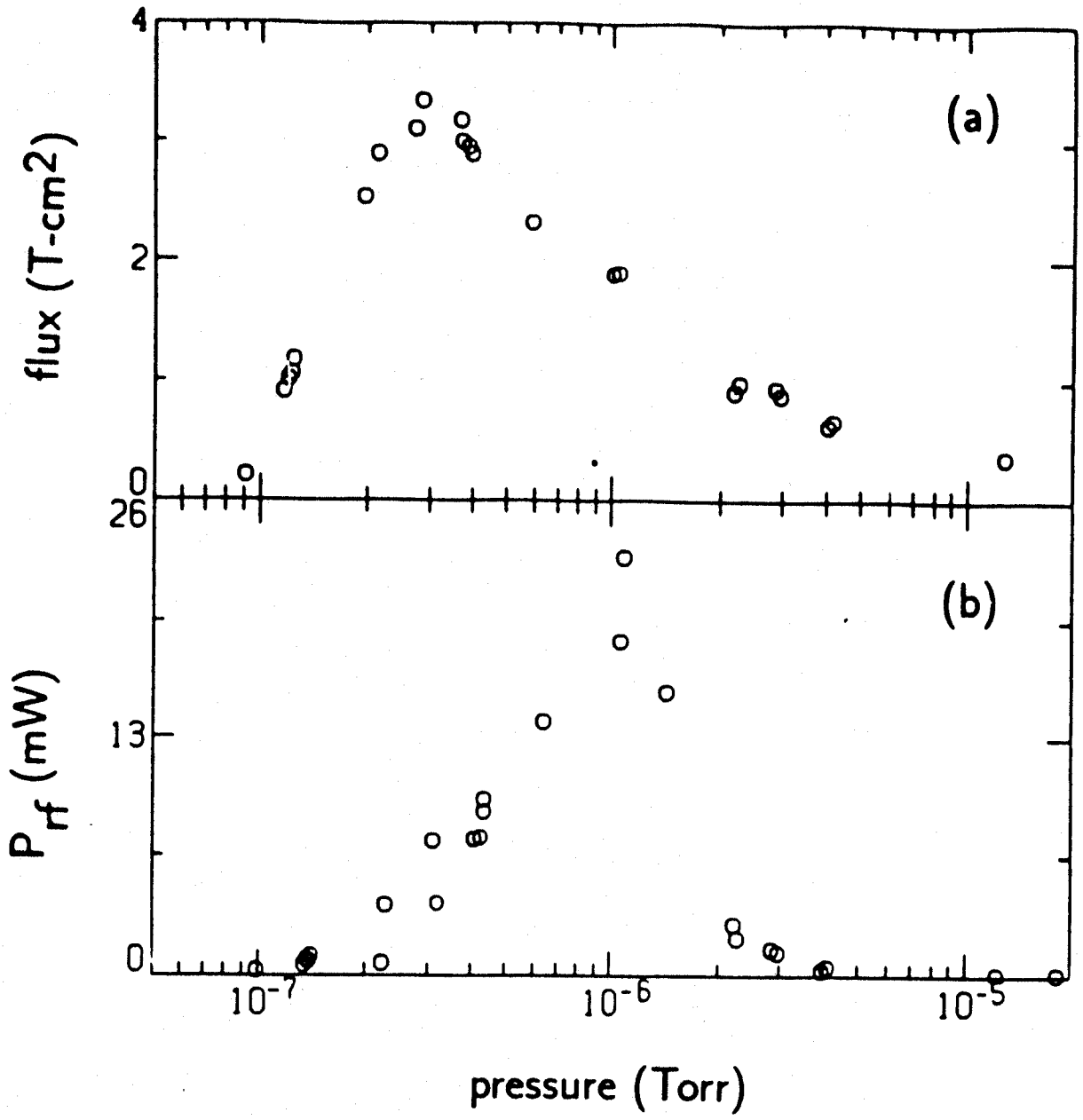

Fig. 33) (a) The diamagnetic flux and (b) the power of the total unstable rf emission as a function of the neutral pressure during the ECRH. Each point is the average over a 30 ms window 1.3 seconds after the rf is turned on.

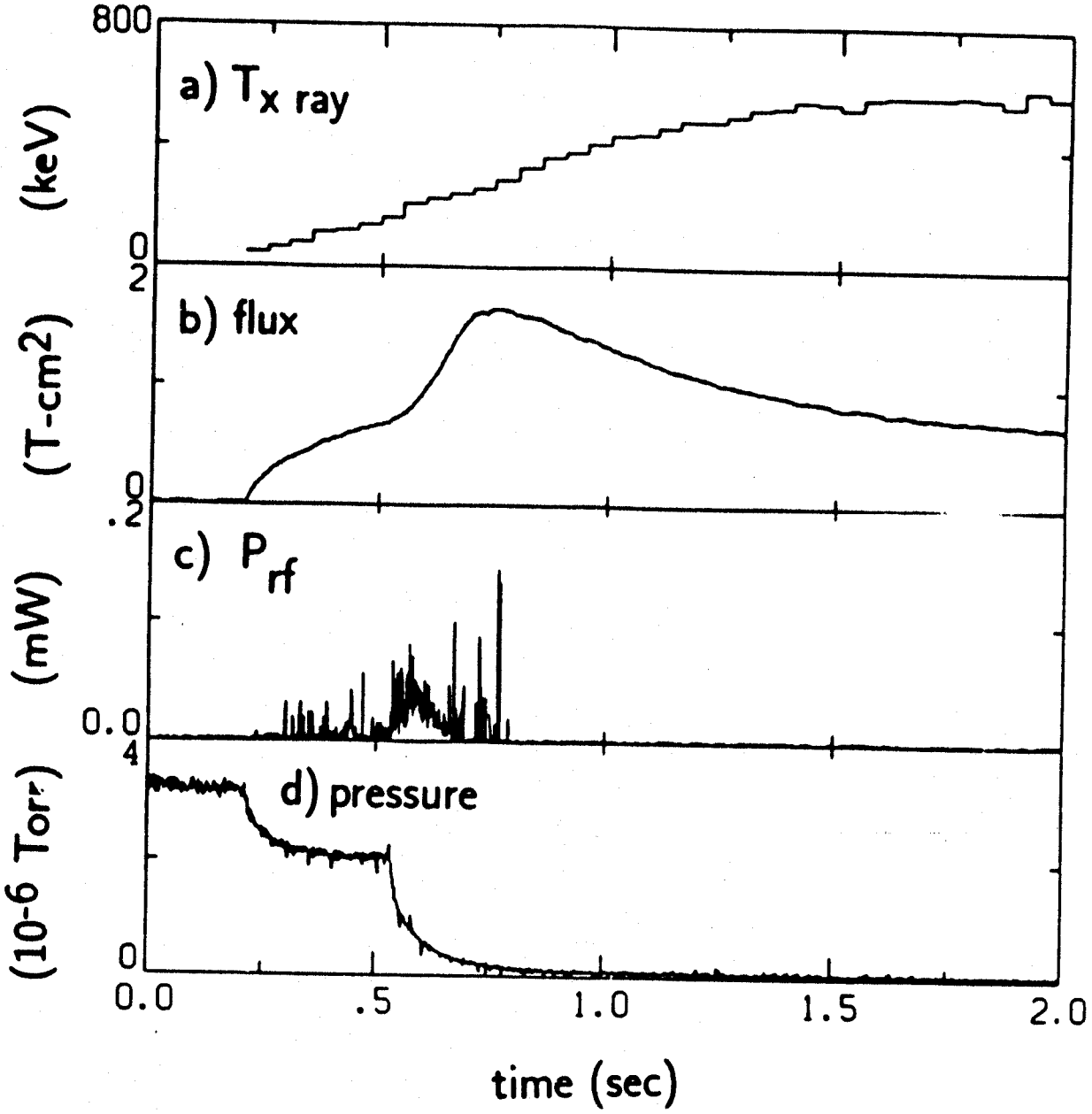

Fig. 34) Data which shows the stability of the hot electrons to the whistler mode. The gas is turned off at 0.6 sec. and the ECRH is turned off at 2 sec. The hot electrons remain for several seconds after the cold and the warm electrons have decayed. There is no unstable rf emission at this time. (a) Hot electron temperature. (b) Diamagnetic flux. (c) Power of total unstable rf emission. (d) Gauge pressure.

highest growth rates occur theoretically is in good agreement with the experimentally observed frequencies of unstable rf emission from the Constance B plasma. For a midplane magnetic field of 3 kG (midplane cyclotron frequency of 8.4 GHz) unstable emission occurs experimentally in the range from 6.7 GHz to 8.7 GHz for low pressures (compare to fig. 35), and 6.7 GHz to 10.5 GHz (the ECRH frequency) for higher pressures. In addition, the theoretical calculations indicate that the particles with the greatest contribution to the instability are those with energies in the 5-50 keV range. Using a bi-Maxwellian loss cone distribution for the hot electrons, as is suggested by the x-ray data, the code predicts that the hot electrons should be unstable and that emission will occur at frequencies near 1-2 GHz. This is not observed in the experiment though.

The power loss due to the microinstability has been measured. Power loss is due primarily to rf emission and to electron endloss induced by unstable waves kicking electrons into the loss cone. Both types are dependent on operating conditions, but appear to be dependent in the same way. The maximum amount of power loss occurs at a particular neutral gas pressure where the rate of production of plasma is greatest. The power loss is dependent on ECRH power slightly less than linearly. For 1 kW of ECRH power the maximum power loss due to unstable rf emission is approximately 14 Watts. The corresponding power loss due to instability-induced endloss is approximately 10 Watts for electrons less than 5 keV. For electrons greater than 5 keV this can only be estimated since a calibrated electron energy analyzer for these energies is not available on Constance. An upper bound can be set at 50 Watts, although it is probably much lower than this since it has been determined through other methods that the hot electrons do not

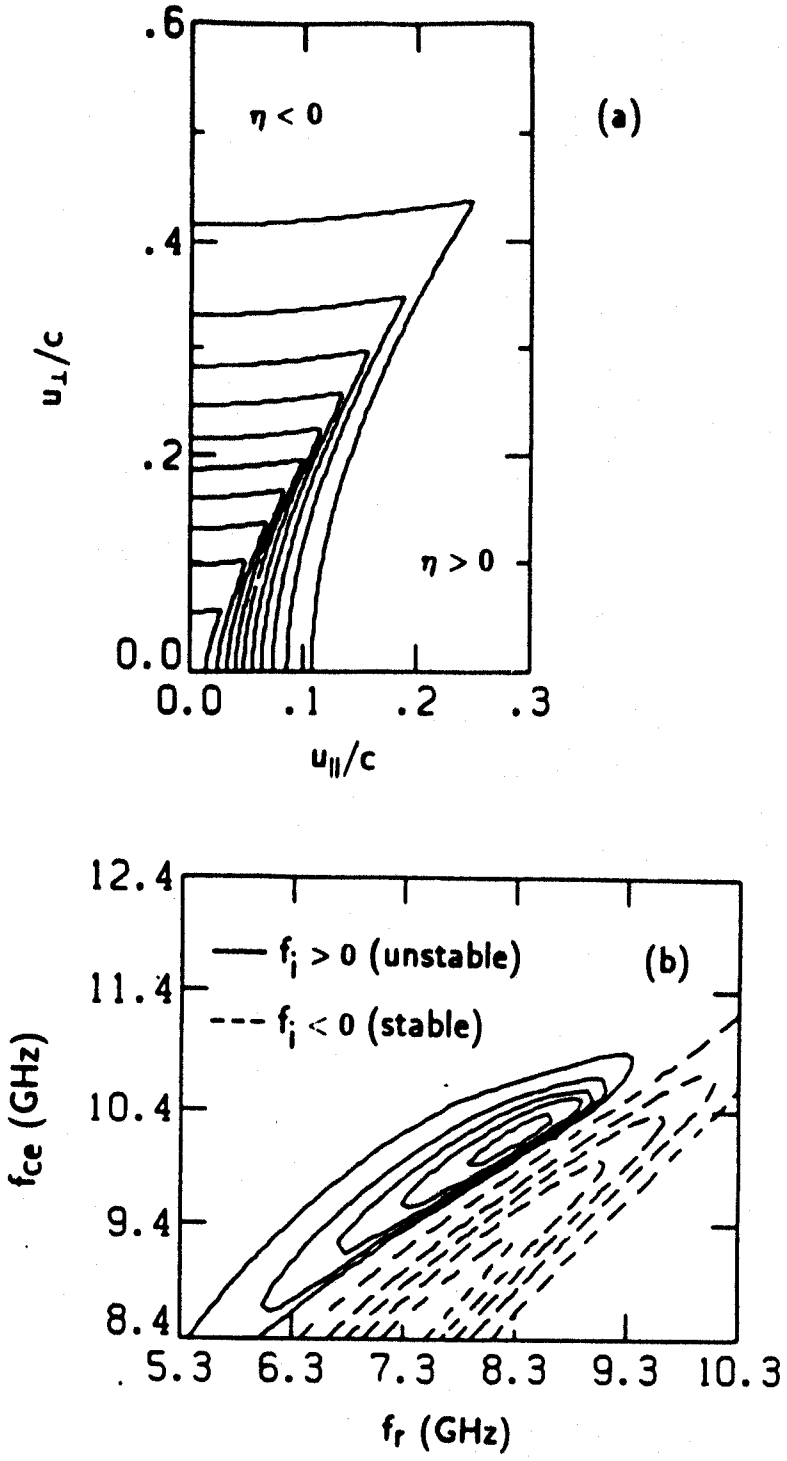

Fig. 35) (a) Contours of the ECRH distribution function in relativistic velocity space for T_χ = 10 keV, T_{η^+} = 5 keV, and T_{η^-} = 0.25 keV. (b) Contours of f_i for these temperatures. The vertical axis is the local cyclotron frequency and corresponds to the position along a field line. The horizontal axis is the real frequency of a wave that satisfies the cold plasma dispersion relation with $k_\parallel = 0$.

contribute greatly to instability. Whistler losses typically account for less than 10% of the input klystron power.

Under certain rare operating conditions large bursts of instability are observed which lead to 20% drops in density and diamagnetism (fig. 36). In these circumstances, essentially all the cold plasma is dumped. Unfortunately the conditions for the occurrence of arge dumps has not been well documented. There appears to be some correlation with poor vacuum conditions but this is not well-established

G. Other Instabilities

Hot electron dumps have been seen in the low neutral pressure decay of the diamagnetic loop signal. The scintillator probe shows large bursts coincident with the small staircase drops in beta (fig. 37). There is no microwave emission associated with this activity. This instability was seen only under conditions of very good machine base pressure ($< 4 \times 10^{-8}$ torr).

Fast b-dot probe measurements also resulted in the discovery of some instability activity. Studies were made of the magnetic fluctuations which occur on fast time scales, such as the whistler instability bursts. These measurements showed the existence of two types of fast b-dot fluctuations. In the first instability the magnetic fluctuations have no dominant frequency components and are preceded by end loss bursts, a few hundred nanoseconds earlier (fig. 38). These endloss bursts are correlated with the whistler emission. In the second type of fast magnetic instability, a large

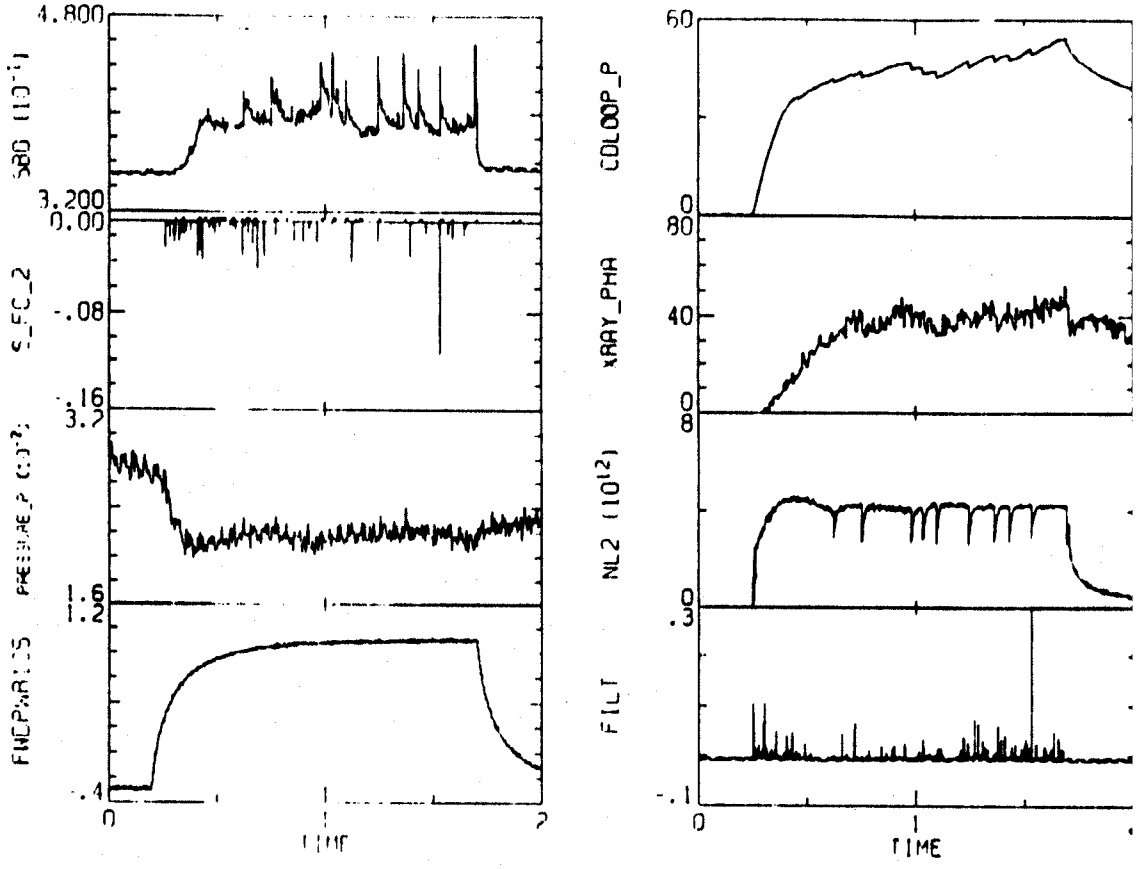

Fig. 36) Large plasma dumps. Shot conditions are B=2.9 kG and P=2.5 kW.

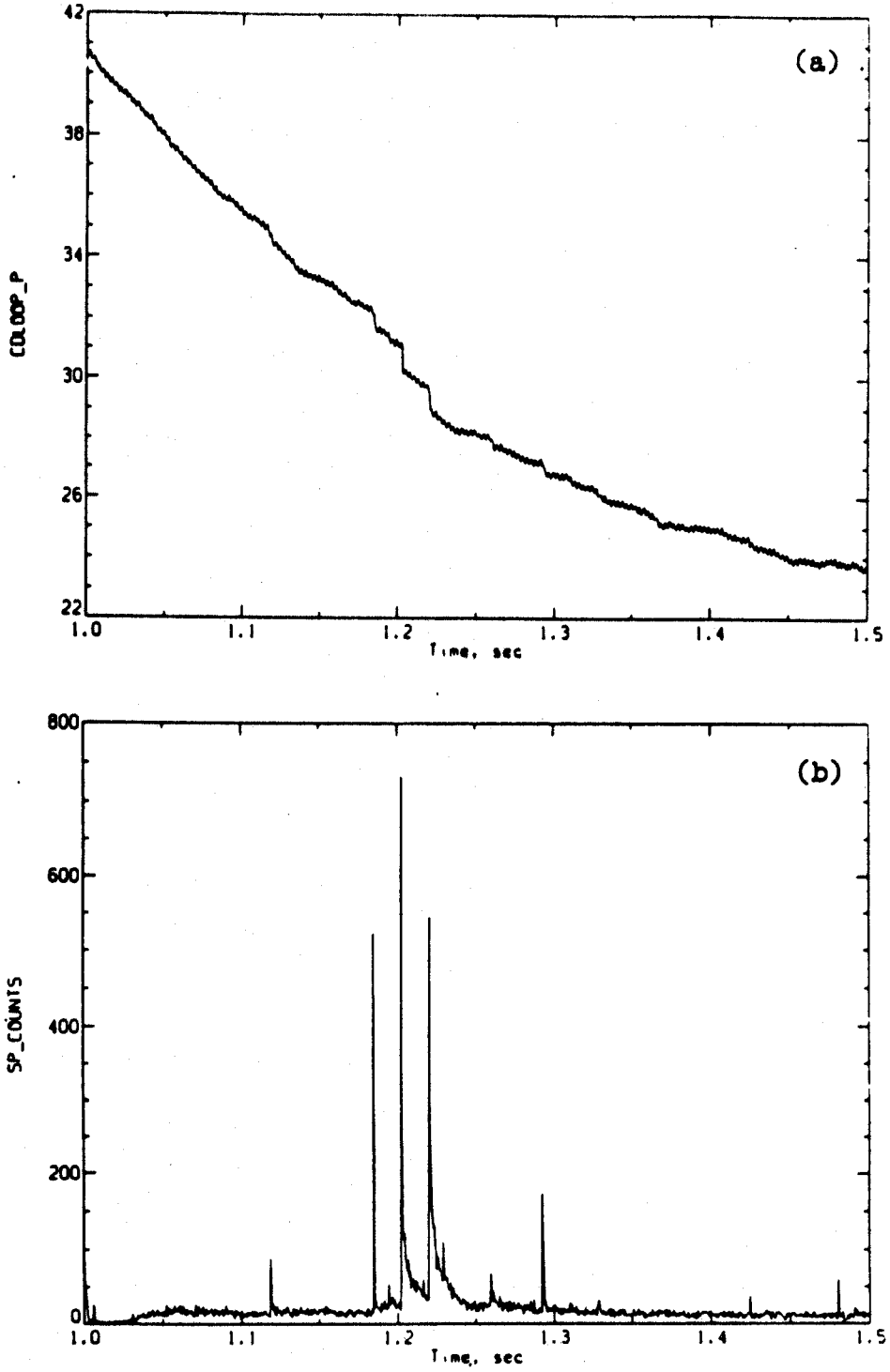

Fig. 37) Hot electron dumps in the afterglow plasma. The (a) rapid drops in diamagnetism are correlated with (b) bursts of E > 150 keV hot electrons detected by the endwall scintillator probe. There is no microwave emission observed with these bursts. B=3.2 kG, P=1 kW.

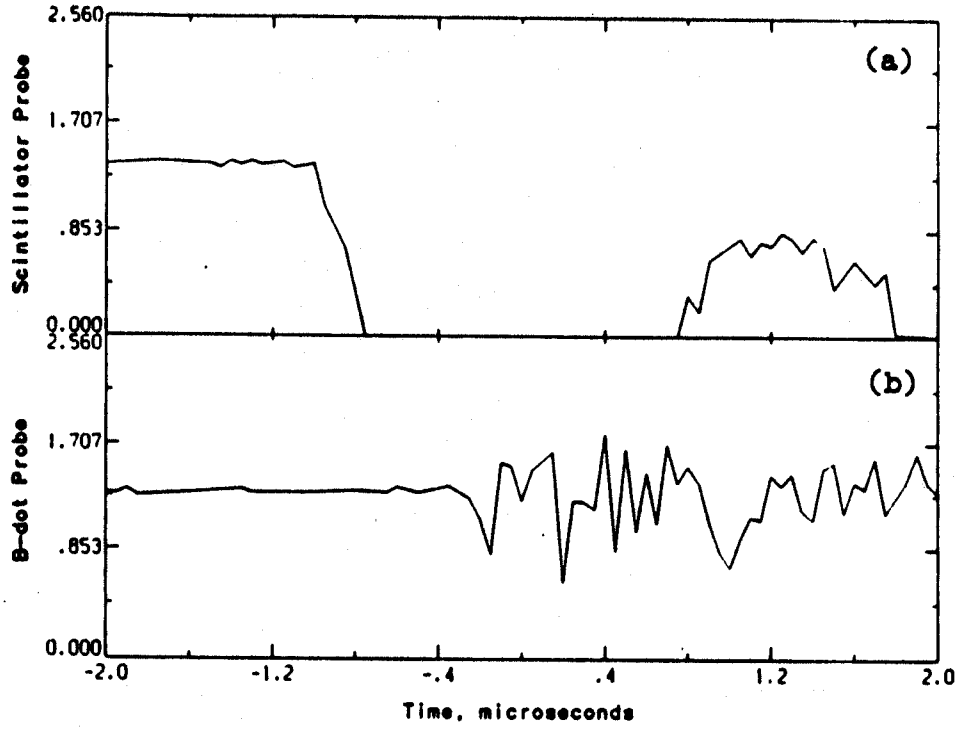

Fig. 38) M gnetic fluctuations (b) which are preceded by the loss of hot electrons (a).

burst of 4 MHz oscillations occurs which is followed by end loss fluctuations (fig. 39). The end loss occurs 50 to 200 nanoseconds after the magnetic fluctuations. A 4 MHz oscillation is also seen on a floating probe at the plasma edge. We note that 4 MHz is in the neighborhood of the ion cyclotron frequency (~5 MHz) and the hot electron drift frequency (~7 MHz).

The presence of probes in the plasma can result in interesting fluctuations (fig. 40). There is no microwave emission corresponding to the reset oscillations seen on the density and other signals. This activity may be a fueling related phenomenon.

H. Equilibrium Measurements

The goal of the equilibrium studies experiments is to determine the hot electron pressure profile in the plasma. This is a difficult experimental task since the hot plasma can only be probed either in a volume averaged sense or locally, well away from the hot electrons. The approach in Constance has been to measure the diamagnetic fields generated by the plasma and compare them to the results predicted by computed model pressure distributions. The first models used a $P(\psi,B)$ equilibrium where alpha was chosen so that the flux surfaces were circles at the midplane. Various flux dependencies including profiles peaked on and off the axis were explored. In view of the visible light pictures the present pressure models have been chosen so that the flux surfaces correspond with the drift surfaces of deeply trapped particles as in figure 16.

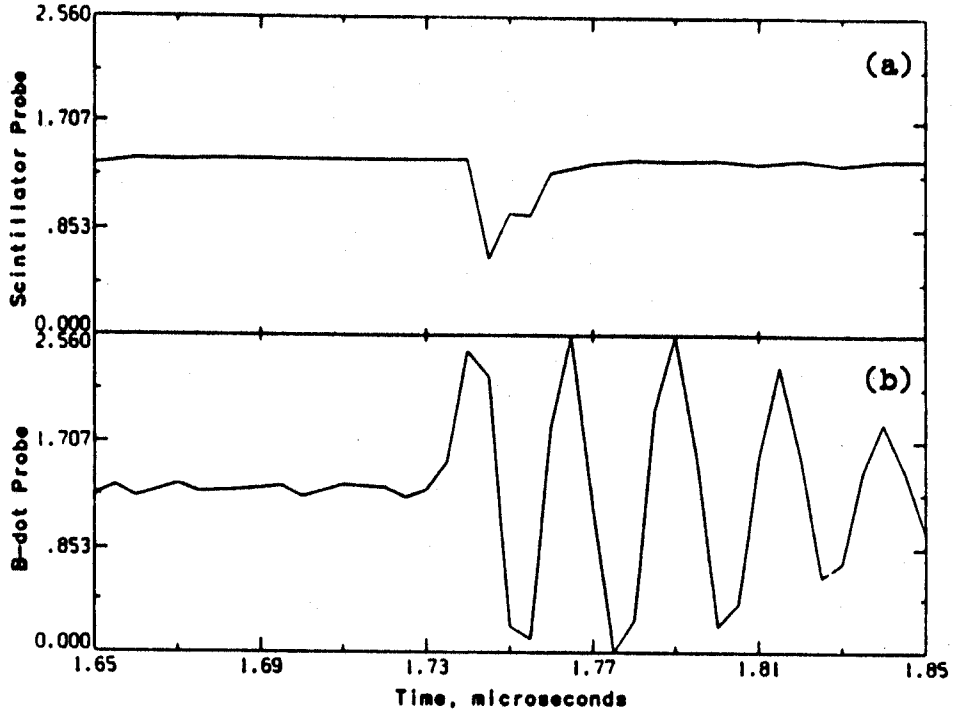

Fig. 39) 4 MHz magnetic oscillations (b) which precede the hot electron endloss (a).

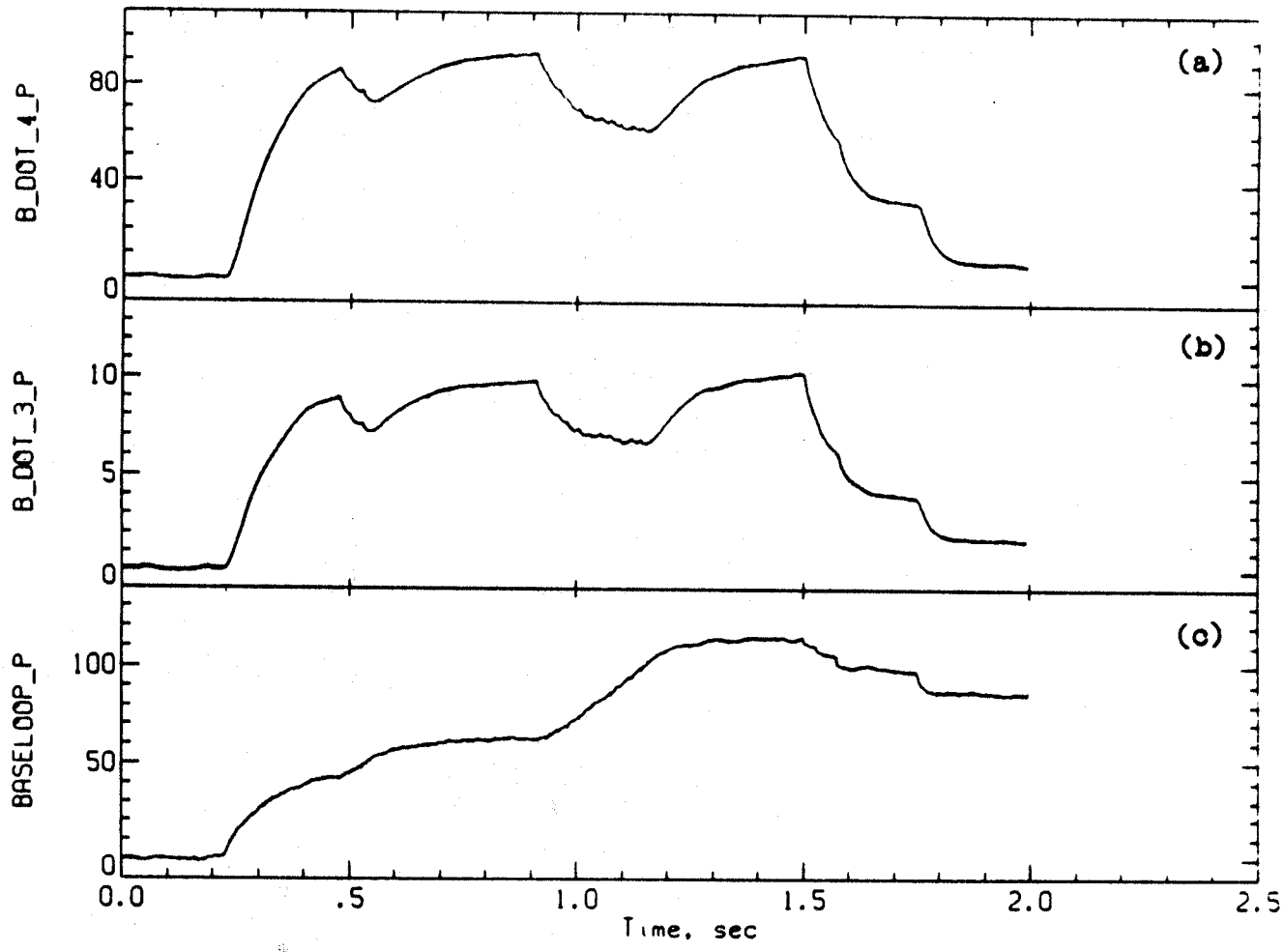

Fig. 40) Diamagnetic loop and b-dot probe signals as a function of time when a 1/4" diameter probe is inserted 1" from the axis at z=3.75" south. Baseloop is the signal from the diamagnetic loop which is shaped like the baseball seam.

An important aspect of the experimental work has been the construction and testing of electronically stable (drift-free) amplifiers and integrators. This was difficult to achieve for the several second long pulse lengths but has now been done. Probes have been made to measure B_z, B_x, and B_y but most of the measurements to date have been made with the B_z probes. The b-dot probes for the equilibrium studies typically have up to 1000 turns of wire in order to achieve the necessary sensitivity for the measurements. The probes are mounted inside 1/2" or 3/4" diameter stainless steel sheaths.

Prior to making the bulk of the measurements extensive numerical modelling was done to calculate the diamagnetic fields outside the plasma for the different pressure profiles. These calculations showed that to within the accuracy of the measurements it was not really possible to differentiate between the profiles by measuring only the B_z magnetic fields outside the plasma. The reason that greater differences are not seen is that the diamagnetic depressions of the vacuum magnetic field are strong inside the plasma (on the order of beta) but are small outside the plasma and fall off as r^{-3}. However, the calculations have shown that the ratio of the diamagnetic loop signal to the b-dot probe signal is a more sensitive measure of the pressure profile than the local magnetic field measurements (fig. 41). These calculations also showed that a negative diamagnetic field could be measured on the narrow side of the plasma fan. This turn-over point is potentially a sensitive measure of the profile. B_x has also been shown to vary strongly between some pressure profiles.

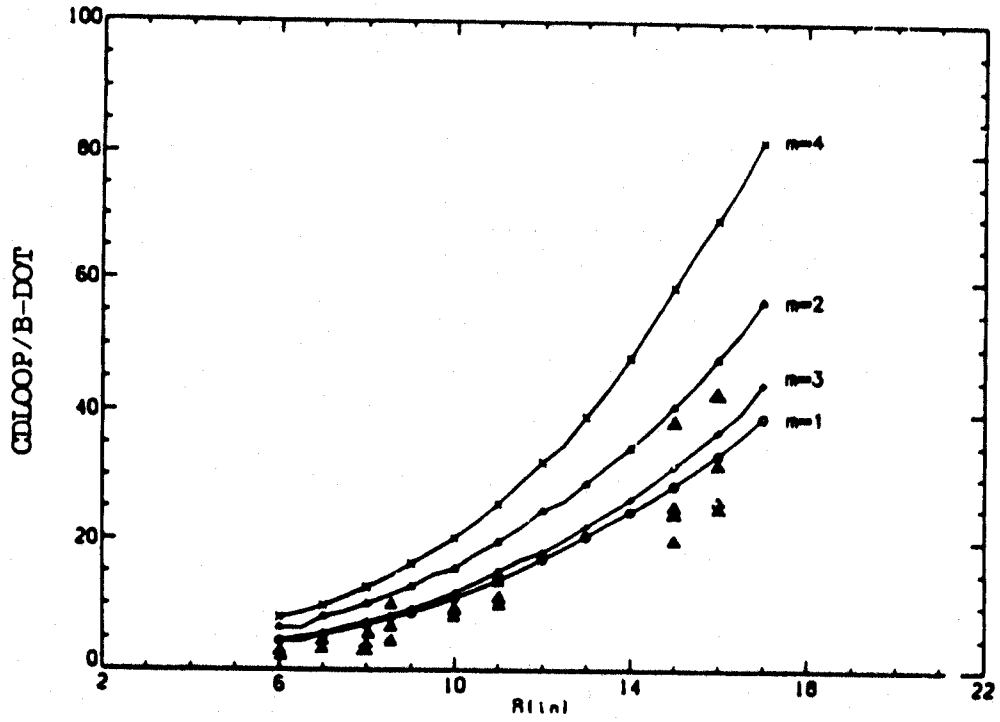

41) The ratio of the diamagnetic loop signal to the local b-dot signal as a function of the position of the b-dot probe, for different pressure profile models. M=1 and m=2 are gaussian profiles, m=3 is a hollow profile, and m=4 is a flat profile. The experimental data is shown in the large, closed triangles.

An important part of the modeling effort has been the development of an accurate analytic expression for the Constance magnetic field. The new B-field model is accurate to within 5% over the entire range of the magnetic well. This enables us to accurately model the plasma behavior at the edge, which is crucial to the magnetic measurements.

The measurements have verified the $^1/_{r^3}$ dependence of the diamagnetic field fall-off and local diamagnetic fields of up to 20 Gauss have been measured 15 cm from the plasma. The excellent stability of the electronics allows fields as low as 0.2 G to be measured. The shape of the plasma is found to be established within 100 ms and remains constant during the ECRH pulse for most conditions.

The measured radial variation of B_z and B_x at several axial positions is being compared to the code predictions to determine which pressure model is the best fit to the data. This profile will then be examined to see if, in conjunction with the xray pinhole pictures, the NaI profiles and the hot electron endloss profiles, a consistent picture of the hot electron equilibrium can be obtained.

Attempts at making magnetic probe measurements inside the hot electron plasma have also been made. Skimmer probes of 1/4" diameter can be inserted all the way to the axis at z=-4" (reference figure 2) without perturbing the plasma. However the b-dot probes are 1/2" or 3/4" in diameter and cannot be put into the hot plasma without changing it. A linear time behavior on the b-dot probe which is different from the diamagnetic loop behavior is the

signature of a perturbing probe (fig. 42). This is a localized perturbation which probably causes currents to flow in the plasma around the probe tip. When the probe coil is moved back from the edge of the sheath the signal reverts to the normal time behavior, i.e. it resembles the diamagnetic loop signal.

The three-dimensional equilibrium code VEPEC, developed by D. Anderson at LLNL, has been used to model Constance results in the past [7]. However, now that we believe that the hot electron pressure profile is hollow, this code cannot be used. VEPEC is an MHD code and will go numerically unstable with hollow pressure profiles.

I. RF Induced Losses

The use of rf to heat mirror plasmas, either in the ion or electron cyclotron range of frequencies, leads to enhanced diffusion or particle loss. The degree to which rf diffusion affects the power balance will depend on the strength of the rf diffusion relative to collisional and other diffusion mechanisms. ECRF induced velocity space diffusion of hot electrons in a quadrupole mirror is being studied in detail in Constance B. The hot electrons in Constance are moved around in velocity space due to three mechanisms: (1) collisions with other electrons, and with hydrogen and impurity neutrals and ions, (2) ECRH electric fields, (3) microinstability electric fields, and (4) the synchrotron radiation reaction. The focus of the research has been on the dominant electric field mechanisms.

In Constance the relative importance of collisions, microinstability, and ECRH can be adjusted by controlling the neutral gas pressure and the

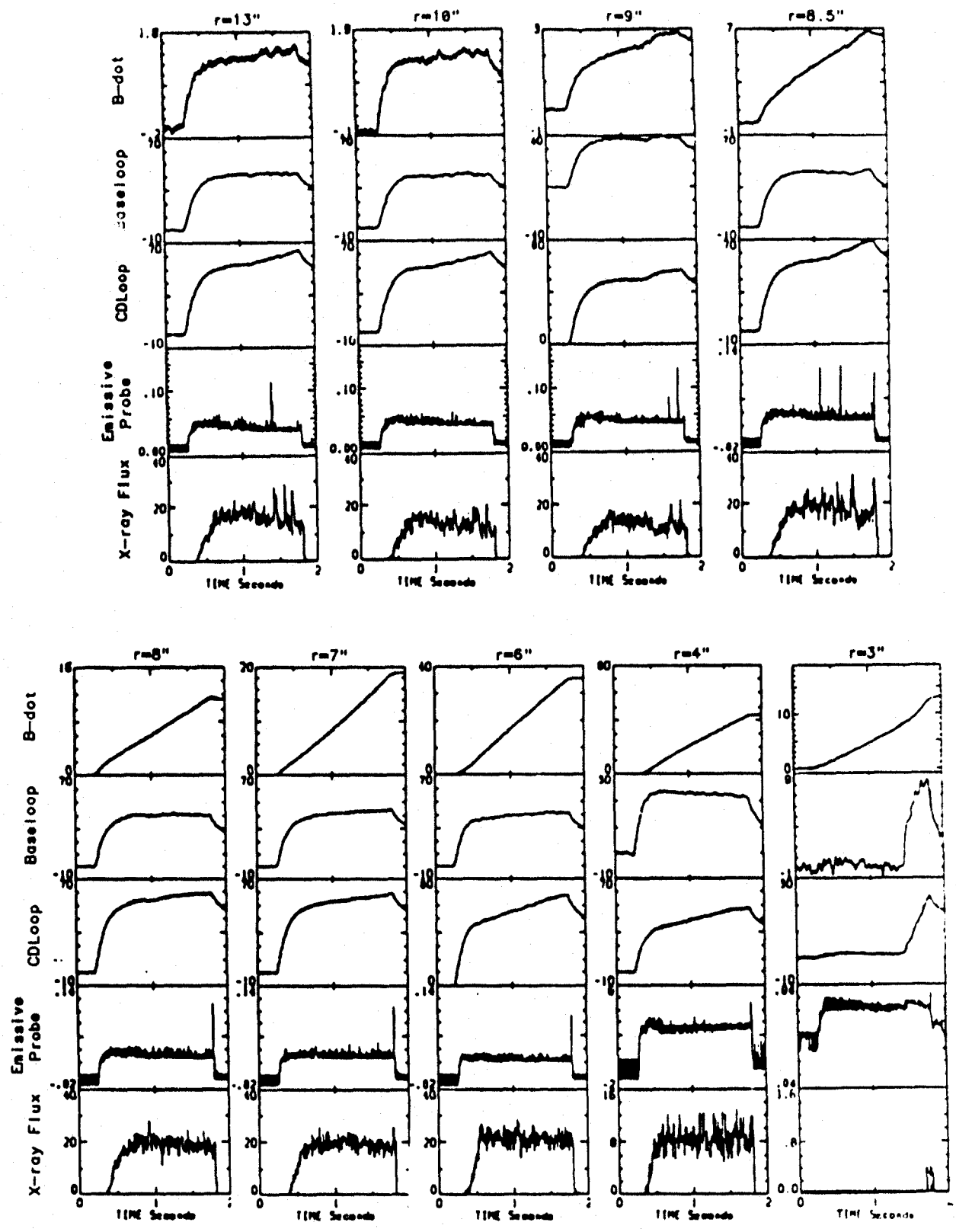

Fig. 42) The time behavior of a b-dot probe located 4" south of the midplane changes as it is moved in toward the axis, even though the diamagnetic loop signal is basically unchanged.

microwave power. Figure 43 shows clearly the faster decay of the diamagnetism when the second rf pulse is turned on - i.e. that the ECRH increases the loss rate. In figure 44 the endloss power as measured by a plastic scintillator probe is shown as a function of time for different combinations of gas and rf. From experiments such as these it has been seen that the loss rate of hot electrons (E > 150 keV) can be enhanced by up to 100 times the collisional loss rate. In experiments where the power used to heat the plasma is varied, the steady-state rf-induced hot electron endloss has been found to increase as the square of the rf power relative to the collisional loss (fig. 45). A linear portion of this is due to the increase in the rf field strength and the rest is due to changes in plasma conditions. When the magnetic field is varied, the ratio of rf to collisional endloss (> 150 keV) is a complicated function of the magnetic field which peaks at low fields, where the nonrelativistic ECRH resonance is located near the mirror peaks (fig. 46).

The hot electron endloss due to the ECRH diffusion is greater than that due to the microinstability. Figure 47 shows that hot electron endloss as measured by the scintillator probes peaks in magnitude at a much lower neutral pressure than the microinstability does. Also 50-80% of the scintillator probe signal is in the DC level with the remaining fraction in the microinstability bursts (fig. 48).

In experiments where the initial plasma is formed under the same conditions but the afterglow plasma is subject to a second ECRH pulse of varying power, the loss rate of the diamagnetism increases linearly with the power in the second pulse (fig. 49). The E > 150 keV electron endloss

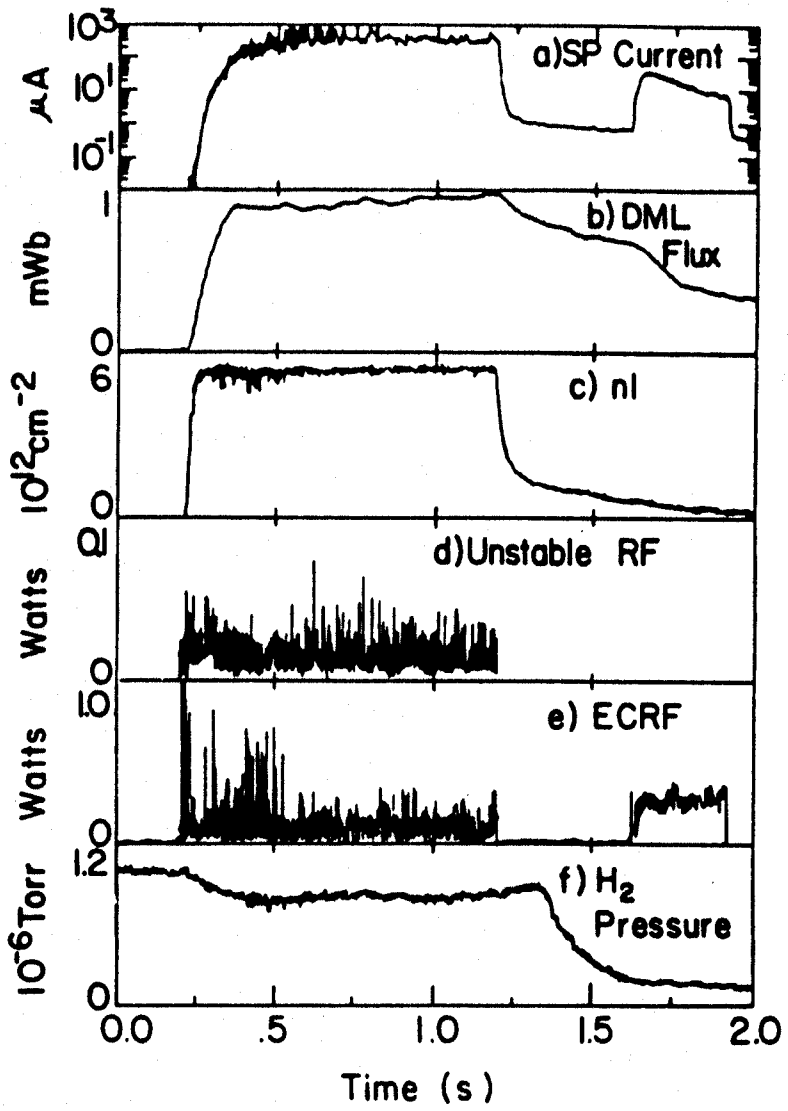

Fig. 43) Rf induced hot electron endloss experiments. 2 kW of ECRH is pulsed a second time in the low pressure decay of the hot electron plasma. Note that the decay rate of the diamagnetism is faster when the ECRH is on. The hot electron endloss power for electrons of E>150 keV is directly measured using the scintillator probe.

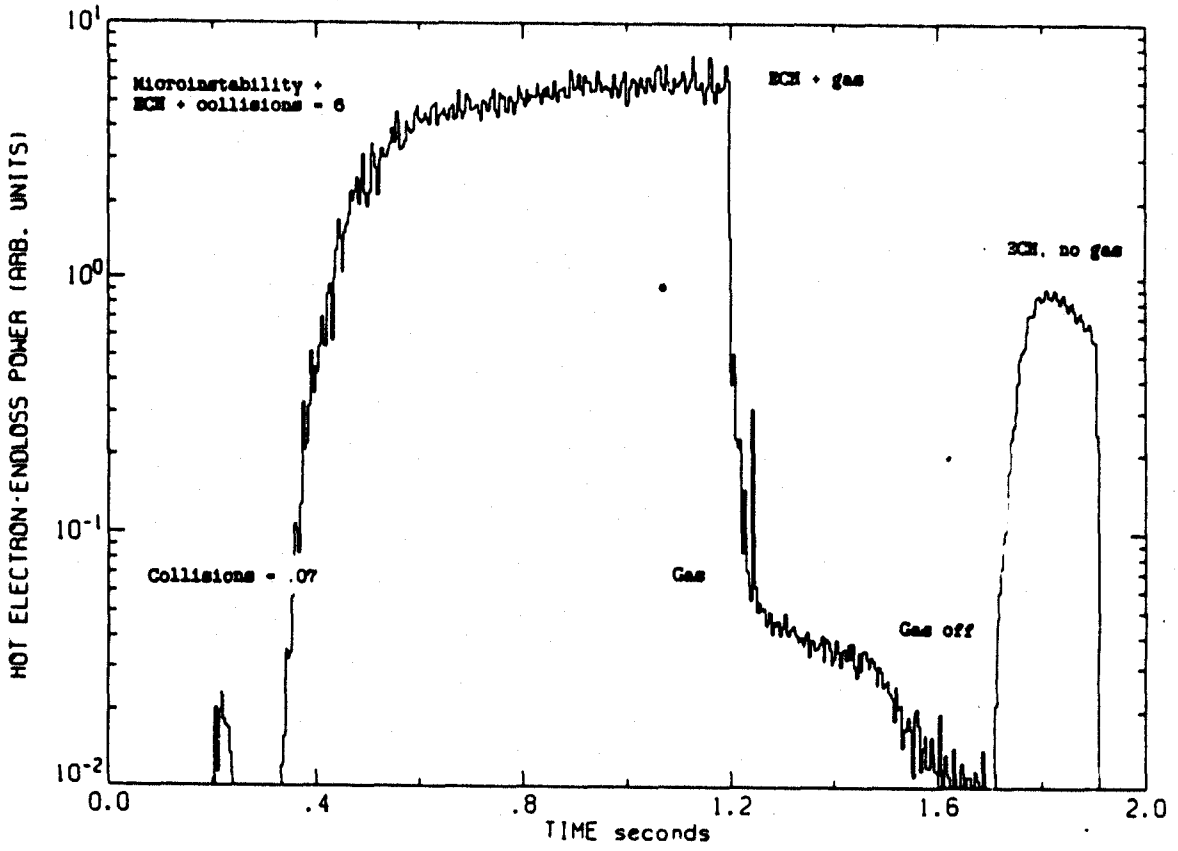

Fig. 44) The relative contributions of ECRH, microinstability, and collisions to the hot electron endloss. B=3.2 kG, P=2 kW.

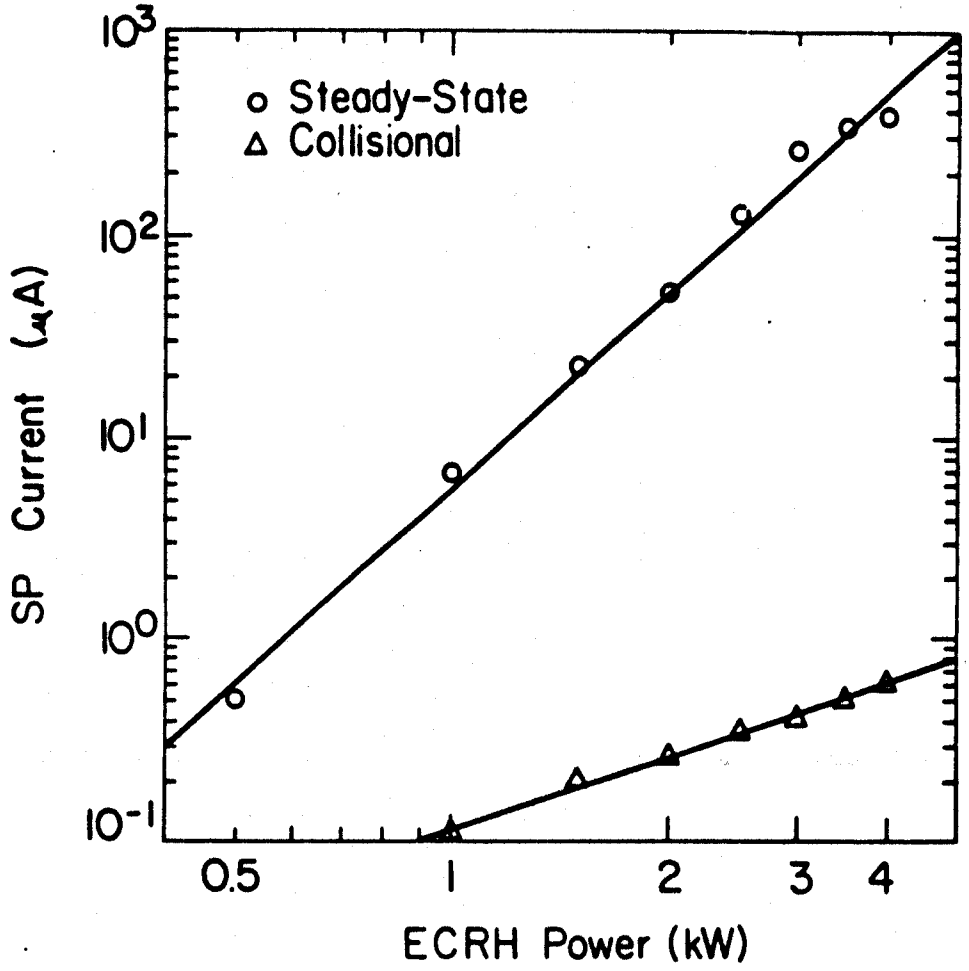

Fig. 45) Hot electron endloss vs. heating power as measured by the scintillator probe current. The points represent averages over 0.1 sec at the end of the ECRH pulse for the steady state case, and after the rf is turned off for the collisional case. B=3.2 kG.

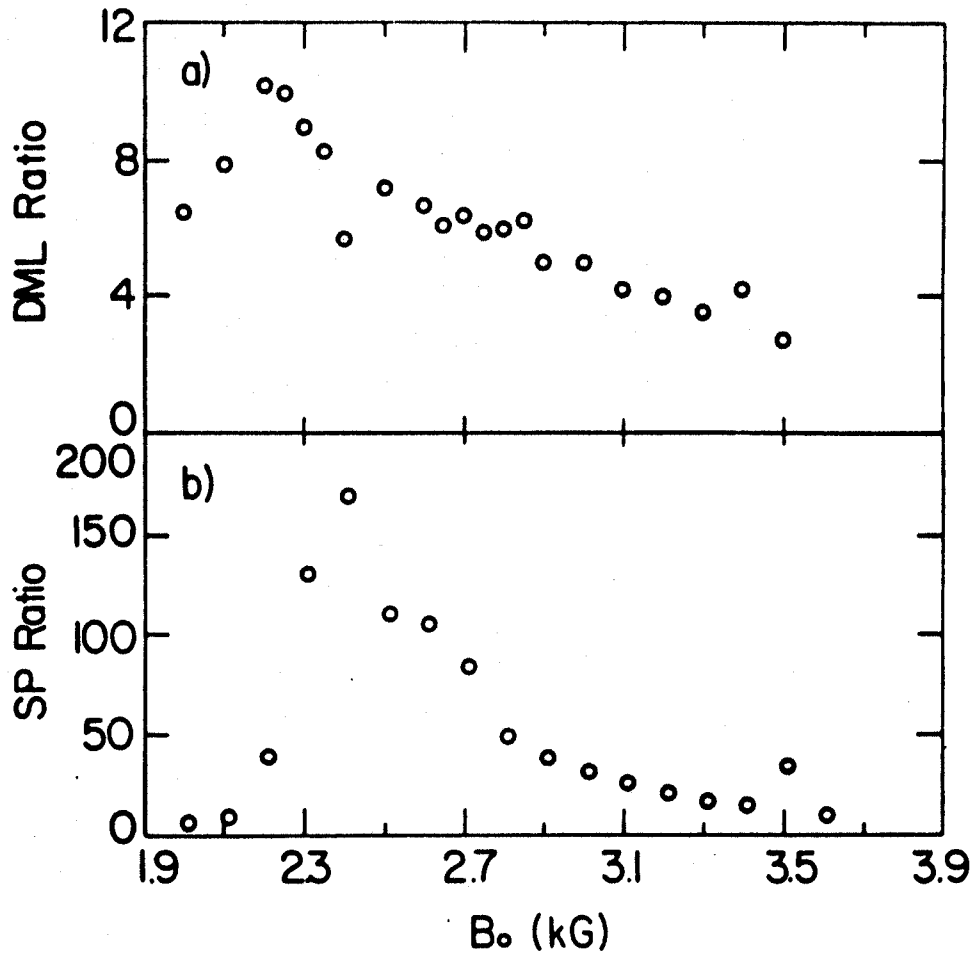

Fig. 46) The ratio of rf-induced loss to collisional loss vs. midplane magnetic field as measured by (a) diamagnetic loop decay rate and (b) scintillator probe current. The rf-induced part is taken from the second pulse and the collisional level from the first ECRH pulse. Both ECRH pulses are 4 kW.

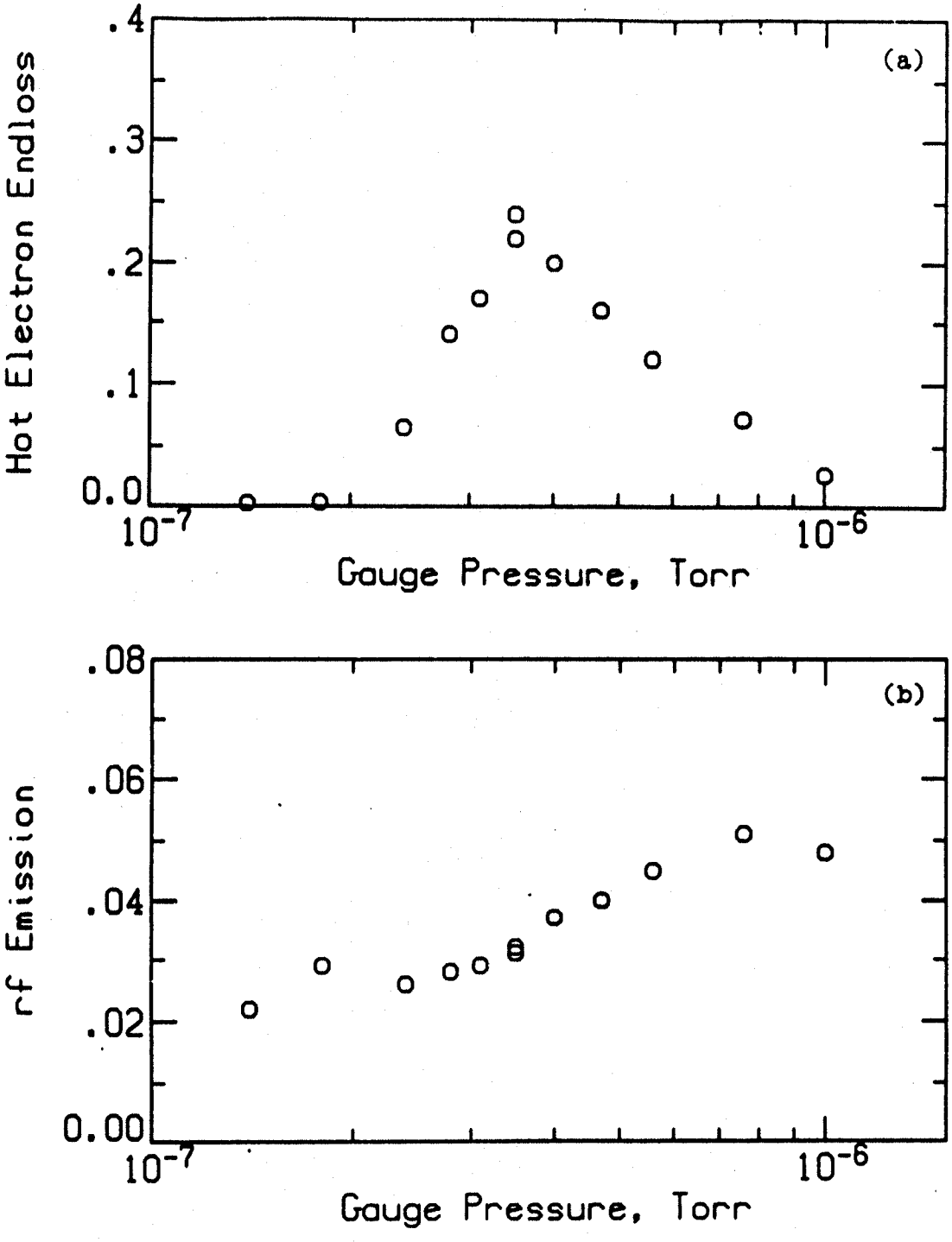

Fig. 47) Hot electron endloss and microinstability emission as a function of neutral pressure.

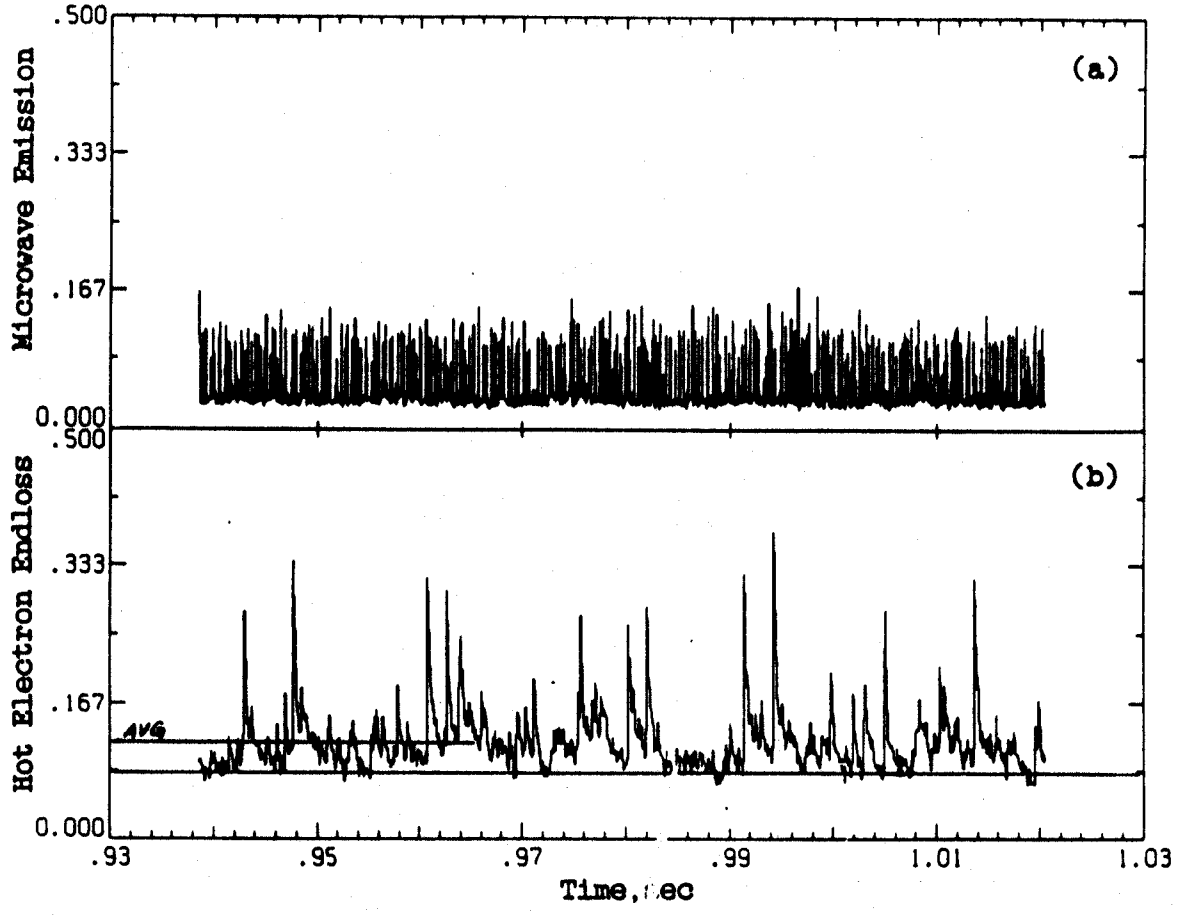

Fig. 48) Relative contribution of microinstability and ECRH diffusion to the hot electron endloss. The average value of the microinstability-induced endloss bursts are shown relative to the DC value which is due to the ECRH.

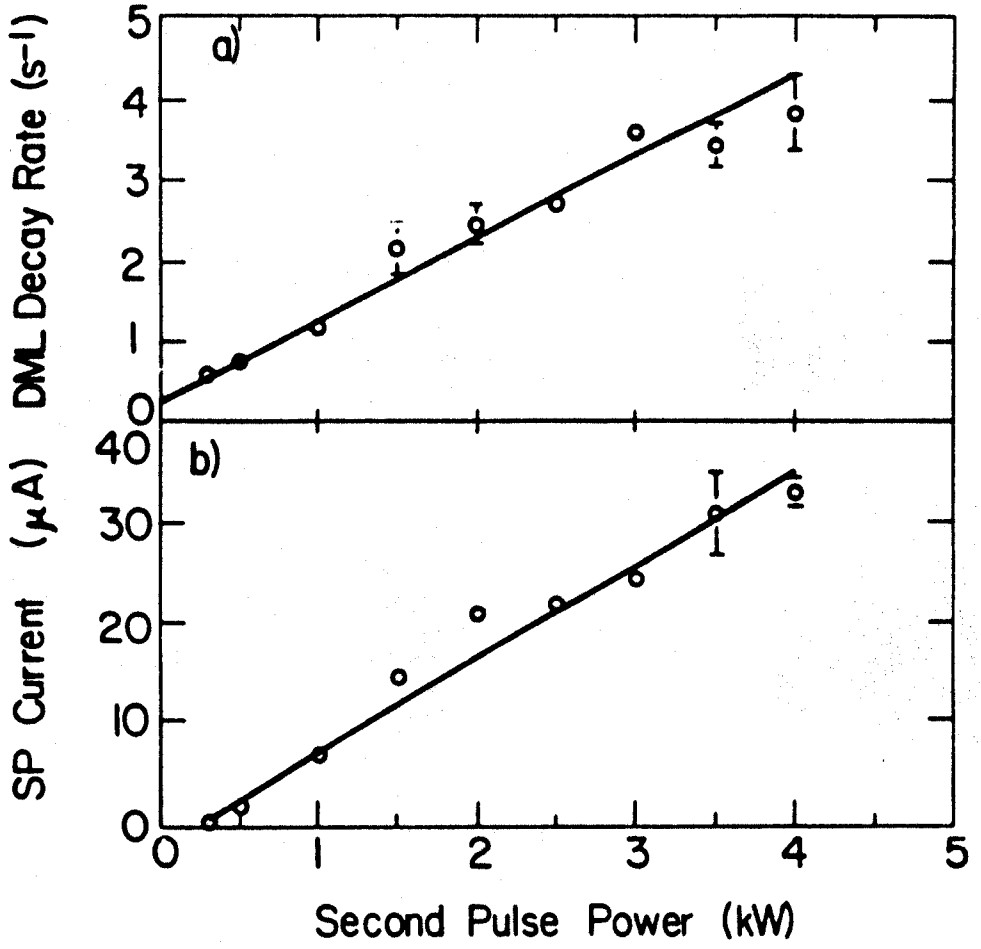

Fig. 49) RF-induced loss versus second pulse power as measured by (a) the diamagnetic loop decay rate and (b) the scintillator probe. The error bars represent shot-to-shot variation. The initial plasma is formed with 2 kW of heating power and B=3.2 kG.

increases linearly with the second pulse power above some threshold power. The existence of a power threshold for high energy electrons may be evidence of superadiabaticity.

According to the single particle heating theory [8] the stochastic barrier as calculated using Constance parameters and the measured 15 V/cm electric field is on the order of 20 keV. This implies that the hot electrons must be superadiabatic. They have long wave-particle resonances and the multiple resonances which arise because $k_{||} \neq 0$ and due to second harmonic heating are important. For these reasons, the existing quasi-linear models of ECRH heating are not valid for Constance and cannot be used to predict the ECRH-induced diffusion into the loss cone. An orbit code is being written to model the experiment.

J. Hot Electron Heating Rates

Using the hard x-ray pulse height analysis system the time development of the hot electron temperature has been measured. The initial heating rate at a neutral pressure of 5×10^{-7} torr is 600 keV/sec/kW. The data is shown in figure 50. The initial rate of rise of the hot electron temperature decreases with increasing neutral pressure, but not proportionally.

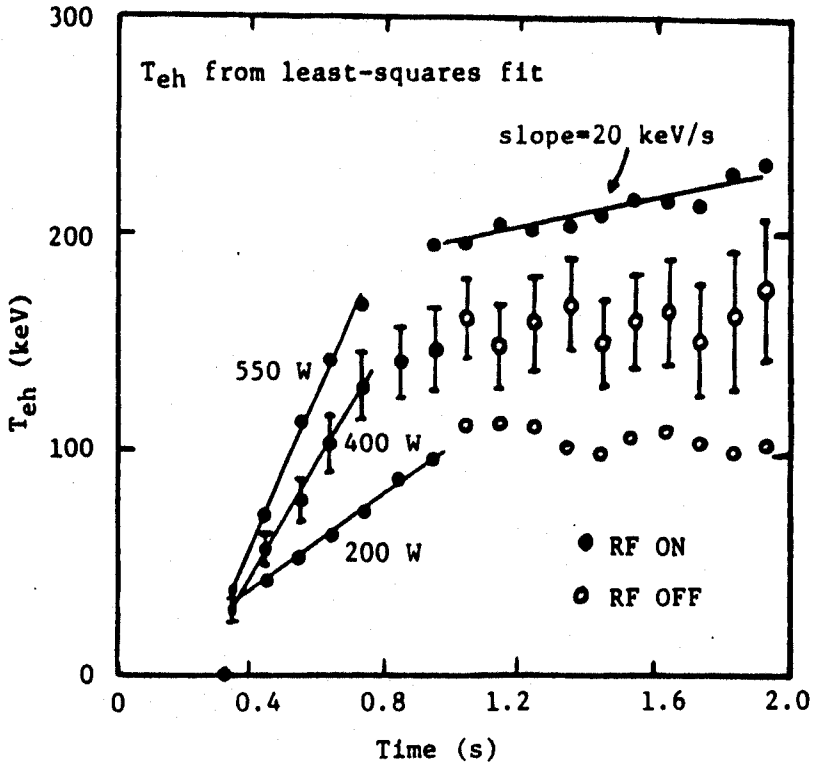

Fig. 50) The hot electron heating rate scales linearly with ECRH power.

K. Potentials

The potential structure in the machine was measured early in the course of the program using emissive probes and endloss analyzers. The results are shown in figure 51. The emissive probe cannot be used inside the field lines which are tangent to the resonance zone without burning up. Outside the mirror peak, measurements can be made on those field lines however. It may be noted that there are strong electric fields at the plasma edge.

The potential measured by the foregoing techniques is the positive ambipolar potential which must exist to confine the electrons in a mirror machine. However, consideration of the ion confinement dictates that there must be a local potential dip in the region of the hot electrons, i.e. within the resonance zone where the potential cannot be measured with probes. The confinement of the hot electrons is long compared to that of the cold ions so that the usual loss process ordering is reversed and a potential must develop to confine the ions locally. This potential will be on the order of the ion temperature. Calculations indicate that for our parameters it will be on the order of 15 volts when the rf is on and drop to less than 5 volts when the rf is off. To understand the ion confinement it would be very important to measure this potential. Note that impurity ions will be well confined in a hot electron mirror since the confinement time increases exponentially with the ion charge.

The good confinement of the ions in a hot electron machine has led to the use of ECRH mirrors as sources of highly stripped ions for accelerator physics [9]. Ions can be stripped to high charge states by the hot

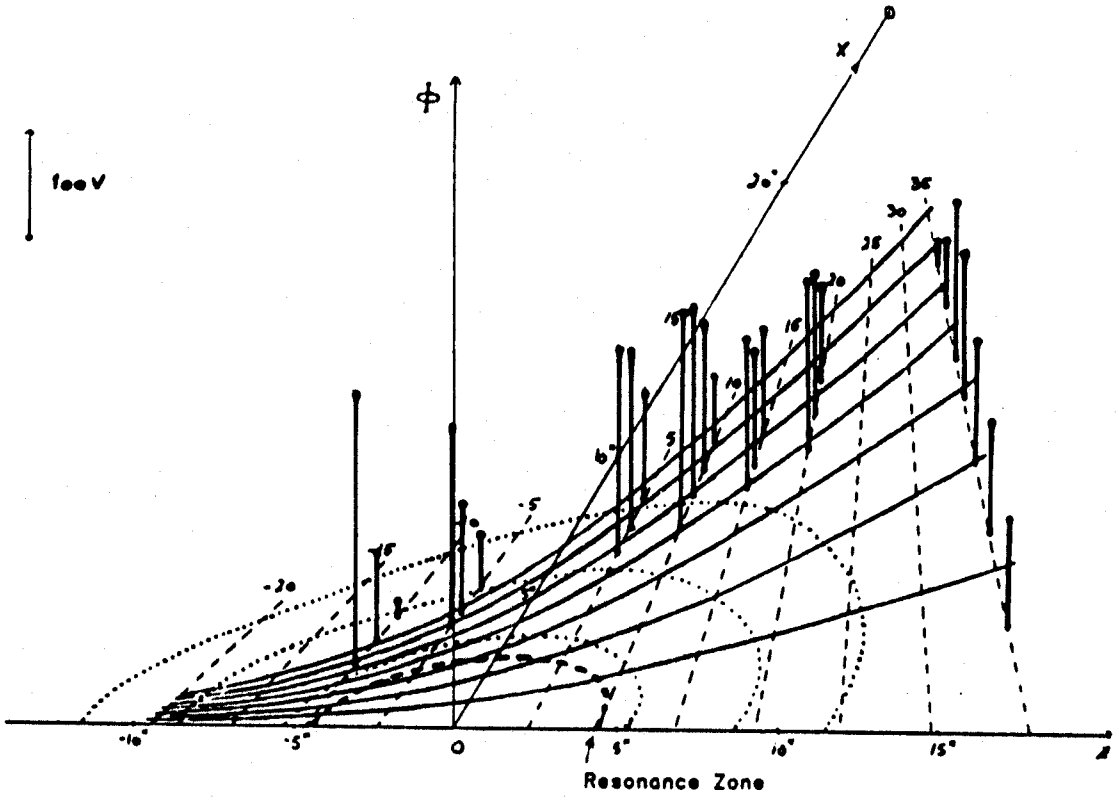

Fig. 51) Potential measured by the emissive probe as a function of position in the plasma. The length of the vertical bars indicate the magnitude of the potential at that point.

electrons because of their long confinement times. Brau [10] has calculated that for the typical Constance parameters, helium-like argon, Ar^{+15}, should exist in the plasma. Efforts to measure the argon charge state in Constance have been initiated.

L. X-ray Impurity Measurements

As described in Section C, the germanium soft x-ray detector measurements showed that the x-ray spectrum was Maxwellian down to ~ 2keV. At the low energies x-ray lines could be resolved in the spectrum. The data is shown in fig. 52 where the argon and titanium K-edge lines are identified. Analysis of the spectrum indicates that, for these plasma conditions, the argon and titanium targets produce 24% and 13% respectively, of the continuum x-rays. Titanium is generated by the getters. The titanium comes into the plasma directly from the emitting getters, not from the gettered wall surfaces, since when the getters are turned off, the titanium line disappears.

These results suggest an explanation for some of the "anomalous' x-ray flux signals. Fig. 53 shows the behavior of the x-ray flux signal for different neutral pressures. Note that at low pressure the flux increases after the rf is turned off. One expects the flux to decrease since the cold ions ($\simeq$ half the density) are lost at ECRH turn-off. This implies that the ions are not the majority of the targets. The soft x-ray data tells us that impurities are important. Figure 54 shows the x-ray flux in two shots with

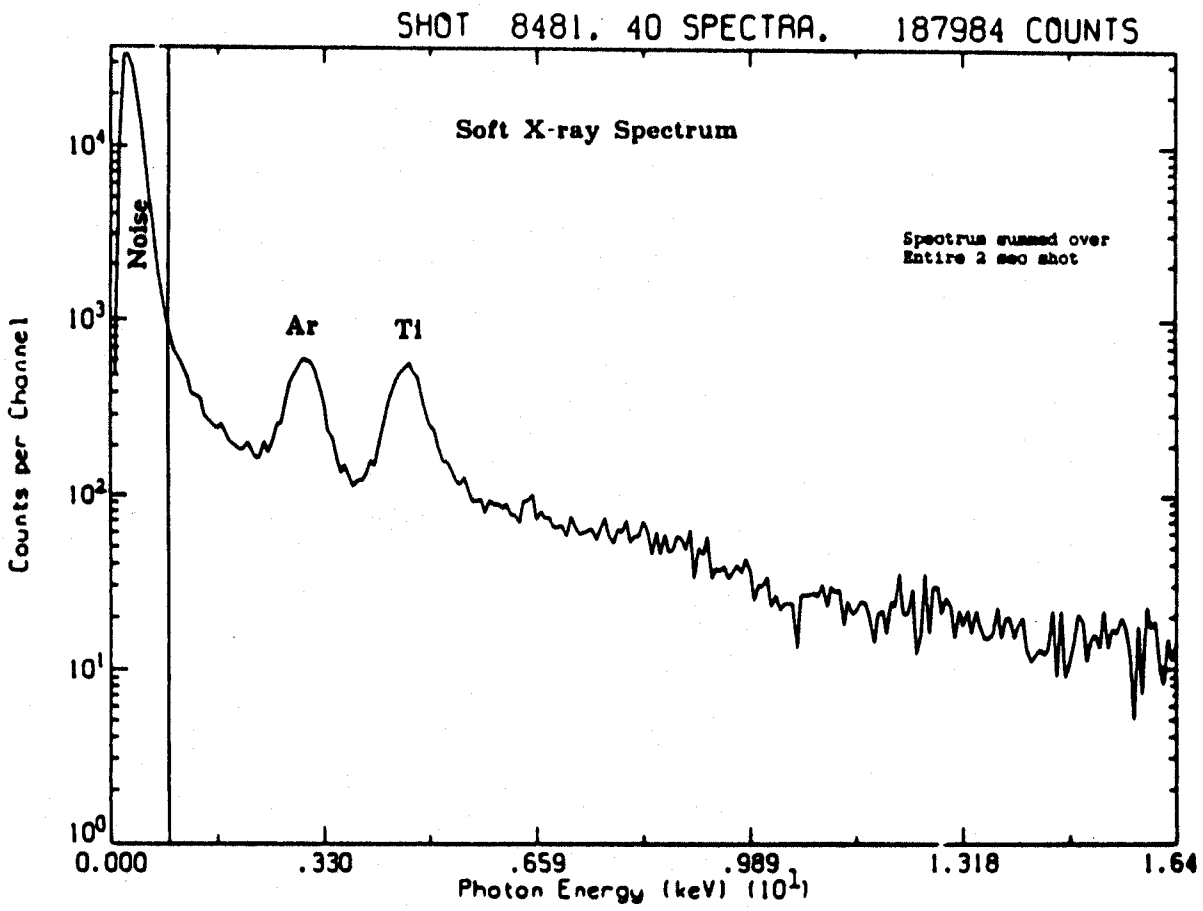

Fig. 52) Soft x-ray spectrum measured with the germanium detector shows the argon and titanium lines.

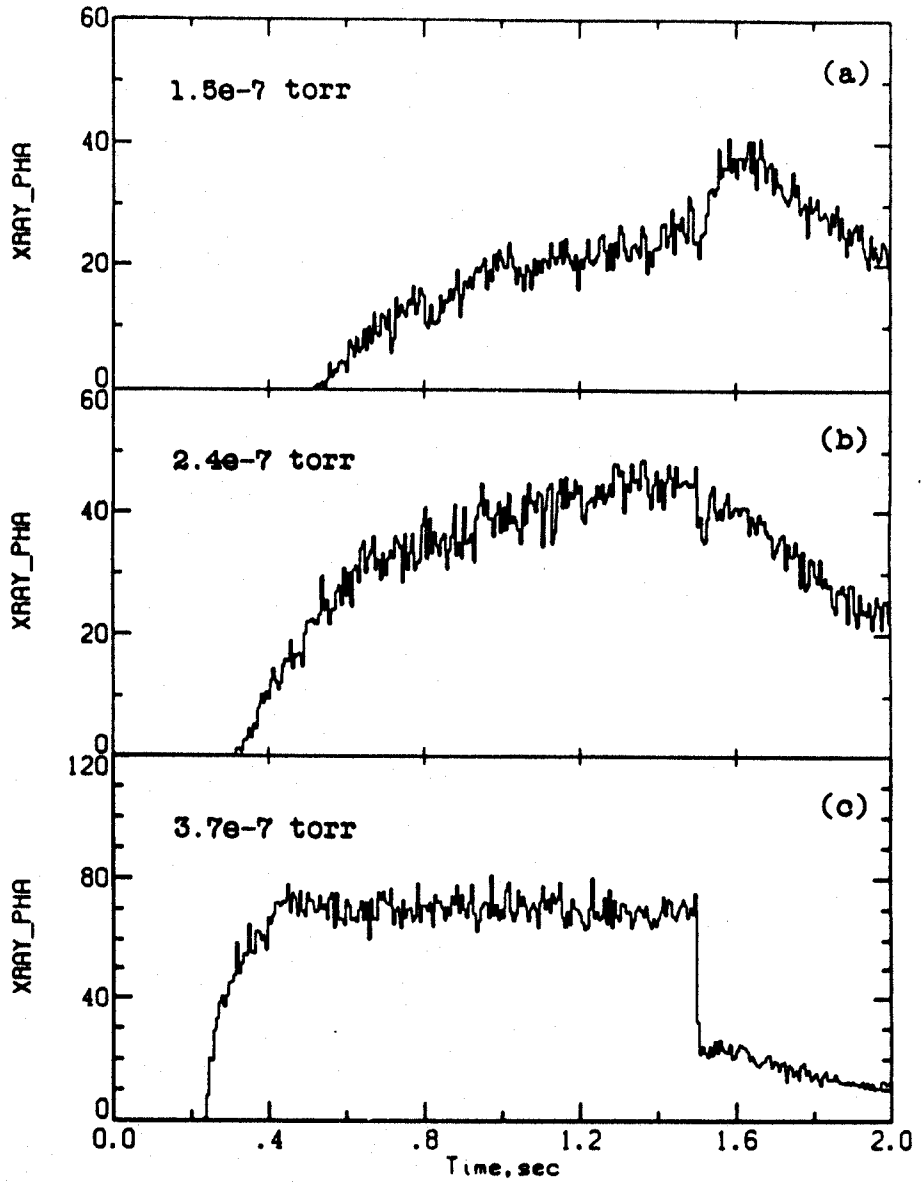

Fig. 53) X-ray flux signal for different neutral pressures.

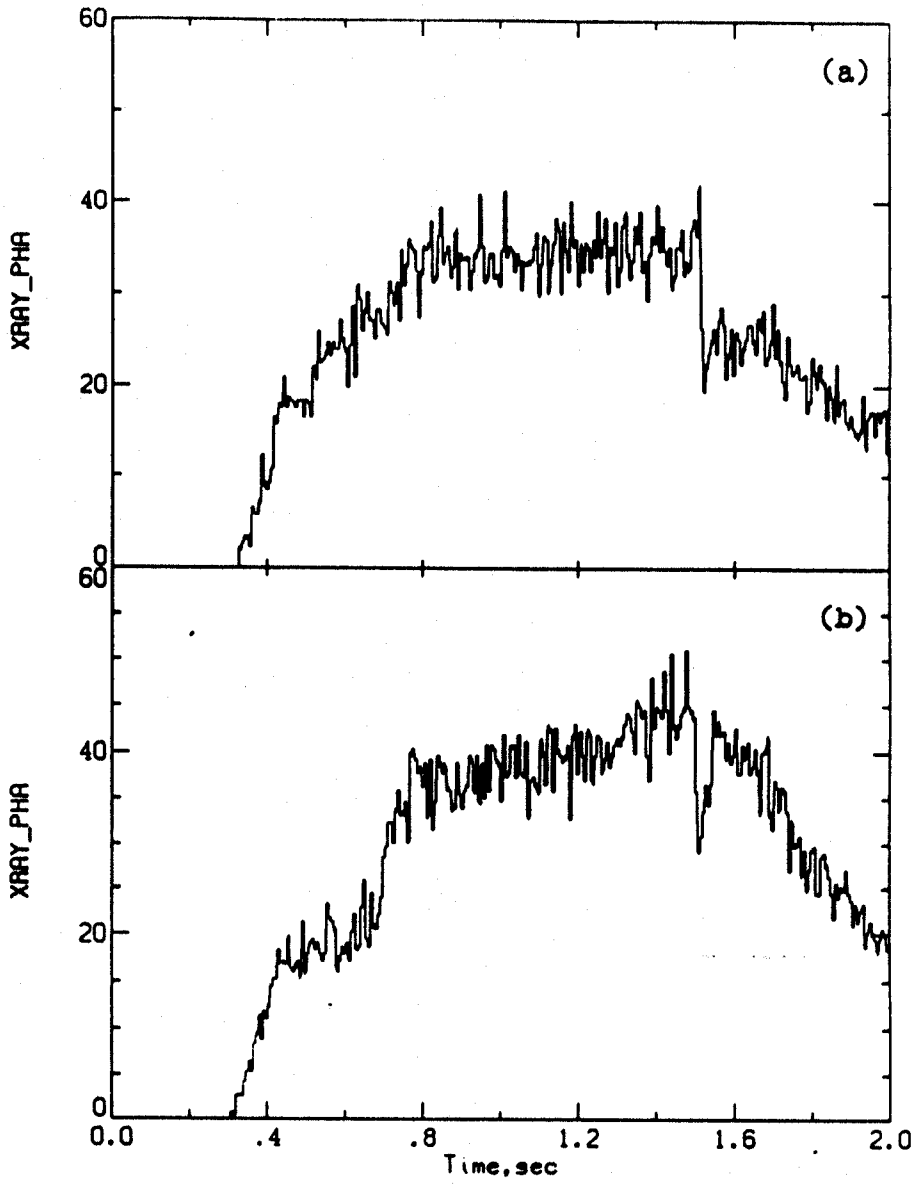

Fig. 54) The difference in the x-ray flux with (a) the getters off and (b) the getters on. The gas pressure is set to be the same in both cases.

the same neutral pressure but one shot has the getters on, and in the other the getters are off. Note that the flux drops as expected when the getters are off. The increase in flux when the getters are on and the pressure is low is probably due to impurities falling into the plasma. Impurities are excluded by the plasma's positive ambipolar potential when the ECRH is on.

We also note that the surface barrier detectors (SBD's) are an excellent monitor of the impurity line emission. They are sensitive in the low keV range where the titanium and argon lines are the dominant feature of the x-ray spectrum. When the getters are turned off the SBD signal drops almost to the x-ray background level.

M. Potential Control

Experiments in potential control using one biased end wall began as early as January 1984. Later both end walls were biased using large rectangular plates at both ends. These experiments showed that the potential and density profiles could be changed using these technique (figs. 55, 56). It was also noted that changes in the hot electron decay time could also be seen (fig. 57).

The next step was the design of end wall rings for radial potential control experiments. The baseball magnetic field produces fans with very high ellipticity ($\simeq$40) so that the midplane plasma maps to almost a line at the endwall. This makes the placement of rings and diagnostics very difficult. Therefore recirculariz:ation coils (fig. 58) were designed to increase the mapped plasma width at the endwall. With the coils the

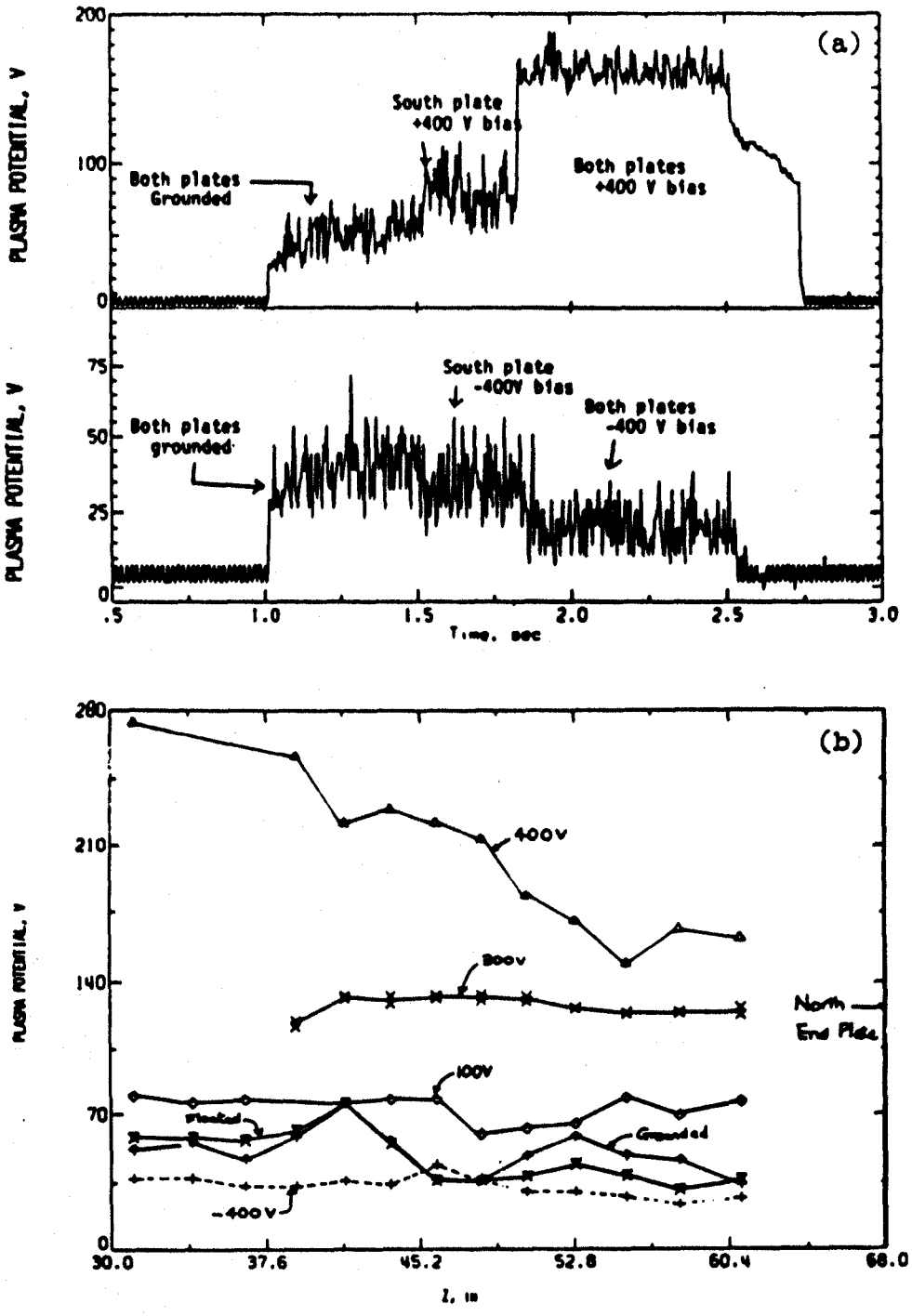

Fig. 55) (a) Change in plasma potential as end wall plates are biased. (b) Change in axial potential profile with end wall bias.

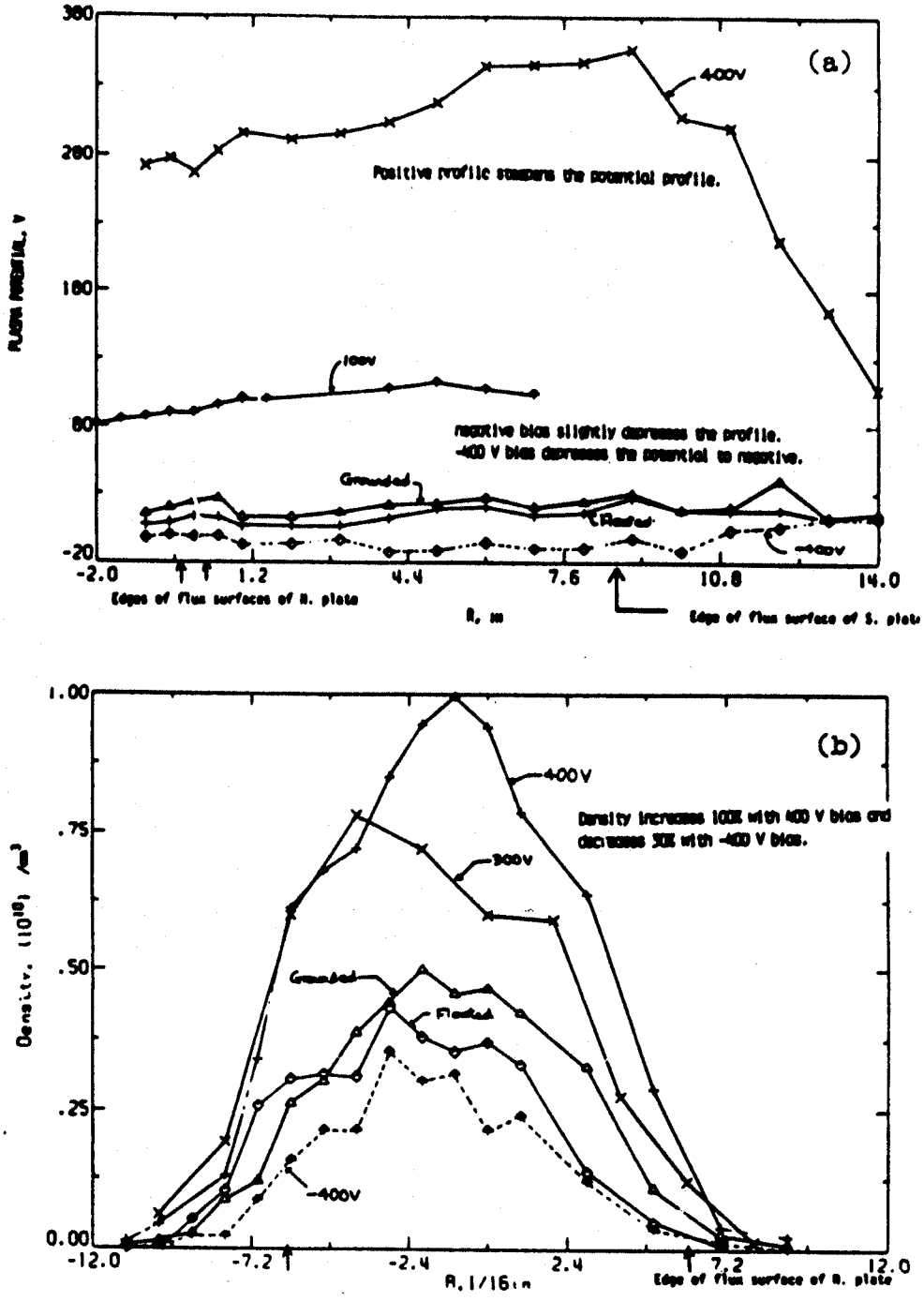

Fig. 56) (a) Change in radial potential profile with end wall bias. (b) Changes in the radial density profile with end wall bias as measured with a Langmuir probe.

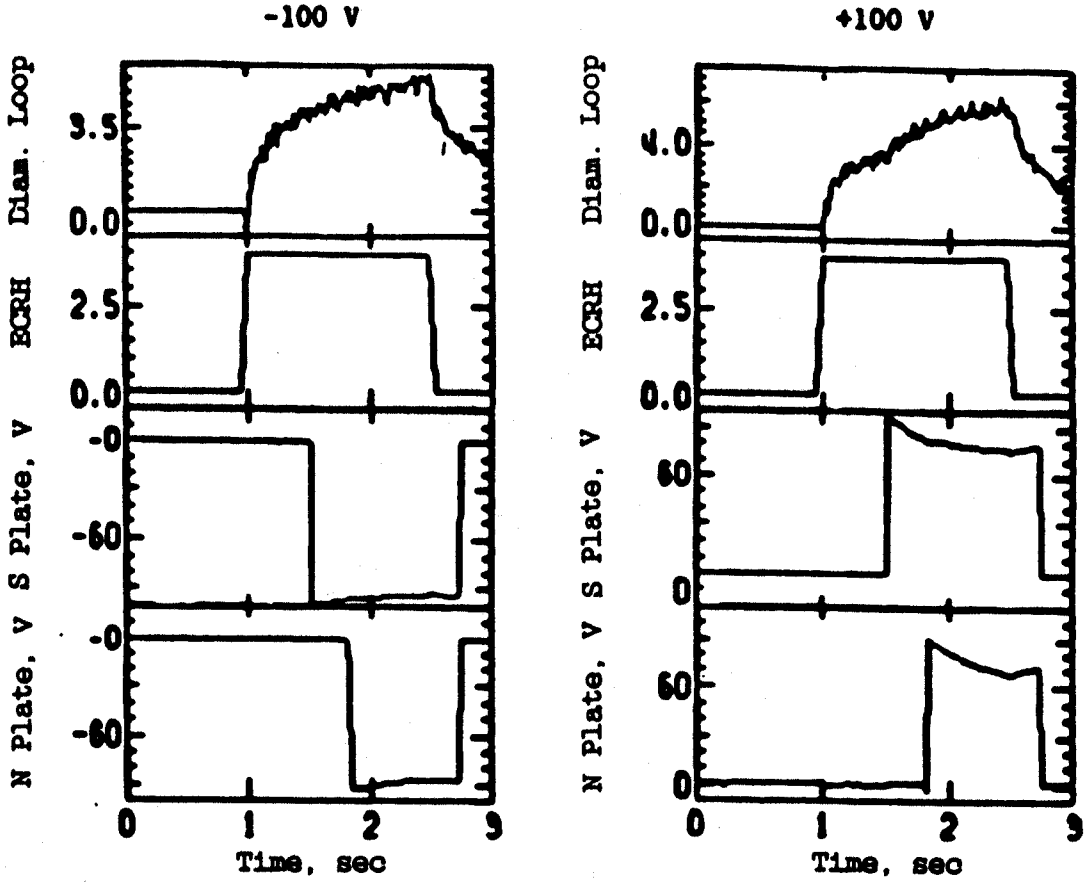

Fig. 57) Changes in diamagnetism with end wall bias. The diamagnetism is increased for positive plate bias.

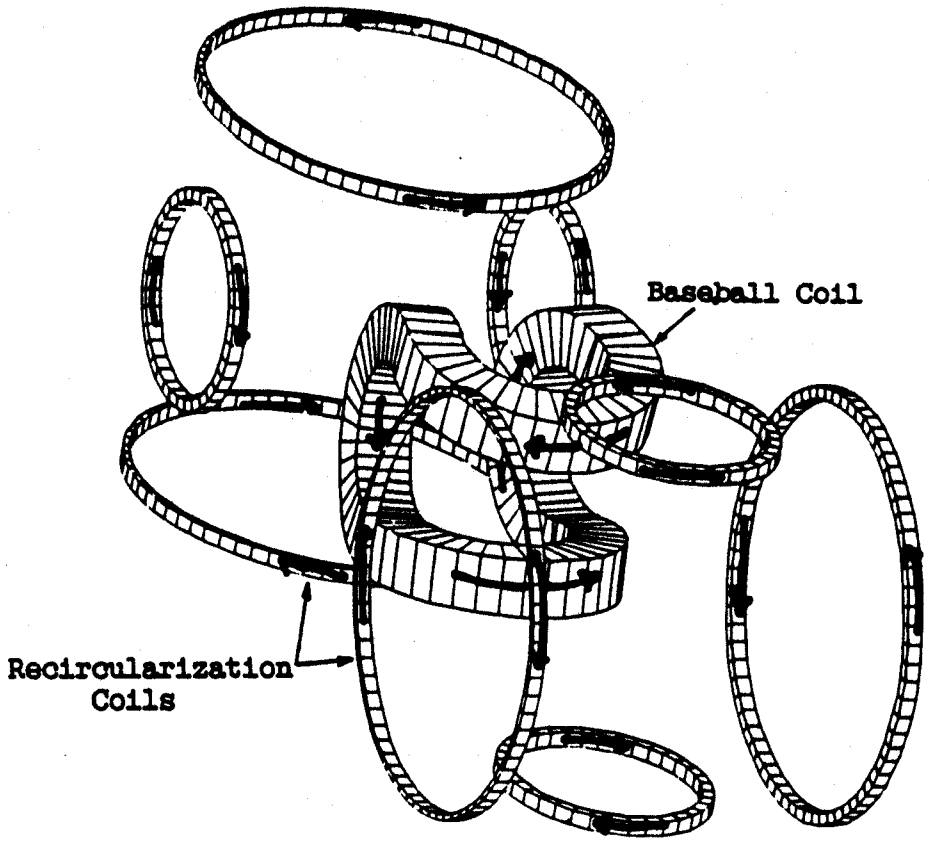

ig. 58) Fan tank recirculariz ation coils shown in position relative to the baseball coil. The arrows indicate the direction of current flow in each of the coils.

ellipticity at the endwall is ~8. These coils were delivered in October 1985 and will be installed by July 1986.

The success of any radial potential control experiment depends on the accuracy to which the field line mapping is known. Therefore alignment procedures have been developed and extensively tested. We have found that an e-beam can burn a pattern into phosphor-coated plexiglas so that a permanent record of the mapped beam position can be made. We will use such a plate mounted at the same position the potential control plates will be mounted and use a star-shaped e-beam to burn a pattern onto the plates. The plates and the diagnostics are mounted in a frame connected to the vacuum chamber by turnbuckles so that the position can be easily adjusted. We know from previous alignments that the south fan maps low and at an angle, and the north fan is displaced to the west. This is due to an inherent asymmetry in the magnet itself.

N. ICRH and Drift Pumping

In August 1985 the antenna and matchbox for the ICH and drift pumping experiments were installed on Constance. RF pumping is a technique whereby ions are caused to move radially due to a resonance between an applied field and the ion's bounce or drift motion. This radial flow is necessary in the thermal barrier of a tandem mirror to keep ions from collisionally filling in the barrier and thus destroying it. It is desirable to have the ions move stochastically so that a larger class of ions experience the resonance. In the Livermore drift pumping schemes stochasticity is induced by the use of multiple frequency applied fields. A different drift pumping technique

has been developed at MIT in which the necessary stochasticity is introduced by ICRH.

The Constance experiments use the ion bounce resonance. A 150 kW, 20 ms, 155 kHz transmitter was built which produced a perturbed magnetic field, $\bar{B}$, of 125 gauss. The antenna (fig. 59) generates a spatially varying B_x which perturbs the geodesic curvature and leads to radial transport. The ICRH transmitter operated at 1 kW CW at frequencies from 3-5 MHz.

The experiments lasted for 5 weeks and were the first rf pumping experiments in the mirror program. The design $\bar{B}$ fields for rf pumping were produced by the antenna but no effects on the plasma parameters were observed. The ICRH alone caused increases in the plasma potential even in the absence of an ion cyclotron resonance in the machine, implying direct electron heating. A second effect was plasma pumpout at low densities.

The second phase of the ICRH experiments was carried out in April and May of 1986. A new double half turn antenna was installed and the former drift pump transmitter was converted to operate at the ion cyclotron heating (ICH) frequency, and produced 10 kW in the frequency range from 1-6 MHz. This allowed heating of either hydrogen or helium plasmas.

The visible spectrometer was used to measure the Doppler-broadened emission lines and the cesium cell charge exchange analyser was brought on line to measure the ion temperature. In radial scans the spectrometer showed that the profile changed from a hollow profile to a peaked one with

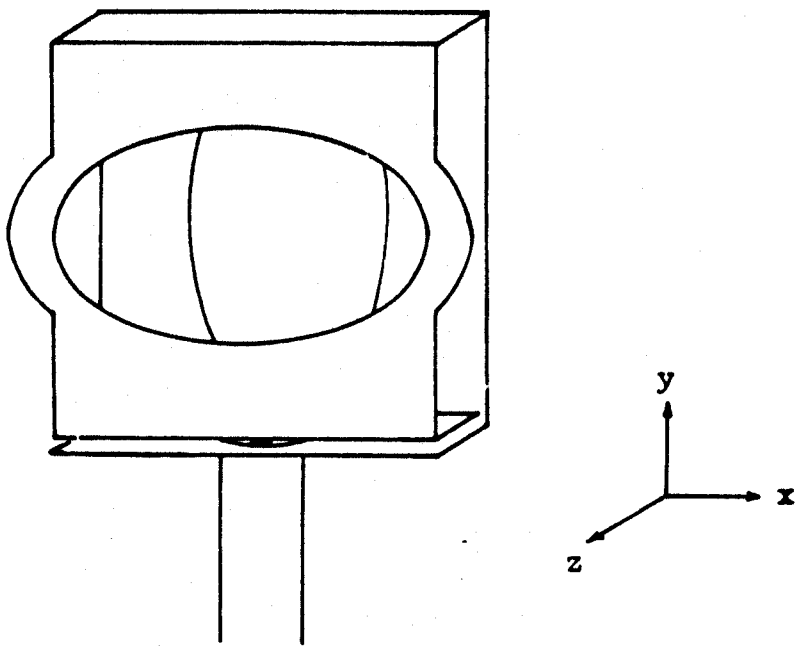

Fig. 59) Drift pump antenna used in the July and August 1985 drift pump experiments.

he application of ICRH, indicating a loss of cold plasma near the edge. ith sufficient power, all the cold plasma is lost and the density drops to 0% of its pre-ICRH value (fig. 60). We call this the "candle effect" ecause the plasma is "blown away" by the ICRH. This effect does not equire an ion resonance in the machine to occur, so it is thought to be an lectron effect, caused by the enhanced potentials which the ICRH generates. ith ICRH the potential can be increased by as much as a factor of six.

Endloss analyser data shows that the potential and the endloss emperature are increased with ICRH (fig. 61). The spectrometer data ndicates a broadening of the singly ionized helium line during ICRH. owever, the ion temperatures seen by the spectroscopy are a factor of 4 ess than the ion endloss temperatures.

. Particle and Power Balance

At this time the power balance in the Constance B device is not ntirely understood. One of the reasons for this is that the profiles of ensity and temperature are not well enough known. Depending on the profile nd volumes which are used, one can account for anywhere from 40-140% of the ower. The main sources of power loss are the ECRF-induced losses and cattering of the hot electrons on neutrals and cold electrons. The histler microinstability accounts for less than 10% of the power drain. ith endloss arrays we should be able to pin down the particle and power alance in Constance B. These arrays are being designed. Table 4 shows an

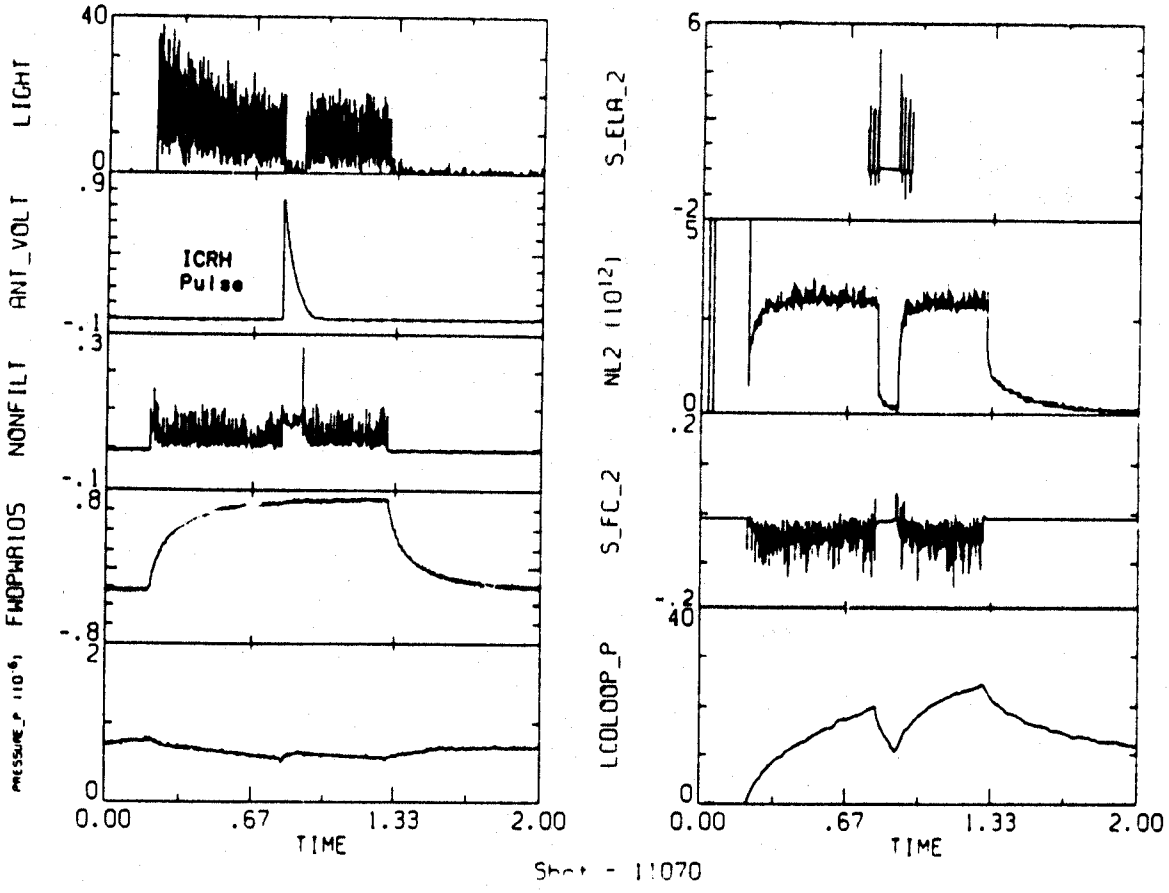

Fig. 60) ICRH "candle effect" data. If the ICRH power is high enough and the gas pressure is low enough, the cold plasma is extinguished by the ICRH. When the cold fueling electrons are expelled, the diamagnetism begins to decay.

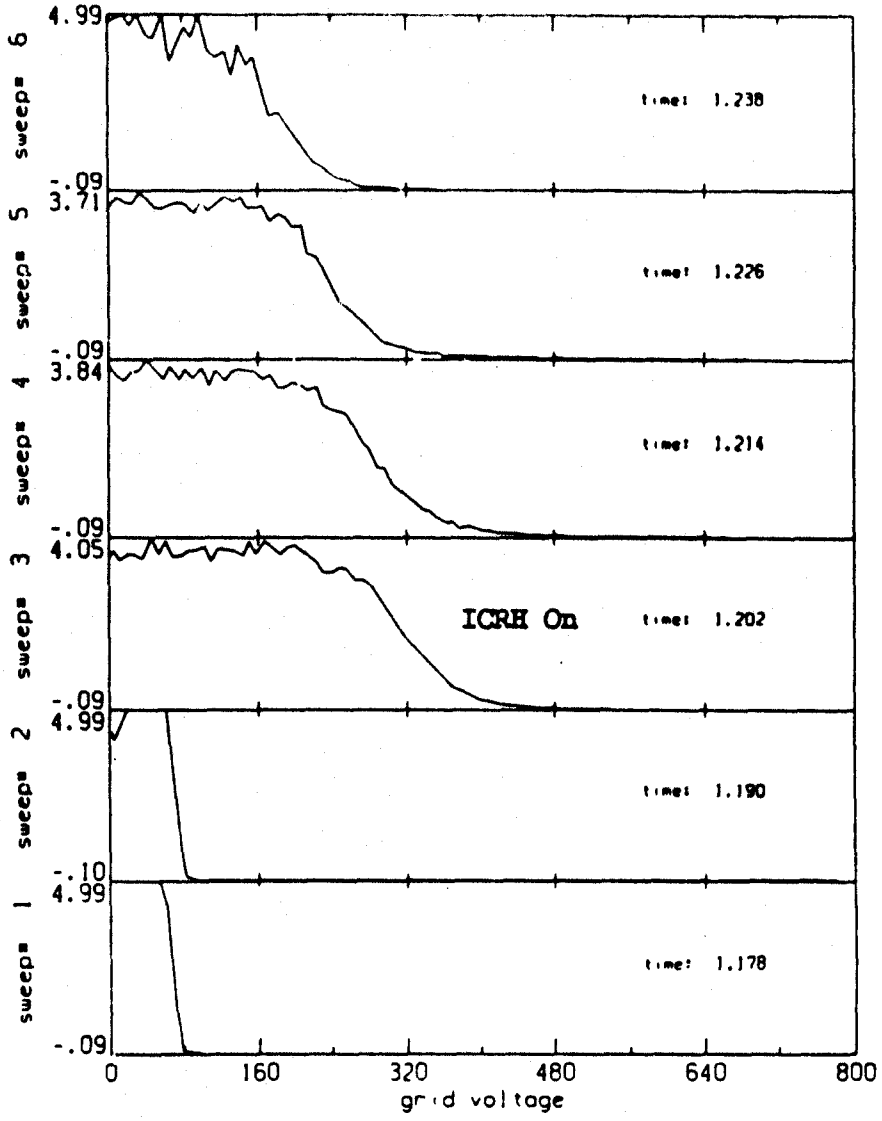

Fig. 61) The change in the potential and the ion end loss temperature due to ICRH (8 kV plate voltage).

example of the power balance accounting which has been done. In this case, sixty percent of the ECRH power is accounted for.

Table 4. Power Balance

For 1 kW of ECRH Power:

Cold electron endloss	25 W
Microinstability induced hot electron endloss	90 W
ECRH induced hot electron endloss	280 W
Unstable rf emission	40 W
Microinstability induced warm electron endloss	80 W
Ionization and excitation*	35 W
Reflected power	~50 W
	600 W

*Calculated

A power balance code is being developed to simulate the machine performance. The code now includes collisonal scattering, drag and ionization. RF losses are not yet included, but will be added as the empirical scaling is available. Impurity losses will also be incorporated.

P. Octupole Constance AP

In November of 1984 work began on the design of an octupole mirror cell machine which would have been called Constance AP (Advanced Plug). This machine (fig. 62) would have been constructed using parts of the Constance II mirror experiment now in storage. During the first 6 months of 1985 the design was worked on by 1 graduate student full-time and 2-3 scientists as a part-time effort. The magnet design and the particle drift analysis were carried out using the LLNL codes effi and XGC49, respectively. The final magnetic geometry is shown in figure 63. The saddle coils were chosen over

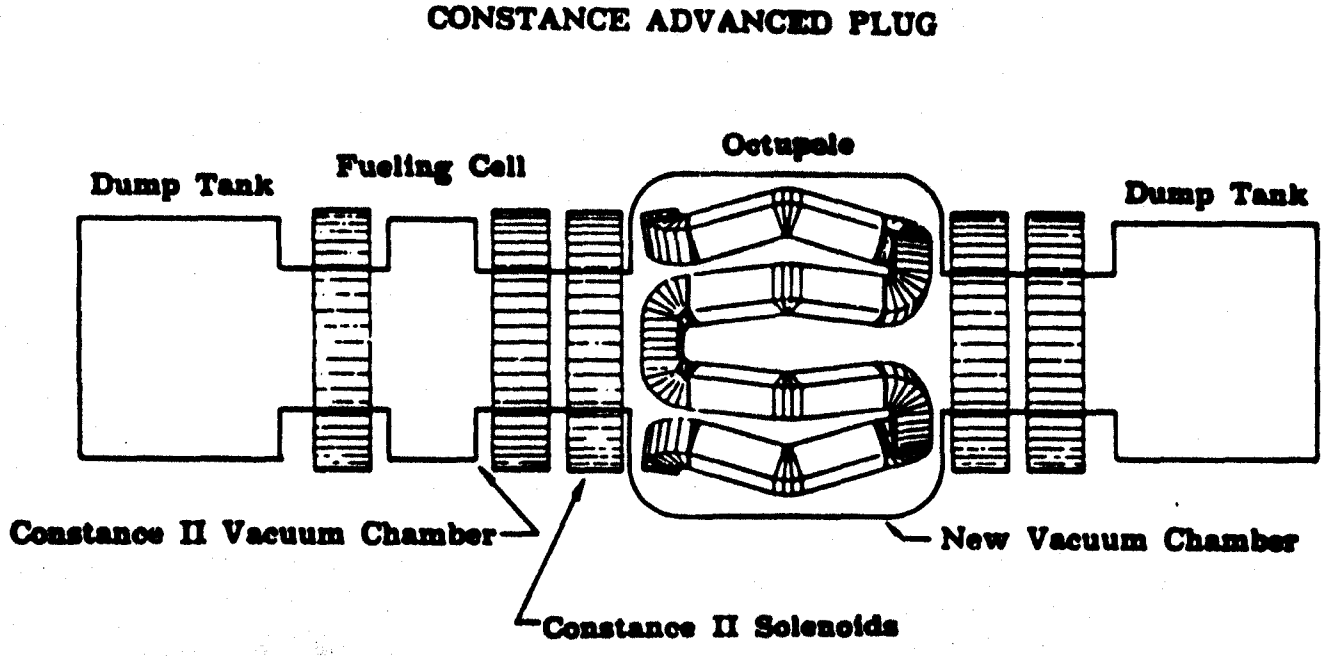

Fig. 62) Early drawing of the Constance-AP experiment. The octupole coil is shown inside the vacuum chamber in this design. In the final design, saddle coils were used which could be mounted outside the vacuum chamber.

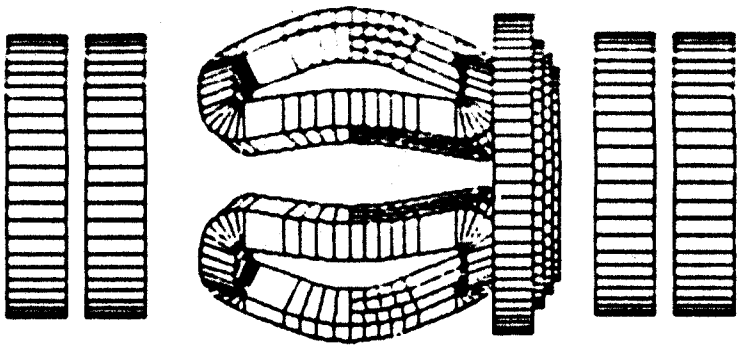

(a)

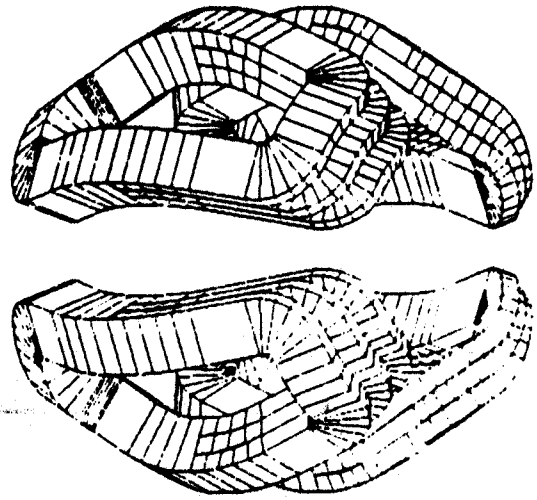

(b)

63) (a) Side view of the Constance-AP octupole coils showing the saddle coils and the stepped correction coil. The end solenoids are existing Constance II coils. (b) 3-D view of the octupole coils.

a continuous wind octupole for their relative low cost and the ease of fabrication. Details of the magnet design can be found in reference 11. This project was mothballed due to budgetary constraints but could easily be restarted if it were desirable to do so.

Q. Epilogue

This report has compiled the basic data which has been collected on the Constance B mirror machine in its first 2.5 years of operation. We hope that this data will be better understood in the future as more experiments are done. In future years new information will be compiled in the form of an annual report.

References

[1] Ard, W.B., R.A. Blanken, R.J. Colchin, J.L. Dunlap, G.E. Guest, G.R. Haste, C.L. Hedrick, N.H. Lazar, J.F. Lyon, and D.J. Sigmar, 4th Conference on Plasma Physics and Controlled Nuclear Fusion Research, Madison, WI (IAEA, 1971) Vol. II, P. 619.

[2] Mauel, Michael E., "Wave Propagation in Ultra-relativistic Plasma", internal memorandum, Jan. 25, 1985.

[3] Chen, Xing, "Diamagnetic Loop Calibration", internal memorandum, Feb. 25, 1985.

[4] Beals, David M., "An Acousto-optic Spectrum Analyzer", B.S. Thesis, Massachusetts Institute of Technology, June 1985.

[5] Cohen, B.I., editor, "Status of Mirror Fusion Research 1980", UCAR 10049-80, Lawrence Livermore Laboratory, Jan. 2, 1980.

[6] Garner, Richard C., "Hot Electron Microinstabilities in the Constance B Mirror Experiment", Ph.D. Thesis, Massachusetts Institute of Technology, in preparation.

[7] Anderson, D.V. and B. Lane, "Numerical Studies of Finite Beta Equilibria in the Constance Mirror Experiment", Bull. Am. Phys. Soc., 29 (1984).

[8] Lichtenberg, A.J. and G. Melin, "Diffusion in Electron Cyclotron Resonance Heating Magnetic Mirrors", Phys. Fluids, 16, 1660 (1973).

[9] Geller, R., "Electron Cyclotron Resonance (ECR) Multiply Charged Ion Sources", IEEE Transactions on Nuclear Science, vol. NS-26, No. 2, April 1979.

[10] Brau, K., "Atomic Physics Considerations for Constance B", internal memorandum, February 1986.

[11] Liu, Dilys K., "A Report on Octupole Magnet Design for Constance Advanced Plug Experiment", internal report, Dec. 16, 1985.